Marcos Borrego Puche

Doctoral Thesis

Analysis of single stage SPIF process applied to the hole flanging operation

Marcos Borrego Puche

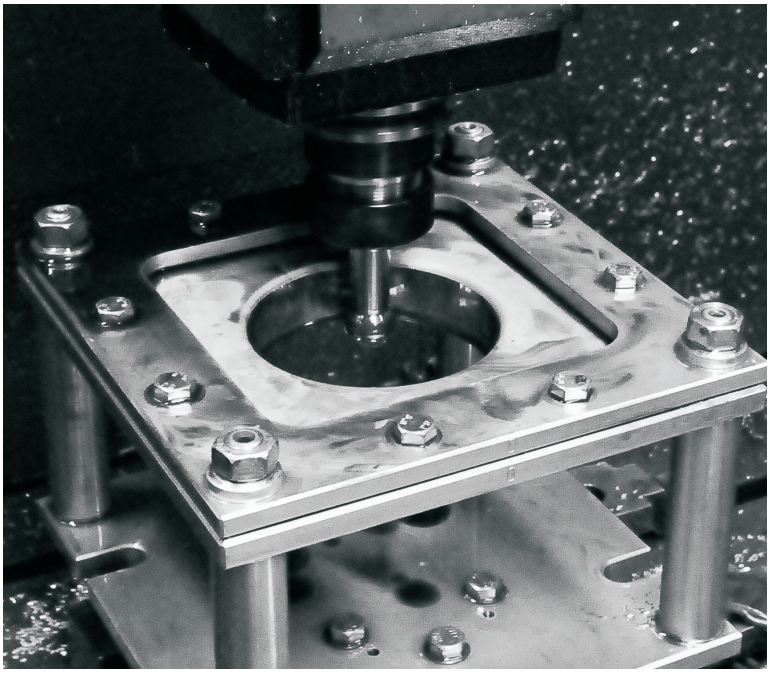

Analysis of single stage SPIF process applied to the hole flanging operation

2018

UNIVERSIDAD DE SEVILLA

Doctoral Thesis

Analysis of single stage SPIF process applied to the hole flanging operation

Author:

Marcos Borrego Puche

Mechanical Engineer

Directors:

Dr. Carpóforo Vallellano Martín

Dr. Domingo Morales Palma

Dpto. de Ingenieria Mecánica y de Fabricación

Escuela Técnica Superior de Ingeniería

Avda. De Los Descubrimientos s/n. 41092

Universidad de Sevilla

Sevilla, 2018

A mi familia

ACKNOWLEDGEMENT

Parecia que nunca iba a llegar el momento de los agradecimientos y sin embargo el momento ha llegado.

Quiero agradecer en primer lugar a los doctores Prof. Carpóforo Vallellano y Domingo Morales por su implicación en este proyecto, tanto en la dirección como en las correcciones.

Al Dr. Andrés Martínez-Donaire, disponible 24/7 para cualquier cuestión.

Al Dr. Gabriel Centeno, guerrillero urbano que se las sabe todas.

A Antonio Guillén, buena persona y mejor amigo, con el que disfruto enormemente en el taller.

A Manuel Sánchez, excelente ganadero ecológico y miembro secreto del equipo "ARUS".

Al Dr. Alfredo Navarro, que poco a poco vamos a cambiar la ingeniería por la botánica.

A José el carpintero, excelente profesional y compañero. Me encanta charlar con él.

A Juan Martínez, servicial y gran alumno de Solidworks.

A Manuel de fluidos, que tiene un coche con un catalizador que no se lo merece….

Al futuro Dr.Andrés Lopez, que como a mi, le sube la adrenalina con lo que otros tiran.

Al grupo del Técnico de Lisboa, por su trato acogedor y familiar:

Prof. Dr. Paulo Martins, visto sus "ferramentas" en otra vida seguro que fue discípulo de Leonardo Da Vinci.

Dra. Beatriz Silva, diligente y dispuesta a reir en todo momento, amante del queso y el vino.

Dr. Carlos Silva, no me lo ha confirmado pero creo que es familia del Sr. Gomes…

Dr. Luis Alves, excelente persona y potencial artesano de cascavéis de falcoaria.

Dr. Valentino Cristino, servicial y gran conversador portugués de ultra mar.

A las secretarias Paula y Fatima, cordiales, serviciales y familiares.

A mis padres Antonio y Ana, los impulsores sin ninguna duda de esta aventura, lo vieron claro desde el principio y animaron sin fisuras. Sólo ellos son conscientes de lo que disfruto con ellos en su casa, también la mia.

A mis hermanos Pablo y Berta, iniciadaos antes que yo y precursores de mi carrera docente. Les deseo lo mejor.

No puedo olvidar a mi tia Lola, doctorada de la vida con casi 80 años de experiencia recientemente fallecida. Cita ineludible de cada miércoles.

Y por supuesto le doy las gracias a Patricia por su "pacencia"" infinita".

Alguno se me olvida, que no me lo tenga en cuenta,¡gracias!

RESUMEN

Tradicionalmente, las operaciones de rebordeado se llevan a cabo en la industria mediante técnicas de prensado convencionales utilizando punzón y troquel. Sin embargo, investigaciones recientes en conformado incremental (ISF) han señalado ventajas significativas de esta operación con respecto a los procesos convencionales. Entre otras son, la flexibilidad, la relación coste-efectividad y una importante mejora aparente en la confomabilidad del material. En este sentido, la presente tesis doctoral ofrece un análisis crítico de la operación de rebordeado de agujero cilíndrico mediante el conformado incremental mono punto (SPIF), realizada en una etapa, desde el punto de vista de la conformabilidad del material y las capacidades geométricas del proceso.

Para comprender y cuantificar las ventajas de las operaciones de SPIF de una sola etapa, se llevó a cabo una campaña experimental de rebordeado de orificios cilíndricos mediante conformado incremental y convencional. Esto se realizó sobre una lámina de aleación de aluminio 7075-O.

Se proporciona un estudio detallado de la evolución de las deformaciones en el flanco. Éstos se midieron utilizando métodos avanzados de videogrametría y fotogrametría. Los mecanismos y modos de fallo de la lámina y la caracterización de la capacidad de rebordeado en ambas operaciones se analizan usando el diagrama límite de conformado (FLD). El efecto de flexión inducido por la herramienta en SPIF y el radio de esquina en el caso convencional ha sido claramente dilucidado, junto con la geometría del flanco y las fuerzas de conformado involucradas.

Finalmente, la comparación llevada a cabo permite extraer las ventajas y limitaciones tecnológicas en el proceso de rebordeado de orificios mediante SPIF de una sola etapa, y descubrir futuras líneas de investigación para mejorar su aplicación práctica.

ABSTRACT

Traditionally, flanging operations are performed in industry by conventional press working techniques using a punch and die. However, recent investigations in incremental sheet forming (ISF) have highlighted the significant advantages of this operation with respect to conventional processes. These advantages include flexibility, cost-effectiveness and a significant apparent enhancement in the formability of a material. This PhD thesis offers a critical analysis of the hole flanging operation by Single Point Incremental Forming (SPIF), which is performed in one stage, from the point of view of material formability and the geometrical capabilities of the process.

To understand and quantify the advantages of a single-stage SPIF operation, an experimental campaign of hole flanging tests by both incremental forming and conventional forming was performed on an aluminium alloy 7075-O sheet.

A detailed study of the evolution of the strains in the flange is provided. These strains were measured using advanced videogrammetric and photogrammetric methods. The mechanisms and modes of failure of the sheet and characterization of the flangeability in both operations were analysed using a forming limit diagram (FLD). The effect of bending induced by the tool in SPIF and the punch edge radius in conventional forming was clearly elucidated with the flange geometry and the forming forces.

The comparison performed in this study enables the identification of the technological advantages and limitations in the hole flanging process by single-stage SPIF and the future research lines for improving its practical application.

GENERAL INDEX

LIST OF SYMBOLS

$A\%$	Percentage elongation
C	Clearance
d	Die diameter
d_f	Final hole diameter
$d_{f,\,max}$	Maximum final hole diameter
d_o	Initial pre cut hole diameter
$d_{o,\,min}$	Minimun initial pre cut hole diameter
D_p	Punch diameter
D_f	Die diameter
E	Young's modulus
$\bar{\varepsilon}$	Equivalent Strain
ε_1	Major principal strain
ε_2	Minor principal strain
ε_1^p	Major principal plastic strain
ε_2^p	Minor principal plastic strain
ε_3^p	Thickness principal plastic strain
ε_{1f}	Major principal strain at fracture
ε_{2f}	Minor principal strain at fracture
ε_{3f}	Thickness principal strain at fracture
$\varepsilon_{1,UT}^*$	Major strain at the onset of necking in uniaxial tension
F_x	Force in X direction
F_y	Force in Y direction

F_h	Horizontal force
F_z	Vertical force
h	Flange heigh
h_o	Height of the stack
K	Strength coefficient
kN	Kilo Newton
mm	Milimeter
mm/s	Milimeter per second
n	Hardening exponent
P	Pressure
r	Lankford coefficient
r_{0^o}	Lankford coefficient in rolling direction
r_{45^o}	Lankford coefficient in diagonal direction
r_{90^o}	Lankford coefficient in transverse direction
r_1	Radius of a sphere
r_2	Radius of a sphere
R	Punch edge radius/tool radius
Ra	Roughness Average
R_c	Clearance thickness ratio
R_d	Radius of the die
R_p	Radius of the punch
rpm	Revolutions per minute
Rz	Average maximum height of the profile
ρ	Radius of curvature

$\bar{\sigma}$	Equivalent stress
t	Thickness
t_o	Initial thickness
$\bar{t}$	Average thickness
t_o/R	Bending ratio
V	Volts
Y	Yield stress
Δz	Step down

LIST OF ACRONYMS

AA1XXX-YZ	Aluminium alloy, series 1(e.g. AA1050-H14)
AA2XXX-YZ	Aluminium alloy, series 2
AA3XXX-YZ	Aluminium alloy, series 3
AA5XXX-YZ	Aluminium alloy, series 5
AA6XXX-YZ	Aluminium alloy, series 6
AA7XXX-YZ	Aluminium alloy, series 7
ACW	Anti-Clockwise
ASTM	American Society for Testing and Materials
CAD-CAM	Computer-Aided Design/ Computer-Aided Manufacturing
CCD	Charge-Coupled Device
CIRP	The International Institution for Production Engineering
CNC	Computer numerical control
CW	Clockwise
DIC	Digital Image Correlation
EP	European Patent
FEA	Finit Element Analysis
FFL	Fracture Forming Limit
FLD	Forming Limit Diagram
FLD_0	FLC under plane strain conditions
FLD_{0incr}	FLC under plane strain incremental conditions
H_2O	Water

HCl	Hydrochloric acid
HER	Hole Expansion Ratio
HFl	Hydrofluoric acid
HNO_3	Nitric acid
HRC	Rockwell C Hardness
ISF	Incremental Sheet Forming
LFR	Limiting Forming Ratio
ORB	Orbital Roller Ball
PTFE	Polytetrafluoroethylene
SFFL	Shear Fracture Forming Limit
SPIF	Single Point Incremental Forming
SPIF-A	Single Point Incremental Forming-Aveiro
TPIF	Two Point Incremental Forming
TR	Average thickness ratio
UNE	Una Norma Española
US	United States
UTS	Ultimate Tensile Streght
VRB	Vertical Roller Ball

INDEX OF FIGURES

INDEX OF TABLES

MOTIVATION AND OBJECTIVES

Hole flanging is a typical operation that is used in the aerospace and automotive industries to stiffen the edges of structural holes, improve their appearance or provide additional support for press fitting or welding to join sheet parts to tubes.

This thesis analyses and compares two forming processes that are used to perform this industrial operation: the well-known and conventional process of hole flanging by press working, which will serve as a reference or base line for comparison, and the innovative process of hole flanging by incremental forming by Single Point Incremental Forming (SPIF) performed in a single stage.

The differences between these processes primarily arise from the manner in which the material is deformed to perform the flange. In conventional press working, a clamped blank with a pre-cut hole is plastically deformed in a single punch stroke, which forces the material around the hole to expand. In circular hole flanging by SPIF, a sheet with a pre-cut hole is deformed by a forming tool that progressively produces the flange following a pre-established trajectory. In the former, the material is subjected to a combination of circumferential stretching and meridional bending; in the latter, the material is deformed by a combination of meridional and circumferential stretching with localized bending induced by the tool.

Single-point incremental forming is a novel technology that has been employed for the last few years to obtain a variety of industrial parts due to its benefits compared with conventional sheet metal forming processes. SPIF is a flexible and cost-effective process that is viable for small- and medium-sized batches and is capable of producing a remarkable enhancement in material formability.

High ductility metal sheets formed by conventional press working processes usually fail due to the onset of localized necking, where plastic deformation concentrates until material fracture. Both failure mechanisms, i.e., necking and ductile fracture are characterized in practice by the Forming Limit Curve (FLC) and Fracture Forming Line (FFL), respectively. The FLC provides the limit strains for the initiation of necking in the sheet, whereas the latter represents the fracture locus for the appearance of tensile cracks in the material.

In general terms, a conventional forming operation is warranted when the strains in the sheet are below the FLC. This criterion is currently the most useful criterion

for evaluating the formability in press working operations. However, the majority of studies of conventional hole flanging analyse the formability via the Limiting Forming Ratio (*LFR*) parameter, that is, the maximum ratio between the final hole diameter and initial hole diameter achievable without failure. Few studies are devoted to the use of the FLC as the analysis tool. None of these studies have provided a detailed description of the flange deformation process or a comprehensive study of the influence of bending induced by the punch profile.

Regarding the hole flanging processes by SPIF, current studies only focus on multi-stage operations. Despite the inherent advantages of SPIF in terms of simplicity, flexibility and sustainability, multi-stage strategies have a large deficit in terms of time consumption. Some attempts have been made to reduce production times by performing hole flanging operations by high-speed SPIF using complex tools; for instance, Bambach *et al.,*2014. However, minimal attention has been paid to what is probably the simplest method for reducing the processing time, that is, to perform the operation in a single-stage. In addition to the preliminary work performed by Borrego *et al.,*2015, current state-of-the-art methods do not include a systematic study about the capability of performing hole flanging by SPIF in a single stage. Therefore, there are no relevant studies of either the analysis of the deformation process of the flange or the mechanisms of the failure that define its formability.

The objectives of this PhD thesis is to fill the knowledge gaps by performing a detailed comparative experimental study of the hole flangeability, i.e., the capability of the sheet material to form a circular flange in both single stage SPIF and conventional press working operations. The geometrical features of the flanges, such as the dimensions, shape and thickness profile, and forming forces, are also analysed. The tested sheet metal tested is aluminium alloy 7075-O with a thickness of 1.6 mm.

The manuscript is structured in six chapters (see Figure 0.1). Chapter 1 provides a brief description of current state-of-the-art methods for conventional and incremental sheet metal formability characterization and hole flanging operations. The mechanical characterization and determination of the FLC and FFL for the AA7075-O sheet is presented in Chapter 2. Chapter 3 analyses the conventional hole flanging operation, with a special focus on the effect of the punch edge radius on formability. The hole flangeability by single-stage SPIF and a geometrical evaluation of the flanges and forming force evolution during the operation are presented in Chapter 4. In Chapter 5, a comparison between both conventional operation and incremental operation is provided, with a detailed discussion of the differences in flangeability, final flange shape and thickness and forming forces.

Chapter 6 presents the main conclusions of this thesis and possible research directions to extend this study in the near future.

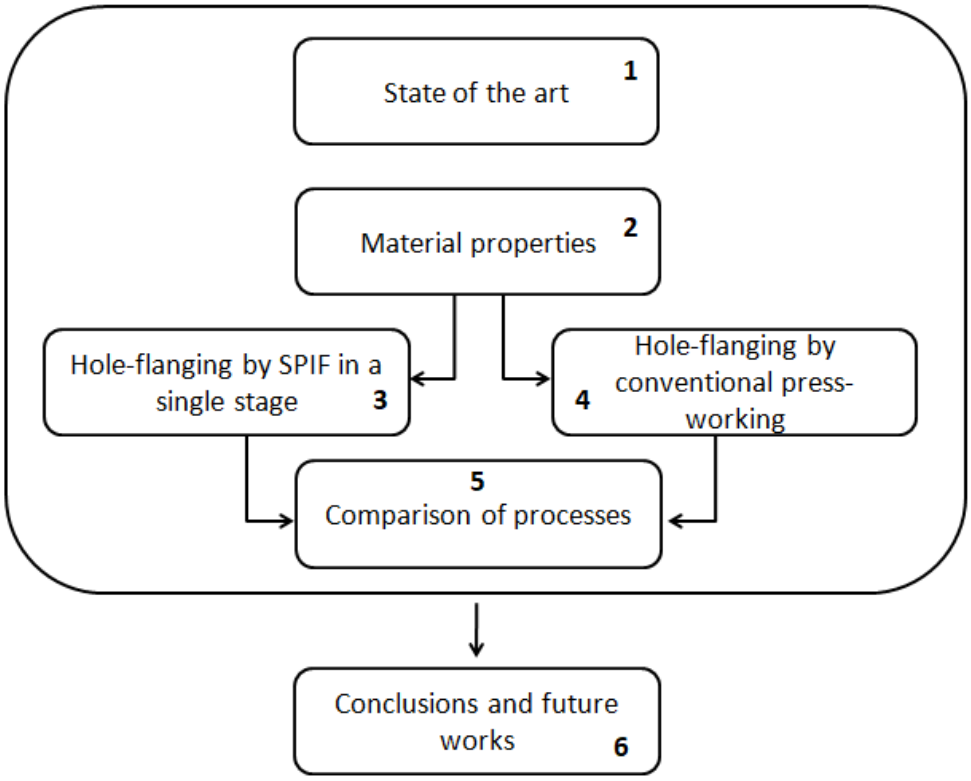

Figure 0.1 Thesis structure

1. INTRODUCTION. STATE OF THE ART

Sheet metal forming processes have substantial industrial importance in highly competitive sectors that require the fabrication of products with high accuracy and geometrical complexity. Industrial production, particularly in countries with expensive labour, experience a high demand for innovation, flexibility and sustainability in their manufacturing processes to maintain high-quality products at competitive prices. The SPIF process has been proposed as an alternative to the traditional conventional press working process.

1.1. Introduction to conventional flanging by press working

When forming a sheet metal part to provide additional support for press fitting or welding to join sheet parts to tubes to improve their appearance or strengthen the edges, the conventional flanging process is one of the last stages of the forming process. This operation is typically employed in the aerospace and automotive industries, in which the flange is generated along the edge of the sheet by the action of a single stroke of a pre-shaped punch (see Figure 1.1).

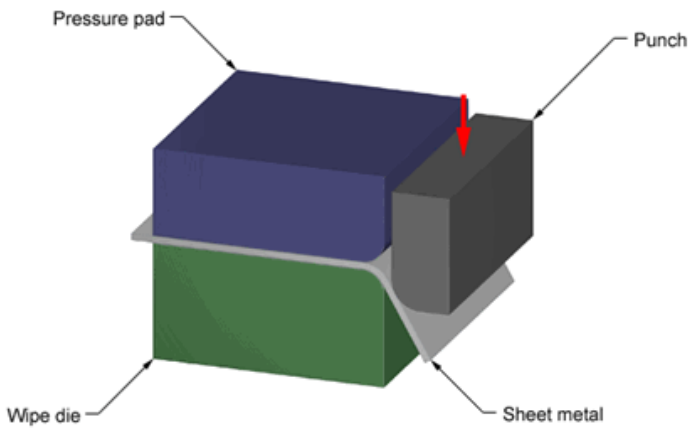

Figure 1.1 Example of flanging by conventional press working (Custompart.net)

Different flange profiles can be generated by varying the die and punch. Depending on the profile of the edge, the sheet undergoes different strain states during the forming process.

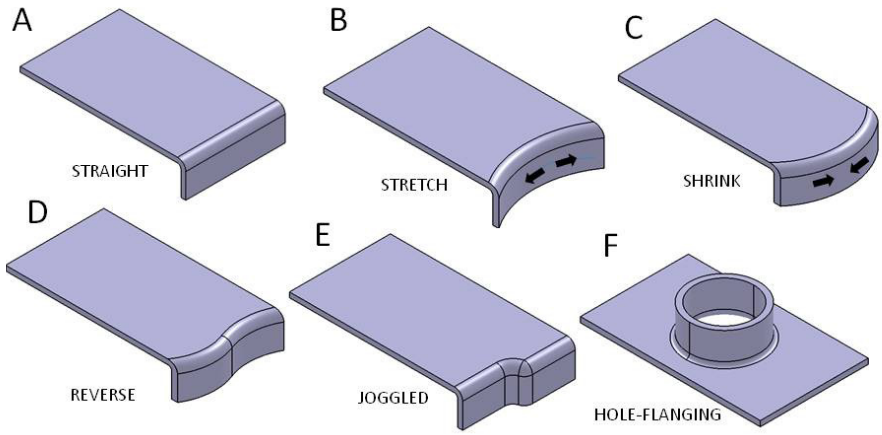

Figure 1.2 Types of conventional flanges: A) straight, B) stretch, C) shrink, D) reverse, E) Joggled and F) hole-flanging

Figure 1.2 shows different types of flanges. Case A shows a straight flange that is primarily formed under bending around the edge. Case B (referred to as a stretch or concave flange) is formed by a combination of bending and tensile loads. Case C is a convex flange (also referred to as a shrink flange), which is produced by bending and compression loads. Other geometries are usually employed in industry. Cases D and E are a combination of the first three cases. Case F is a particular type of stretch flanging in holes (hole flanging) formed by a combination of circumferential stretching and meridional bending; this type of case is explored in this study.

1.2. Influence of different parameters in conventional hole flanging process

In the conventional hole flanging process (Figure 1.3), a clamped blank with a pre-cut hole is plastically deformed and forced to expand. Due to its industrial importance, this process has attracted the interest of researchers who want to understand the deformation process of the flange and the process parameters that control it, such as material properties, anisotropy, punch shape, blank holding force, clearance-thickness ratio or diameter of the initial pre-cut hole.

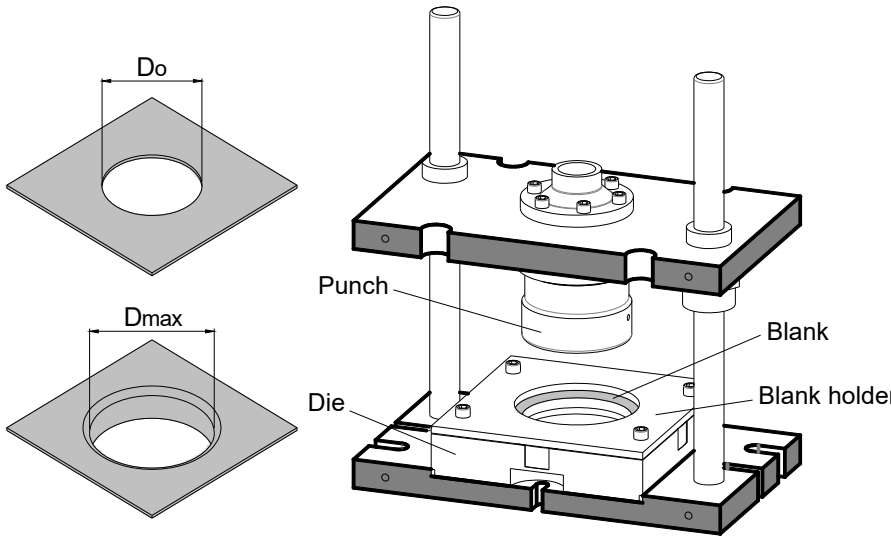

Figure 1.3 Schematic of conventional hole flanging, (left) specimen with an initial pre-cut hole and finished hole flanging, and (right) the conventional press working setup. Montanari et al.,2013

These parameters can be classified into two categories: *material parameters*, i.e., parameters that are directly related to material properties, such as the *yield* stress, and hardening exponent or anisotropy in the case of metallic materials, and *geometrical parameters,* which are related to the boundary conditions and loads. The influences of some of these parameters are discussed in the following section.

1.2.1. Material properties

Although a wide range of materials exist where this forming process can be analysed, only metallic materials (e.g., as aluminium, steel or titanium alloys) will be considered in this case study.

Assuming a generic material hardening law given by $\bar{\sigma}=Y+c\bar{\varepsilon}^{n}$, Yamada *et al.,*1967 investigated the effects of Y and the hardening exponent n in his numeric analysis of the bore expanding test. They noted that circumferential strain increases with n and decreases with Y when the punch load attains its maximum. They also demonstrated that the maximum circumferential stress was located at the edge of the bore, for larger values of n. However, this position can shift to an interior annulus if n decreases and/or Y increases. After ten years, Johnson *et al.,*1977 experimentally concluded that the process geometry and the plastic

properties of the material influence the instability strain in the hole flanging process and that failure of the flange was due to lip fracture.

Some researchers, for instance, Kacem *et al.,*2015, have investigated the influence of the anisotropy (isotropy, normal, and orthotropic anisotropy) and yield criterion (Von Mises and Hill 1948) on hole flanging of AA1XXX. They concluded that the use of the Hill 1948 yield criterion reasonably explains the analysed geometry and forming parameters. They also evaluated the influence of anisotropy on the total final shape, e.g., the accuracy of the final inner radius and the hole circularity error, the flange thinning and the maximum punch load.

1.2.2. Punch shape

Using finite element analysis (FEA), *Tang*,1981 investigated the flange formation with four different punch shapes (hemispherical, ellipsoidal, nearly flat and conical frustum). He concluded that the strain path at the flange tip during the forming process is independent of the punch shape and the maximum strain at the flange edge for an equal hole size and flange height. The strain path at the flange tip was always proportional and had a strain ratio of -0.5 (pure tensile) (see Figure 1.4 right). However, the maximum load exhibited a high dependence with the punch shape (see Figure 1.4 centre).

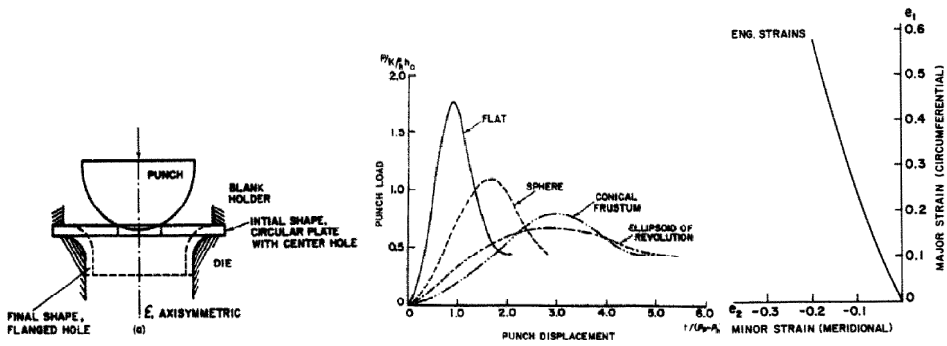

Figure 1.4 Model (left), punch load vs. displacement (centre) and strain paths at the flange tip for different punch shapes (right). Tang ,1981.

Leu *et al.,*1999 employed an incremental elasto-plastic finite-element method to predict the limiting condition of collar-drawing for three punch shapes (conical, cylindrical and spherical). Table 1-1 presents the experimental results. The authors observed that the critical thickness of the hole for necking for all three punch

shapes was equal to the fracture thickness of the material under simple tension. This was used as a necking criterion on the hole periphery for the limiting condition of collar drawing.

Table 1-1 Experimental results for a pre cut hole with a diameter of 16 mm for different punch shapes. Leu et al.,1999

Punch type	Maximum punch load (kN)	Punch stroke (mm)	Final diameter of the hole (mm)	Thickness on the periphery (mm)
Spherical	23.80	28.50	18.29	0.63
Conical	18.31	29.40	18.99	0.65
Cylindrical	41.00	16.50	15.38	0.70

1.2.3. Blank holder effect

Krichen *et al.*,2011 numerically and empirically investigated the blank holding effect on aluminium alloy sheets. Although they concluded that it does not affect the maximum punch load, the shape of the finished product with a residual increase in the outer edge is clearly influenced (see Figure 1.5 right); the maximum load was attained when the test was performed without a blank holder. The author also advised of the use of a blank holding force that at least as great as the reaction force at the beginning of the process.

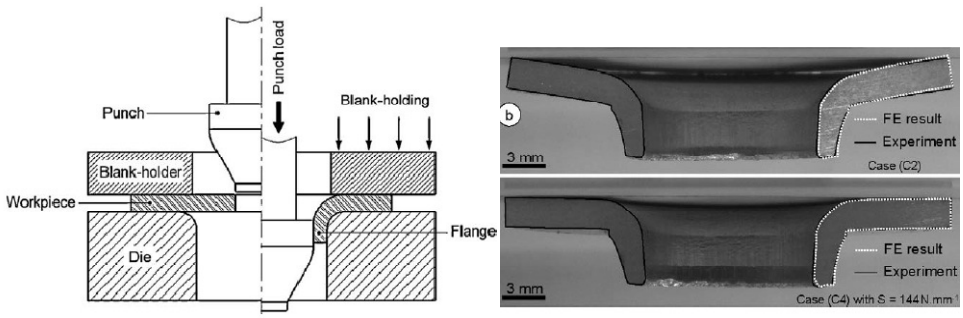

Figure 1.5 Schema of the testing setup (left) and detail of specimens with a blank holding effect (right). Krichen et al.,2011

1.2.4. Ironing and clearance-thickness ratio

Ironing occurs when a flange continuously makes contact with a die and punch during the forming process. Thus, the clearance C between a die and a punch is set lower than a certain value. In the hole flanging practice, one parameter (clearance thickness ratio R_c) resumes the three parameters to be considered to undergo a hole flanging process with or without ironing: sheet thickness t, radius of the punch R_p and radius of the die R_d. The clearance C (as shown in Figure 1.6) is defined as the difference between the radius of the die R_d and the radius of the punch R_p. ($C = R_d - R_p$), and the clearance thickness ratio R_c is defined as the ratio between the clearance and the thickness $R_c = \frac{C}{t}$.

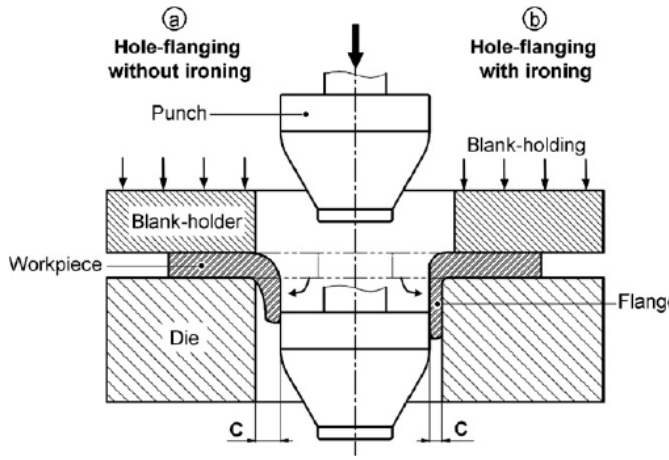

Figure 1.6 Schema of the conventional hole flanging process with clearance indication. Kacem et al.,2011

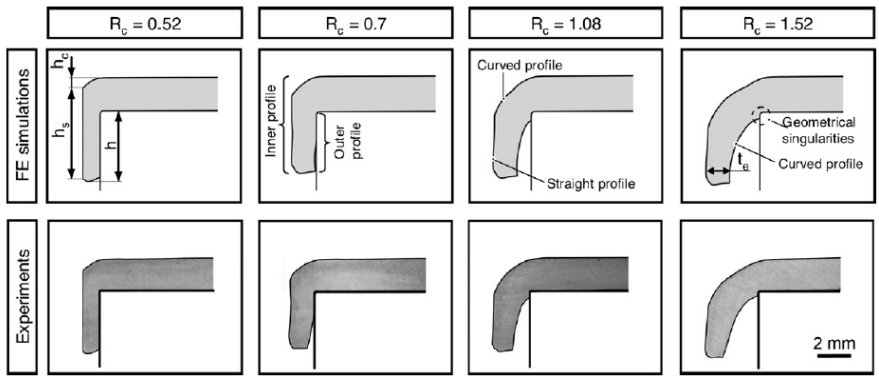

Figure 1.7 FE and experimental shape of flanges for different R_c. Kacem et al.,2011

Kacem *et al.,*2011 investigated the critical value of the clearance-thickness ratio in a 1000 series aluminium with a thickness of 2 mm to distinguish between the two hole flanging conditions. Based on this critical value, the authors were able to predict the flange length, thinning of the flange, final shape and punch load. Figure 1.7 shows the flange profile derived from the numerical and experimental campaign that was performed for different R_c values.Figure 1.8shows the flange length and thinning evolutions according to the evaluated R_c.

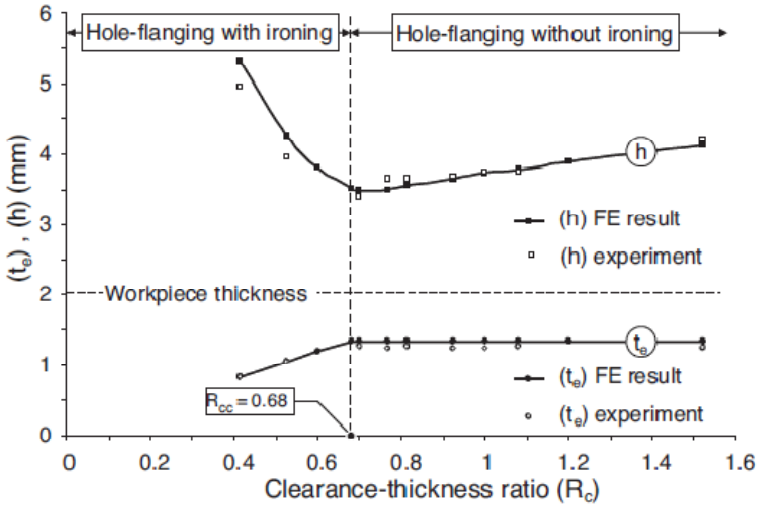

Figure 1.8 Flange length and thinning evolution for different R_c. Kacem et al.,2011

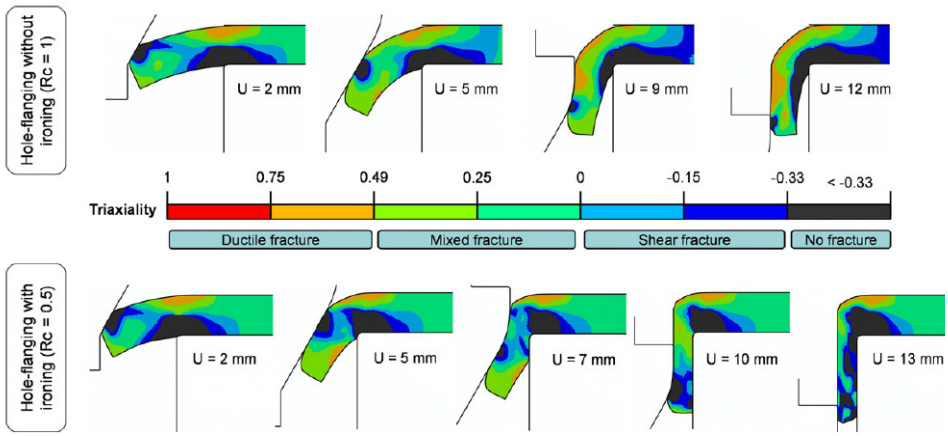

Figure 1.9 Distribution of the stress triaxiality in the conventional hole flanging process on aluminium A1050-H14 with and without ironing. Kacem et al.,2013

In a subsequent study, Kacem *et al.,*2013 investigated the prediction of damage on aluminium A1050-H14 and A6061-O with different parameters, such as the clearance-thickness ratio (R_c) or ironing. Based on the results of an experimental and numerical analysis, they revealed that ironing decreases the damage to the flanged parts since it produces a compressive stress state that tends to close existing voids whereas the clearance-thickness ratio and the diameter of the initial hole significantly affect the damage state of the flange.

Figure 1.9 shows the triaxiality distribution in two hole flanging conditions: without ironing (upper) and with ironing (lower). Due to the imposed geometry between the punch and the die in the resulting flange for low values of the clearance thickness ratio (R_c), a compressive strain state is induced in the flange, which prevents void growth and coalescence.

1.2.5. Initial pre cut hole

Huang *et al*.,2001 numerically investigated the initial pre cut hole effect on the lip wall thinning of a steel sheet. Changing the initial pre cut hole diameter for the same cylindrical punch and monitoring the lip thinning, the authors realized that the maximum reduction in the wall thickness occurred along the periphery of the expanded hole and the tensile stress in the circumferential direction at this location was responsible for failure by cracking or tearing. Thus, they established a useful tool design for engineers by plotting the relationship between the initial hole diameters and expanded the hole diameters for fractured and non fractured specimens. Figure 1.10 shows this relationship by a straight line.

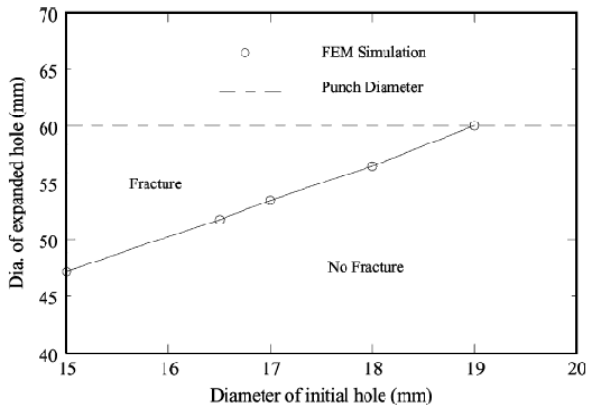

Figure 1.10 Failure map for the conventional hole flanging process at a fixed punch diameter. Huang et al.,2001

The recent work of Soussi *et al.,*2016 analysed the conventional hole flanging process using 1000 series aluminium alloy sheets with a thickness of 0.8 mm while varying the initial hole diameter and clearance-thickness ratio. A failure map that involves these process parameters and the geometrical parameters of the flange, such as the flange height and the edge thickness, was proposed as a tool for product design (see Figure 1.11).

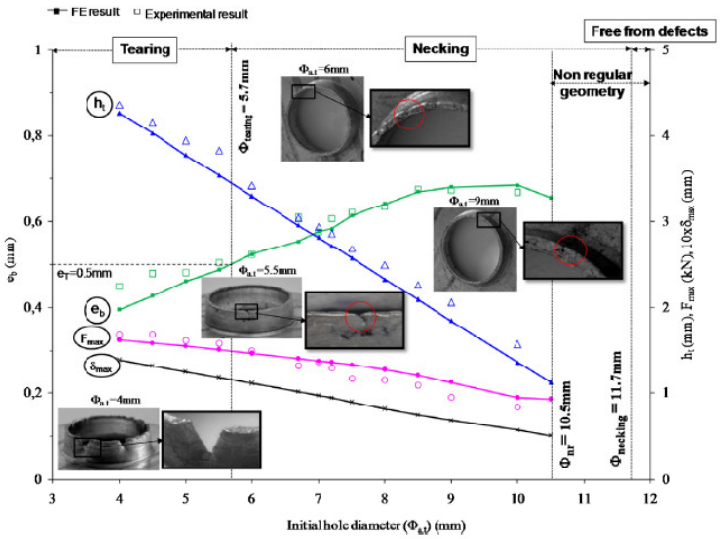

Figure 1.11 Failure map for the conventional hole flanging process based on process and geometrical parameters. Soussi et al.,2016

1.3. Analysis of formability based on LFR

Huang *et al.*2001a, 2001b, 2002 were more concerned with the formability analysis of hole flanging than the previous authors as they use the concept of *LFR*, which is a parameter that quantifies the formability of this particular case of stretch flanging. In practice, the forming severity in conventional circular hole flanging is measured by the hole expansion ratio $HER=d_f/d_o$, and the process formability is quantified by the maximum *HER* attainable by a material without failure:

$$LFR = HER_{\max} = \frac{d_{f,max}}{d_{0,min}} \tag{1-1}$$

where $d_{f,max}$ and $d_{o,min}$ are the maximum inner diameter in the finished part and the minimum pre cut hole of the blank, respectively. For conventional hole flanging, the *LFR* was evaluated assuming $d_{f,\,max}$ to be the punch diameter.

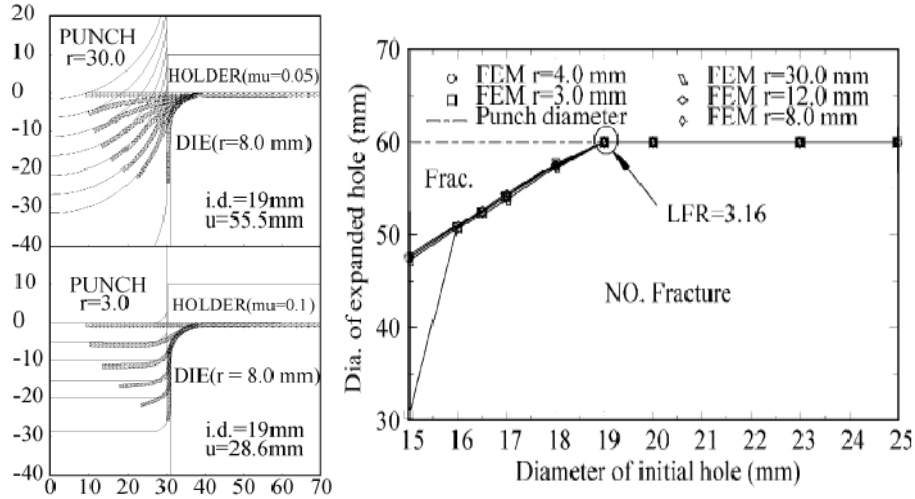

Figure 1.12 Relation between the diameter of the expanded hole and diameter of the initial hole for various punch profile radii. Huang et al.,2001

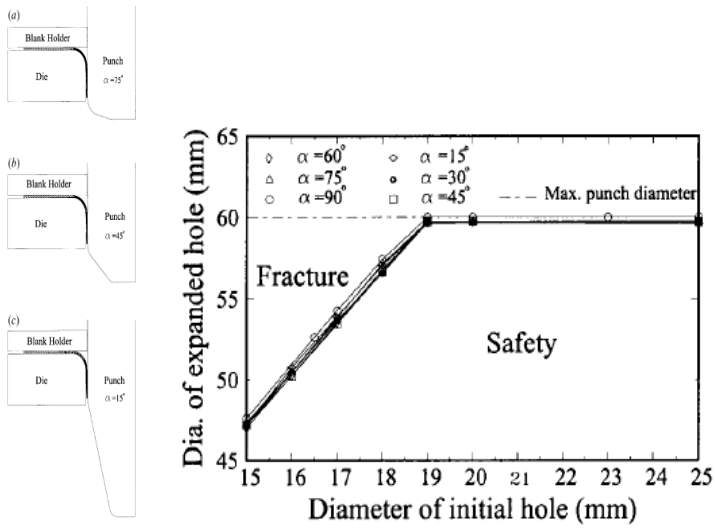

Figure 1.13 Simulated relations between the diameter of the expanded hole and diameter of the initial hole for various truncated conical punches. Huang et al.,2002

Huang *et al.* 2001, 2002 numerically and experimentally investigated the *LFR* of a hole flanging process for low-carbon steel sheets using various cylindrical punch profile radii (see Figure 1.12) and the truncated cone of different angles (see Figure 1.13).

The authors noticed that the *LFR* is independent of the punch radius. However, the punch profile has a significant influence on the final flange shape and maximum punch force of the process. They observed that the maximum reduction in the wall thickness occurs along the periphery of the expanded hole. Therefore, failure at the edge of the flanged hole is controlled by the tensile stress in the circumferential direction.

1.4. Introduction to Incremental Sheet Forming in its variant SPIF

Incremental sheet forming (ISF) is a new process for manufacturing sheet metal parts that fulfils the requirements of flexibility and viability for small- and medium-sized enterprises and is especially indicated for small production batches or prototyping.

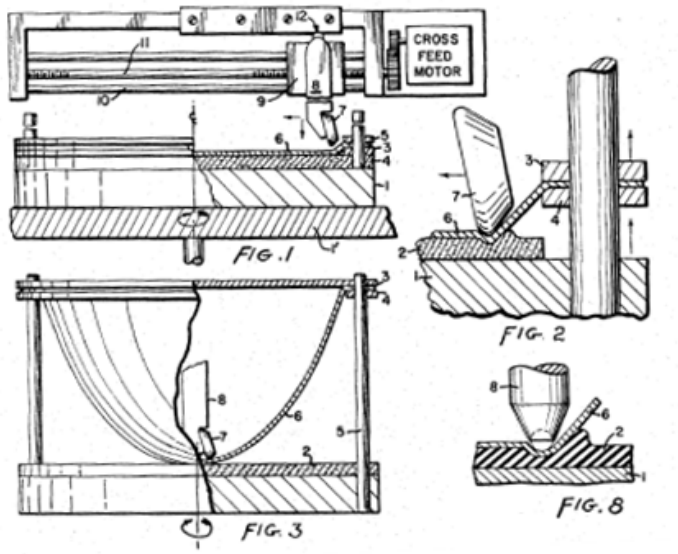

Figure 1.14 Image of apparatus and process for incremental dieless forming. Patent US3342051A

In 2010, Emmens *et al.* published a brief review of the history of ISF. Although two US patents from 1967 exist [US 3342051] and [US 3316745] with the authorship of E. Leszak and Berghahn, respectively, in Emmens´ opinion, the work performed by Mason in 1978 established the foundations of the modern ISF and proposed a process using a spherical roller that can generate any shape surface by controlling its trajectory in three axes.

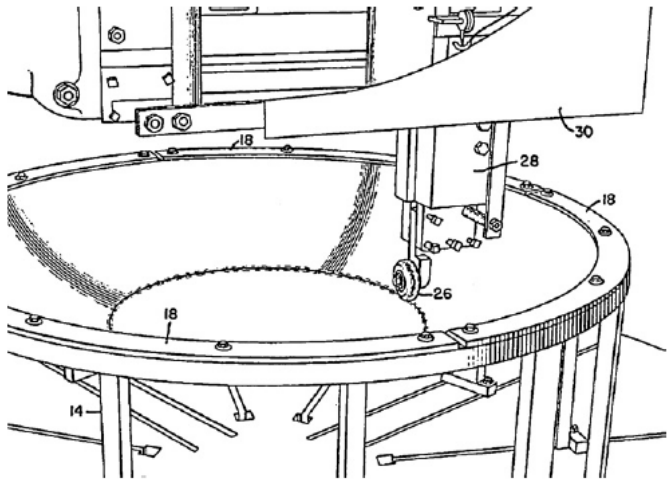

Figure 1.15 Method of dieless forming surfaces of revolution. Patent US 3316745

The patent [US 3342051], "Apparatus and process for incremental dieless forming" (see Figure 1.14), was designed to incrementally conform a blank sheet under the action of a wheel or ball against a flat elastic base. Varying three parameters, the rotation speed of the face plate, the cross-feed rate and the amount of pressure applied to blank, the author was able to produce a considerable amount of shapes. In the second patent [US 3316745] (see Figure 1.15), Berghahn proposes a manufacturing process of disc-like products, where the blanks are clamped and rotate while the forming tool (a roller) moves inward along a radial line.

Although Berghahn´s and Leszak´s patents were presented as spinning variants, in my opinion, Berghahn´s patent could be considered as an early ISF process as it conserves the essence of single point incremental forming and is latterly recognized as an ISF process in studies performed by Mason 1978 and Kitazawa 1993.

The development of the ISF process started in Japan after the interest of a congress in Kyoto (Mason and Applelton 1984); it was the starting line for Iseki and co-workers to work on a manufacturing machine of non symmetrical parts

manually operated on an x-y table that was the object of a paper in 1989 (Iseki *et al.,*1989). At this time, the CNC machine was expensive, weak for supporting forming loads and considered to be unsafe. The research of Iseki *et al.* (Iseki *et al.*,1991, 1992a, 1992b, 1994, 1996) demonstrates that an apparently low stiffness CNC machine can incrementally conform steel, stainless steel and titanium sheet metals with a thickness of 0.7 mm.

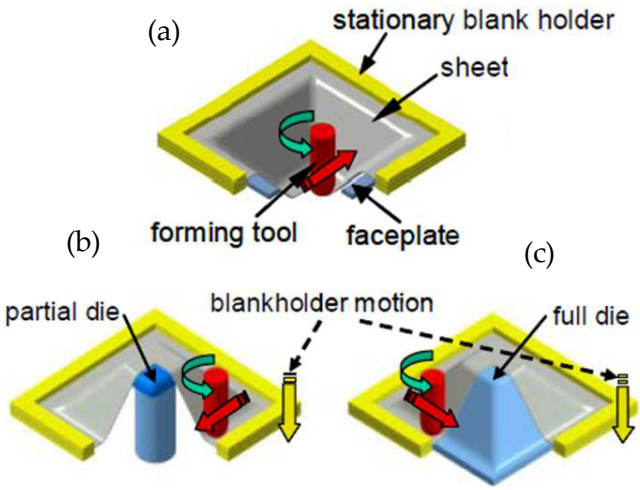

Figure 1.16 Illustration of SPIF a) and TPIF b) and c) with partial and full die. Jeswiet et al.,2005

The use of commercial three-dimensional CNC milling machines has caused the massive development of this technology, especially in Japan, where the concept of single point incremental forming (SPIF) appeared to differentiate it from two-point incremental forming (TPIF), which was introduced by Matsubara in 1994.

As illustrated in Figure 1.16 a), in the SPIF process, the blank is rigidly clamped to the blank holder and deformed under the action of a forming tool that can rotate and move in the three axes. The forming tool, which usually has a hemispherical tool tip, moves according to an established path that was previously calculated in a CAD-CAM software. The material is incrementally formed by pressure due to the action of the tool tip.

In case of TPIF, the forming tool keeps the capacity of rotating and moving in the three axes. However, these movements must be synchronized with the vertical movement of the blank holder. The second difference and the reason for the name of this variant is the way the material is formed, in this case, by the action of the forming tool against a full die underside (Figure 1.16 c) or helped by an underside partial die to create an upward counter force on the sheet (Figure 1.16 b).

In 1993, in the CIRP meeting, several western researchers were impressed by the simplicity of the process, which generated the first publication on this domain in the western world (Luttgeharm 2001, [US 6748780]).

Most of the patents registered from year 2000 are more concerned about the technological development than the process. They are interested in TPIF as a process, probably due to the ease of achieving the required shape compared with SPIF. Some achievements include the patent by Tuominen of Twincam OY, Finland 2002 [EP 1560668], as shown in Figure 1.17, which includes two robots despite the lack of stiffness that is generally attributed to robots, and the concept by Zhang 2007, as shown in Figure 1.18, to accelerate the incremental forming process in TPIF.

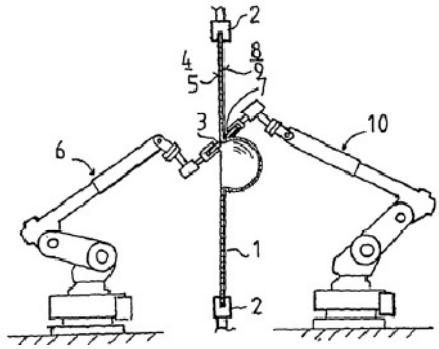

Figure 1.17 Patent by Tuominen of Twincam OY, Finland EP 1560668

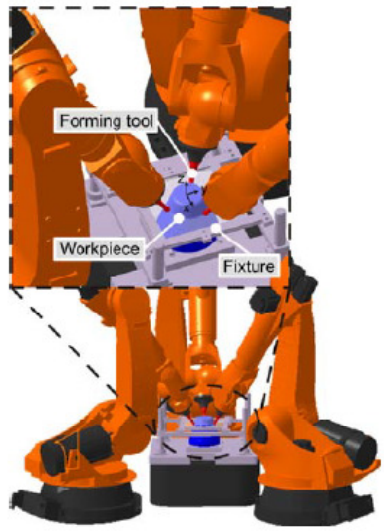

Figure 1.18 Concept of Zhang with three robots. Zhang,2007

SPIF, which is the simplest variant of ISF, has important drawbacks regarding the dimensional accuracy compared with TPIF. Its use is not in the scope of industry; thus, few patents have been registered in recent years about the process to increase the dimensional accuracy and reduce the springback effect of the blanks.

For the patent requested in 2005 by the Univ. of Leuven, Belgium, [EP 1899089], as shown in Figure 1.19, the SPIF device is equipped with a heating device.

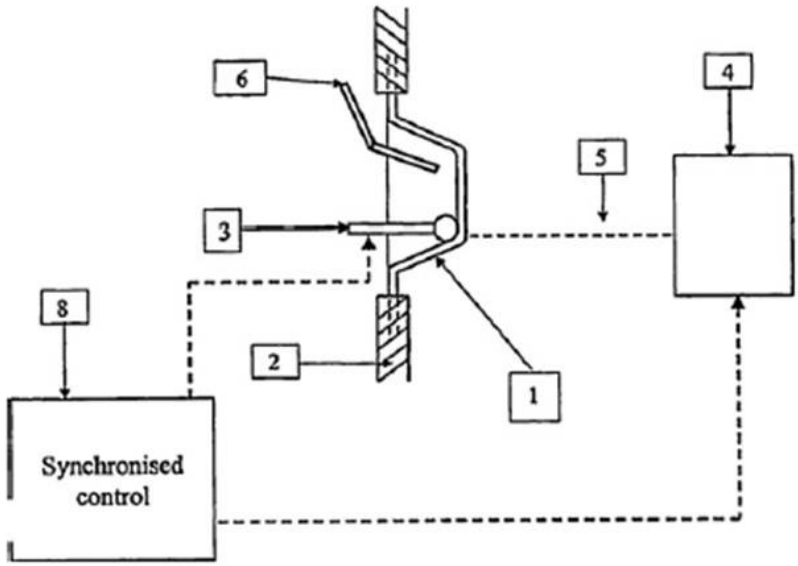

ISF with additional heating as patented by Univ. Leuven [EP 1899089].
1 = sheet, 3 = punch, 4 = heater, 5 = heat flux, and 6 = cooler.

Figure 1.19 Patent number [EP 1899089] from Univ. Leuven 2005

Although car manufacturers initially boosted the study of this process by registering a large amount of patents and manufacturing a variety of pieces (reflective surface of prototype headlights; heat/noise shield, which is used over exhaust manifolds (Figure 1.20, Jeswiet *et al.,*2001)); service panels (Figure 1.21, Amino *et al.,*2002, 2014); hood and fender (Rodriguez *et al.,*2006), which is used by other industries;customized ankle support (Ambrogio *et al.,*2005) or cranial plate (Figure 1.22, Bagudanch *et al.,*2015) in biomedical applications and appliances (solar cooker, Jeswiet *et al.,*2005) and for processing recycling panels, as demonstrated by Jackson *et al.,*2008 and Takano *et al.,*2008.

Figure 1.20 Formed by SPIF headlights and manifolds by Jeswiet et al.,2001

Figure 1.21 Service panels before and after SPIF forming by Amino et al.,2002, 2014

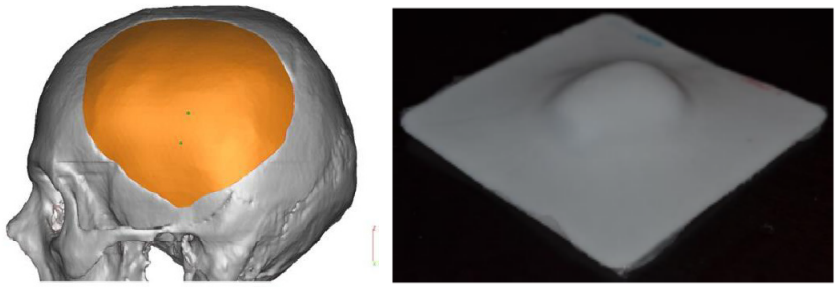

Figure 1.22 Cranial plate capture (left) and SPIF cranial plate (right) by *Bagudanch et al.,2015*

The following advantages make this process variant useful for prototyping in small- and medium-sized production, apart from an increase in formability: lower cost than the conventional sheet metal forming process, can be executed in a conventional CNC machine, flexible design, changes can be easily implemented, production directly from CAD file and small force requirements compared with conventional sheet metal forming process in the case of small thickness metal sheets or soft materials. Although most research groups employ an adapted CNC machine, probably for economic reasons, some research groups have designed new devices that can support 13kN axial force and 6.5 kN lateral force with 6

d.o.f., as shown in Figure 1.23, due to the development of harder materials and the need to test metal sheets with higher thicknesses.

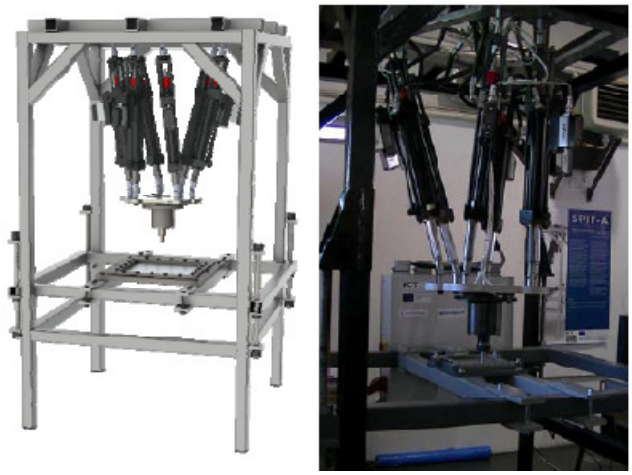

Figure 1.23 CAD model (left) and built machine (right) of SPIF-A. Alves de Sousa et al.,2014

1.5. Formability in SPIF

Formability in sheet metal forming is usually evaluated using a Forming Limit Diagram (FLD). A FLD represents the in-plane major vs. minor strain of a sheet and can include different curves to divide the strain space, such as the Forming Limit Curve (FLC) for the onset of necking and the Fracture Forming Limit (FFL) for fracture. The FFL shape is a straight line that corresponds to a fracture failure mode by tension (Mode I), which is typical of metal sheets. Recently, Isik *et al.,*2014 experimentally determined by SPIF, torsion and in-plane shear tests of AA1050-H111 sheets a third failure curve for fracture by in-plane shear (Mode II). This curve is known as the Shear-FFL (SFFL). Figure 1.24 shows a schema of experiments and experimental results in the FLD including FFL and SFFL.

Using a conical or pyramidal geometry, the authors showed the enhanced formability limit of SPIF processes above the FLC. Many factors involved in the forming process can interfere in the enhancement of the formability of this process.

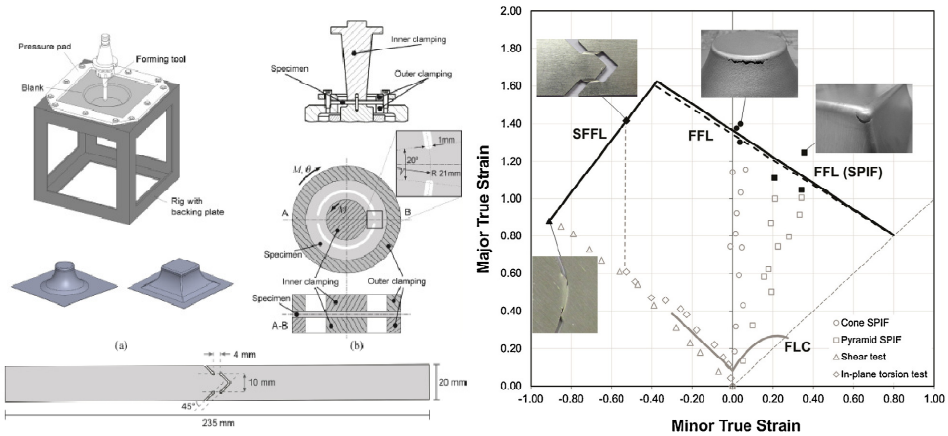

Figure 1.24 Geometries (left) of tests used to calculate (right) SFFL and FFL in AA1051-H111, isik et al.,2014

1.5.1. Suppression of necking

To explain this enhanced formability, numerous papers discuss different mechanisms that affect, e.g., localized bending, via thickness shear and triaxiality, such as Martins *et al*.,2008, Emmens *et al.,*2009a, 2009b and Malhotra *et al.,*2012. Many authors have investigated the factors that produce these beneficial effects.

Silva *et al.,*2011 based their research on the tool radius effects and the stabilizing effect of dynamic bending under tension on AA1050-H111. With a large tool radius, this process seems to be capable of increasing the forming limit curve above that commonly found in stamping to ensure localization by necking. In the case of a small tool radius, the stabilizing effect is not sufficient for ensuring localization and a failure mechanism change to fracture without necking.

In their research on AISI304, Centeno *et al.,*2013 highlighted that the postponed or suppressed necking in ductile metal sheets deformed by SPIF, which enable failure directly by ductile fracture, is caused by not only the tool radius bending effect but also an extensive range of process parameters (tool diameters, step downs, and friction conditions).

Fang *et al.,*2014 proposed an analytical model of the deformation and fracture of the sheet in AA1100that considers the bending and strain hardening effect.

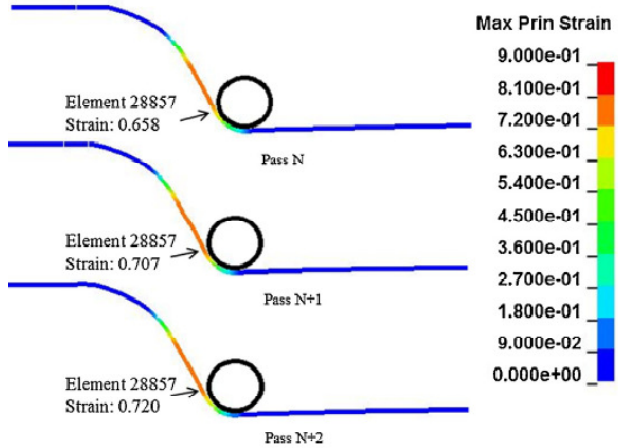

Figure 1.25 Fracture localization due to the bending effect in AA1100. Fang et al.,2014

Fang theoretically proves that fracture occurs first on the outer side of the wall at the transition area between the contact and the non-contact zone due to the bending effect (See Figure 1.25). The strain hardening has a positive or negative effect depending on the thickness ratio.

Li *et al.,*2015 numerically analysed the deformation mechanics and the forming force in SPIF of AA7075-O sheets and concludes that the SPIF deformation process is a combination of stretching, bending and shearing. This combination oscillates depending on the process variables, such as wall angle, friction conditions, and tool diameter.

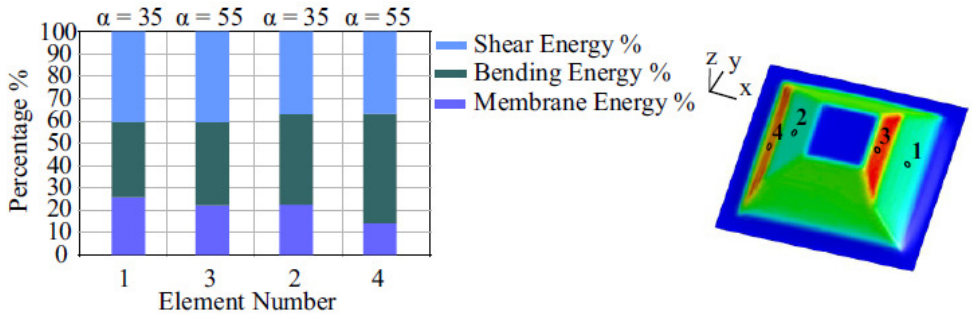

Figure 1.26 Percentage contribution of each deformation mode for four elements under varying wall angles. Maqbool et al.,2017

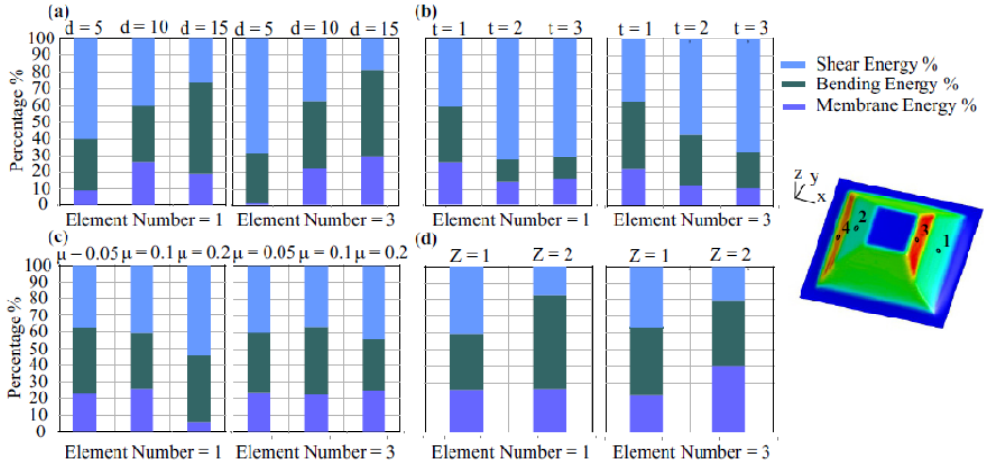

Figure 1.27 Percentage contribution of each deformation mode for two elements under the influence of the a) tool diameter, b) thickness, c) friction and d) step down. Maqbool et al.,2017

As indicated by Maqbool *et al.,*2017 in their study about plastic energy dissipation using an analytical approach, the dominant deformation mode depends on the process variables. According to the desired target, they can be employed in the design forming strategy. Figure 1.27 and Figure 1.26 show the percentage contribution of each deformation mode (shear, bending or membrane) to different process variables, such as tool diameter, thickness, friction, step down and wall angle.

Some mechanisms depend on factors, such as mechanical properties or thickness, whereas other mechanisms are related to factors that are based on the interaction of the tool with the blank, such as tool shape, spindle speed or lubrication conditions. Other mechanisms depend on the tool trajectories: step down, feed rate or tool strategies. These factors are extensively analysed in the next three sectionsInfluence of material properties

1.5.2. Influence of material properties

- **Material properties.**

A relationship between material properties and formability is observed in conventional press working. Fratini *et al.,*2004 investigated the influence of six mechanical parameters on the enhanced formability of the SPIF process for six materials: *K*, strength coefficient; *n,* strain hardening coefficient; *Rn*, normal

anisotropy index; *UTS*, ultimate tensile strength and *A*%, percentage elongation. Table 1-2 (left) shows the list of evaluated materials and properties.

To study the enhanced formability, Fratini needed a reference value of formability to compare the FLD_0 calculated according to Geiger *et al.,*2003 (FLC under plane strain conditions) with the FLD_{0incre} (FFL under plane strain conditions) obtained from tests of truncated cone or pyramids, as these SPIF strain paths are typically very close to the major strain axis in a forming limit diagram.

Table 1-2 Properties of materials investigated (left) and influence of the inputs variables and interactions on FLD_0 and FLD_{0incre} (right). Fratini et al.,2004

Material	K [Mpa]	n	R_n	UTS [MPa]	A%
Copper	390	0.16	0.85	300	26
Brass	1437	0.34	0.88	510	8
DDQ	545	0.27	2.01	290	50
HSS	628	0.25	2.01	350	40
AA1050-O	255	0.18	0.6	76	39
AA6114 T4	540	0.22	0.69	310	24

Predictor	Influence on FLD_0	Influence on FLD_{0incre}
K	High	Medium
n	No	High
R_n	High	Low
UTS	No	No
A%	No	Medium
K·n	High	High
K·R_n	No	No
K·UTS	Medium	No
K·A%	Medium	No
n·R_n	No	No
n·UTS	High	No
n·A%	No	Medium
R_n·UTS	No	No
R_n·A%	Low	No
UTS·A%	No	No

According to the results of their investigation, as presented in Table 1-2 (right), Fratini´s model confirmed that the most important material parameters that influence conventional press working or FLD_0 were the hardening coefficient and normal anisotropy, whereas the highest influence on material formability for incremental forming processes is derived from the hardening coefficient. Also the strength coefficient and percentage elongation have a relevant influence.

Since process mechanics in incremental forming is characterized by stretching and local thinning, the higher is the strain hardening coefficient, the larger is the material formability, which is consistent with the fact that the strain hardening coefficient indicates an indirect measurement of material capability to undergo thinning without plastic collapse.

- **Material thickness**

Hussain et al.,2007 proposed a method that was ratified one year later by Silva *et al.,*2008, to test the thinning limits of sheet metals by performing a series of tests under Negative Incremental Forming conditions (also referred to as Dieless Forming) and comparing these values with values predicted with the Law of Cosines, as presented in Figure 1.28. Truncated cone or pyramids of fixed or variable wall angles are typical selected geometries.

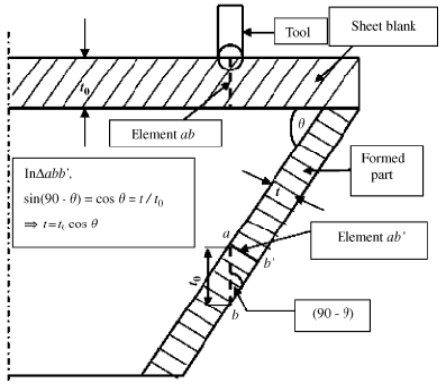

Figure 1.28 Schematic of the Law of Cosines. Hussain et al.,2007

Material thickness is present in the Law of Cosines ($t = t_o \cos\theta$) and was considered in the experimental investigation performed in 2013 by Liu *et al.* for three thicknesses of AA7075-O aluminium sheets: 1.02 mm, 1.6 mm and 2.54 mm. They compared these three thicknesses from several points of view to investigate the influence of mechanical properties, formability and forces. They concluded that the material thickness clearly influences the formability of the SPIF process if the phenomenon of anisotropy increases with the material thickness.
In recent investigations, Hussain *et al.,*2013 tested variable wall angle truncated cones in anextensive range of AA2024-O thicknesses, which enhances the importance of choosing an accurate tool size for the proper thickness; thus, the tool size plays a role.

1.5.3. Influence of the forming tool

SPIF processes are characterized by their low production rates as a result of the local incremental nature. As a consequence of this local forming process, the

surface finish is penalized and the formability is highly dependent of the friction conditions. Thus, the tool shape and size, spindle speed, and lubrication conditions are strongly related.

- **Tool shape**

The simplest tool shape in SPIF is the hemispherical end tool. In 2013, Cawley *et al*. compared angle and parabolic end tools with flat and hemispherical end tools geometries (see Figure 1.29) with the objective of improving the forming limits and expanding the range of potential applications. The test was performed on a variable wall angle conical specimen with a 1.59 mm thick Al-3003-O.

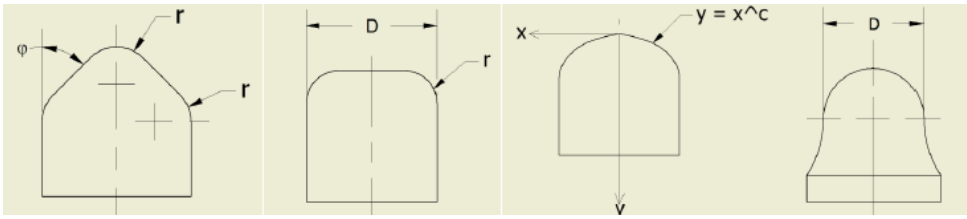

Figure 1.29 Angle, flat, parabolic and hemispherical tool shapes tested by Cawley et al.,2013

In their research, they reaffirmed that a reduced radius contact surface increased the forming limit and worsened the surface quality. They concluded that the use of an end tool or a combination of end tools is the desired option.

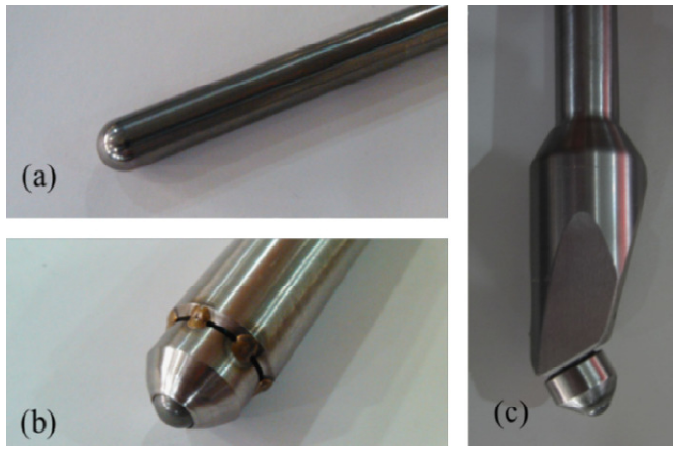

Figure 1.30 a) Rigid hemispherical tool, b) vertical roller ball and c) oblique roller ball. Lu et al.,2014

To study the influence of friction on the surface finish, Lu *et al.*,2014 experimentally and theoretically investigated the differences in surface finish between two types of spherical forming tool: a rigid hemispherical tool and a roller ball in two geometries (vertical and oblique), as shown in Figure 1.30.

Although Lu *et al.*,2014 investigated four grades of aluminium sheet materials, including AA2024, AA5052 and AA6111, AA1100 was employed to perform a series of tests to evaluate the surface roughness *Rz* and *Ra* in truncate cone geometries, as shown in Figure 1.31.

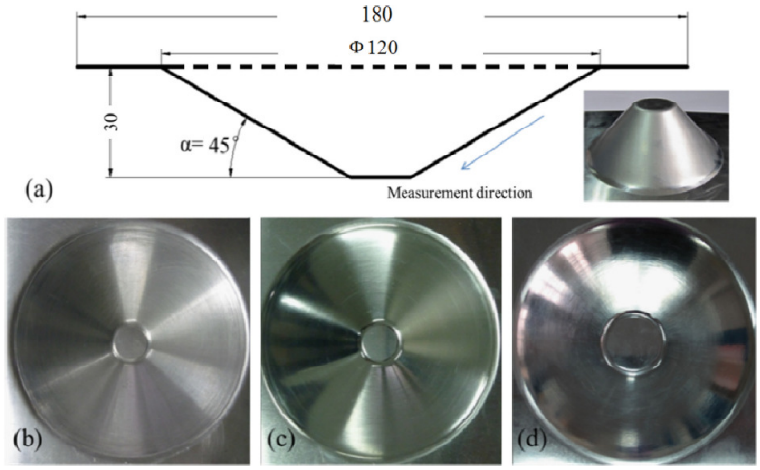

Figure 1.31 a) Truncate cone geometry of surface roughness tests, b) part processed with a rigid tool, c) part processed with VRB and d) with ORB. Lu et al.,2014

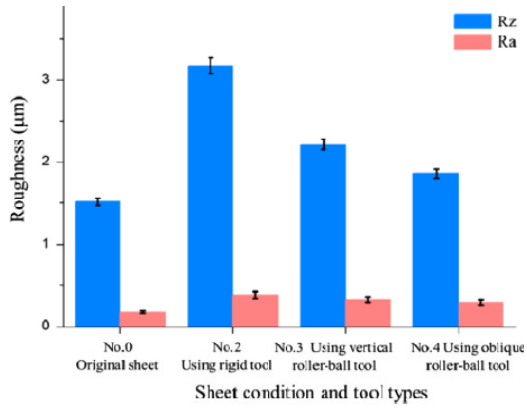

Figure 1.32 Result of surface roughness tests in terms of Rz and Ra. Lu et al.,2014

Figure 1.32 shows the results of the roughness surface tests that were performed on truncated cones in AA1100, which corresponds to Figure 1.31. The investigation shows that the use of any forming tool increases the original roughness of the blank, especially when using rigid tools.

Lu *et al.*2014 also investigated the friction effect on the formability using a series of parabolic truncated cone tests by measuring the achieved maximum for the four selected materials. In all tests that were performed using orbital roller ball tools, the heights of the tested specimens were higher than the heights of the specimens in the tools performed with rigid tools. The authors advised that the throught thickness shear induced in the material was attributed to the friction conditions.

- **Tool size**

Tool size is an important paramenter on formability in materials under SPIF conditions and the effects of this one can not easily appreciated regarding the number of papers in literature, as there are many examples of contradictory effects of the tool size, such as Durante *et al.,*2011-Li *et al.,*2014 with Aluminum AA7075-O and Centeno *et al.,*2014-Golabi *et al.,*2014 with AISI304. According to Hussain et al.,2013, the selection of tool size combined with the metal thickness (t_o/R bending ratio) must be carefully chosen to achieve the maximum formability. A small-sized tool can increase the formability due to the increased bending effect; however, combined with a large thickness, this aspect can cause premature failure due to the indentation of the tool in the sheet

- **Tool rotation**

Research groups have used a ball end tool as the simplest forming tool to start an investigation probably due to the experience with the use of milling machines; the use of spindle speed is always considered.

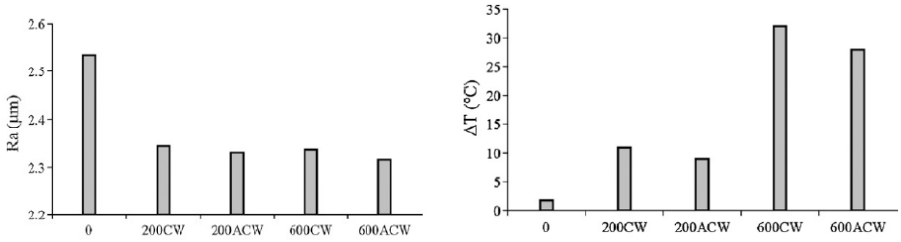

Figure 1.33 Roughness (left) and temperature increment (right) for different levels of tool rotation (rpm). Durante et al.,2009

Durante *et al.,*2009 investigated the influence of tool rotation on the incremental sheet forming process by forming a pyramid frustum in AA7075-T0 with different speeds and both rotation directions. Figure 1.33 shows the results of their research in terms of roughness and temperature increment depending on the rotation speed and directions (ACW, anti-clockwise or CW, clockwise). They also concluded that the use of spindle speed reduces the forming forces, surface roughness and increases the surface temperature of a specimen.

The increase in temperature prompted the investigation by Xu *et al.,* 2013 in which a laser texturized surface tool head was employed to compare it with heat-assisted SPIF methods without sacrificing process flexibility or adding process complexity; see Figure 1.34.

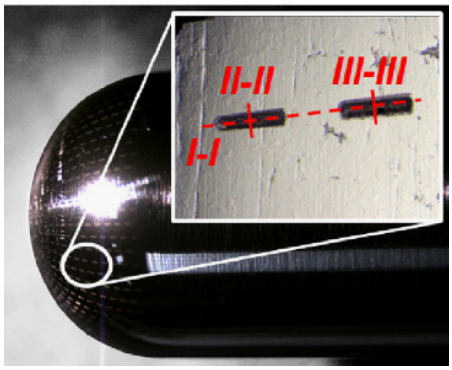

Figure 1.34 Laser texturized surface tool head. Xu et al.,2013

Xu and co-workers investigated the effect of spindle speed in AA5052-H32 in the range of 0 rpm to 7000 rpm using a textured surface tool to compare it with a non texturized surface tool. The results indicated that the formability increases with the spindle speed. At low values of spindle speed, the formability increases with a reduction in the friction coefficient due to the micro channels that act as lubricant reservoirs. At high spindle speed, the friction reduction, compared with standard tools, inhibits the thermal effects that activate dynamic recrystallisation, as recently highlighted by Gupta *et al.,*2018. They investigated the effect of spindle speed on flat-ended tools used to form AA5754-H32 sheets and concluded that increasing the relative velocity between a tool and a blank increases the temperature and introduces dynamic recrystallisation that can alter the properties of the blank, which may not be desirable.

Prior to Xu *et al*, Duflou *et al.,* 2008, proposed a laser-assisted incremental forming that increases the forming limits by local dynamic heating and increases the geometrical accuracy by reducing the residual stresses; see Figure 1.35. Ji *et*

*al.,*2008 proposed the use of a hot air blower, Fan *et al.,*2008 proposed the use of an electric heating device (Figure 1.36).

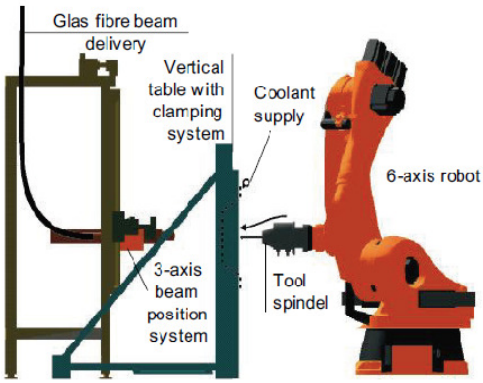

Non-heated		Heated			
wall angle [°]	obtained result	wall angle [°]	spot size [mm]	energy input [J/mm²]	obtained result
30	OK	45	12.0	0.875	OK
35	failed	50	12.0	0.875	OK
32	OK	55	12.0	0.875	failed
34	failed	53	12.0	0.740	OK
33	failed	55	12.0	0.740	OK
		57	12.0	0.740	failed
		56	12.0	0.740	failed
		56	14.0	0.740	OK
		57	15.0	0.740	failed

Table 1: Formability test results for 0.6mm TiAl6V4.

Figure 1.35 SPIF machine with dynamic laser supported heating and formability tests produces 0.6 mm TiAl6V4 sheet with and without heating. Duflou et al.,2008

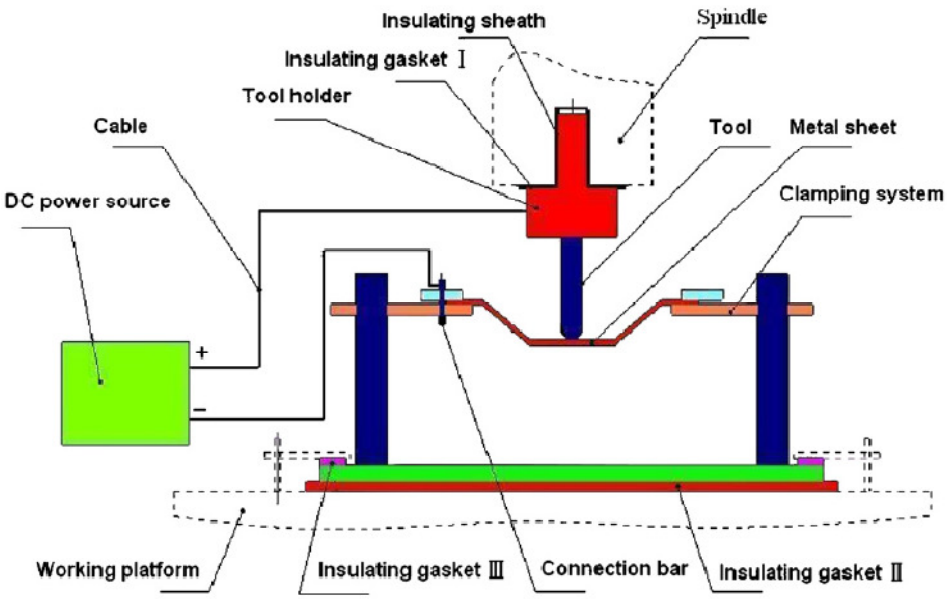

Figure 1.36 Electric heating system proposed by Fan et al.,2008

- **Lubrication**

Researchers usually use a motor, gearbox, special forming oils or grease to reduce friction at low spindle speeds and increase the surface quality produced by machining and step-down traces of the forming surfaces of fabricated specimens, among then Azevedo et al.,2015. To reduce the surface treatment cost compared with pulsed anodic oxidation, micro-arc oxidation (Hussain *et al.,*2008), or electrocodeposition, some researchers, such as Li *et al.,*2018, developed a low-cost lubrication method that is based on the application of a combination of graphite-based grease and oil to increase the surface quality and reduce the forming forces at room or elevated temperatures compared with traditional lubrication methods.

1.5.4. Influence of the CNC program

The Feed rate and step down and tool path strategies are the basic parameters implemented in the SPIF process inherited from CNC machines.

- **Feed rate**

The feed rate does not seem to be an important parameter based on the number of publications that discuss feed rate. Bastos *et al,.*2016 recently published a paper that detailed how they performed a series of conical frustums with feed rates from 1500 mm/min to 12000 mm/min. They tested four different materials and discovered an apparent insensibility to feed rate in terms of formability (see Figure 1.37); in terms of surface quality, however, the feed rate and *Ra* increased (see Figure 1.38).

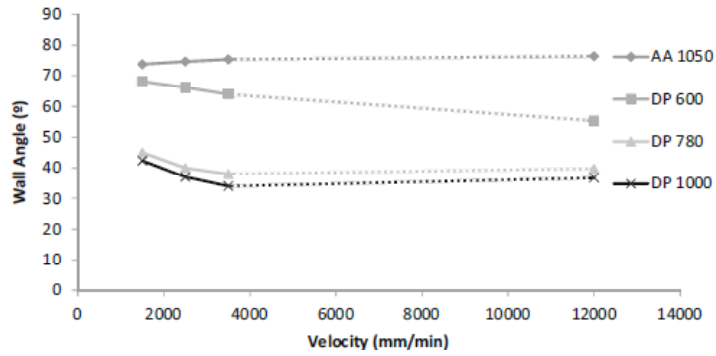

Figure 1.37 Max wall angle for different feed rates and materials. Bastos et al.,2016

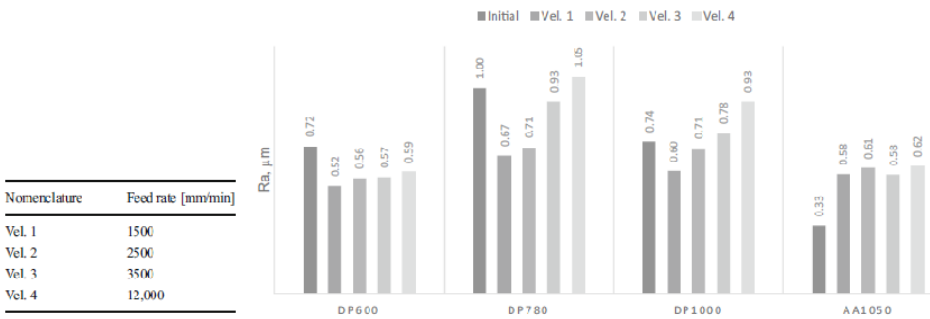

Nomenclature	Feed rate [mm/min]
Vel. 1	1500
Vel. 2	2500
Vel. 3	3500
Vel. 4	12,000

Figure 1.38 Values of Ra for four materials and feed rates. Bastos et al.,2016

The research in this field can only be performed in a specially designed machine similar to the machine employed in Bastos *et al,.*2016, as shown in Figure 1.23, or lathe machines, which constrain the geometry of specimens to axi-symmetrical. The use of high feed rates causes an increase in friction and a redesign of lubrication conditions and tool support conditions to mitigate this force increase. These issue may explain the lack of papers in this domain

- **Step down**

The step down parameter (Δz in Figure 1.39) does not exhibit a distinct influence regarding the number of papers published in literature, in which authors demonstrate contrary sensibility to formability. Durante *et al.,*2011 demonstrated the formability decreases with the step down parameter, whereas other researchers assured an increase in the formability when the step down parameter was decreased (Liu et al.,2013) for the same AA7075-O. In all cases, vertical forming of forces increases with the step down parameter and is limited by the maximum vertical load admissible in a CNC machine.

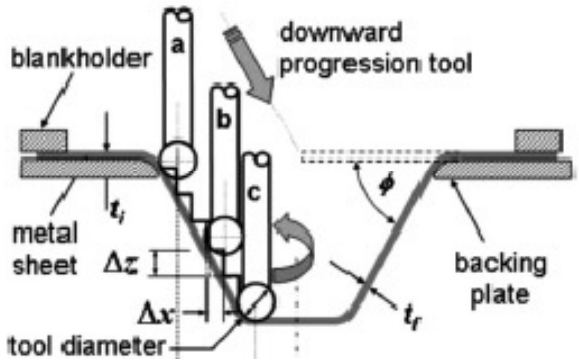

Figure 1.39 Schema of dieless incremental forming. Jeswiet et al.,2005

- **Tool path strategy**

The basic tool path strategy in three-axis CNC machines when performing a formability test on a conical or pyramidal frustum with or without a variable wall angle is the z-level strategy shown in Figure 1.40 (left). Z-level strategies produce a final part with a line or curve, where the tool has stepped down, which can cause premature failure and an undesirable visual impact on a specimen. The occurrence of this line and the peak force produced at every step down in the machine produced a helical path, as shown in Figure 1.40 (right).

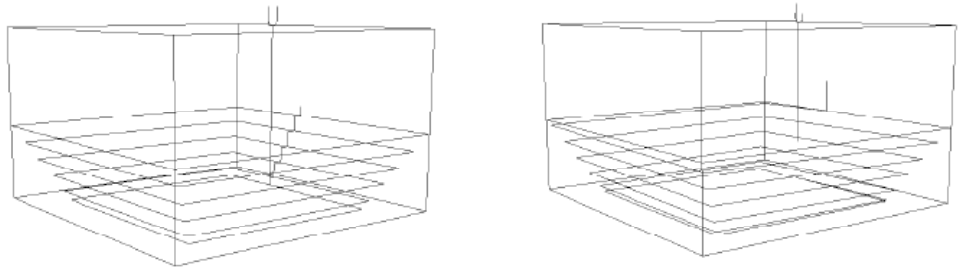

Figure 1.40 Basic tool path strategies: left) z-level and right) helical path for pyramid. Skjoedt et al.,2007

However, the introduction of the helical path does not solve the three main issues of the SPIF process: i) process limits, ii) accuracy and iii) thickness variations.

Different solutions have been published to address these issues in recent years: against excessive thickness variations, Young *et al.,*2005 proposed a double-pass technique to avoid the characteristic thinning band that is present in single pass forming. Ambrogio *et al.,*2005 proposed a sliding blank holder that allowed radial flow of the material towards the forming area, which decreases the thinning and increases the formability.

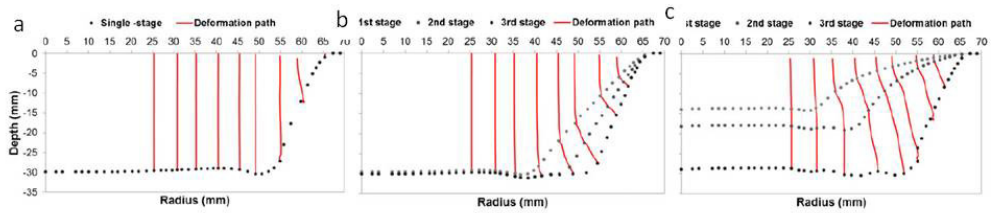

Figure 1.41 70º truncated cone in AA1050 for single-stage strategy, a) conventional three-stage strategy b) and improved three-stage strategy by sequential limit analysis c). Mirnia et al., 2014

As shown in Figure 1.41, Mirnia *et al.,*2014 obtained an improved thickness distribution of a 70^{o} truncated cone in AA1050 by sequential limit analysis compared with single-stage or conventional multi-stage SPIF, which decreases the forming time.

Shamsari *et al.,* 2018 proposed a less sophisticated two-stage hybrid deformation strategy. Compared with SPIF in a single stage, they demonstrated an increase in depth and a decrease in thinning in a truncated cone by the SPIF process, which induces an equibiaxial strain state by hydraulic bulging.

In recent years, due to numerical simulations and the use of five-axis CNC machines, a large number of authors investigated tool path strategies to increase the dimensional accuracy, such as Giraud-Moreau *et al.,*2018 and Fiorentino *et al.,*2018, and optimize the dimensional accuracy by an iterative correction of the tool path. The thickness distribution and process limits have also been investigated with these new machines and methodologies.

1.6. Hole-flanging by SPIF in a single stage

Although the majority of research has been based on a truncated cone, pyramid or variable wall angle conical frustum, current studies show the capability of SPIF to successfully perform circular hole flanging, where a sheet with a pre cut hole is deformed by a forming tool that progressively produces a smooth round flange following a pre-established trajectory,.

The pioneering research on hole flanging by SPIF is relatively recent, as presented by Cui and Gao in 2010. In their research, they perform successful hole flangings using different multi-stage strategies compared with the thickness distribution obtained in each case, as shown in Figure 1.42.

Cui and Gao analysed the formability of the process in terms of the *LFR*, which demonstrates that the use of strategy “a” is more versatile than the other two strategies and achieves a larger *LFR* and more uniform thickness distribution.

Two years after Cui’s study, Centeno *et al.,*2012 attempted to answer some questions regarding the formability aspects that Cui and Gao did not examine, in particular, the influence of a pre cut hole in the formability of SPIF. They concluded that small pre cut holes did not have any influence on the formability of the process if the plastic deformation does not reach the vicinity of the hole edge. However, a new mode of failure is triggered in the contrary case, which entails a

combination of in-plane stretching in plane strain conditions with bending around the perimeter of the flange, which causes a suppression of necking prior to failure (see Figure 1.43 a).

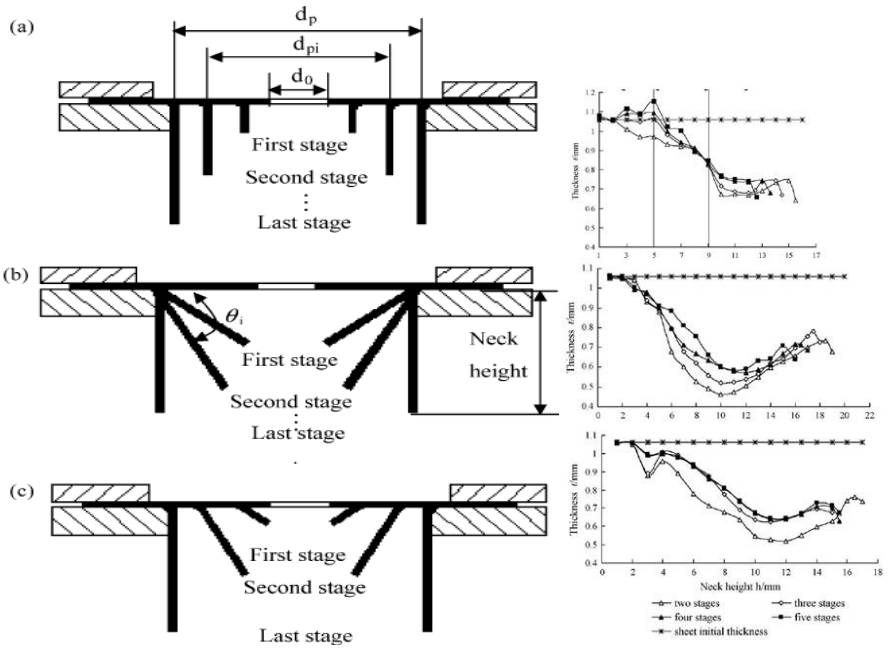

Figure 1.42 Tool path strategies and corresponding thickness distributions for an initial pre cut hole with d_o=35.5 mm and final hole diameter of d_f=65 mm in AA1060. Cui et al.,2010

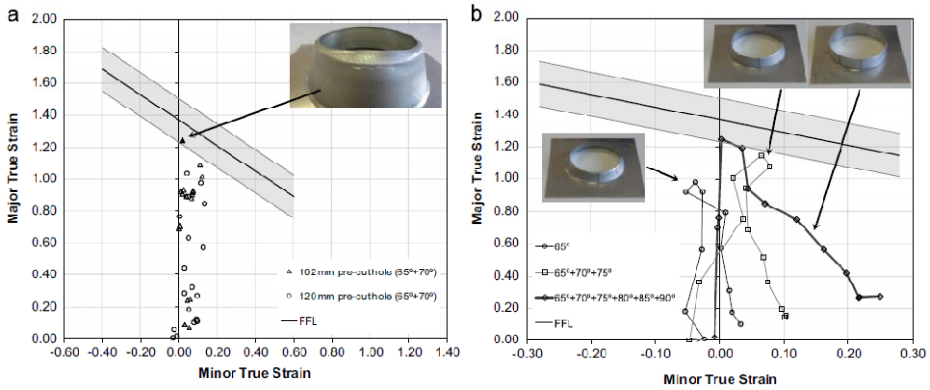

Figure 1.43 a)Experimental strains in conical hole flanging with multi-stage strategies in AA1050 b) and selected steps in the successful production of cylindrical hole flanging. Centeno et al., 2012

Figure 1.43 b) also depicted the strain distribution of outer surface points along a meridional cut in the FLD. The meridional strain distribution follows the plane strain behaviour at the bottom of the specimen due to the equibiaxial strain state near the hole edge.

Due to the particular geometry of the holes, most studies on hole flanging have been devoted to analysing the sheet formability via the *LFR*, and few studies have applied the Forming Limit Curve (FLC) as an analysis tool, such as studies by Martins and co-workers (Silva *et al.,*2013*,* Montanari *et al.,*2013 and Cristino *et al.,*2015). Although the FLC is currently the most useful tool for evaluating the formability of metal sheets during the design process of press working operations, these studies have not provided a detailed description of the flange deformation process or a comprehensive study of the influence of the punch profile. Figure 1.44 depicts some results of the strain analysis in hole flanging by SPIF and conventional FLD.

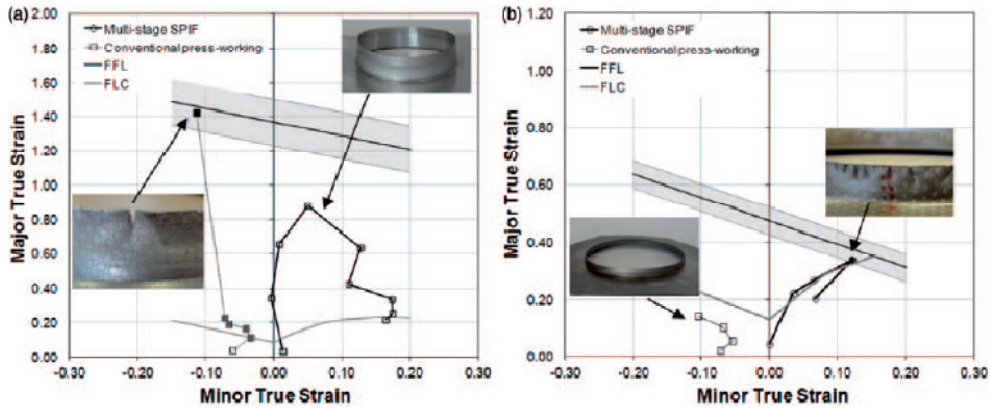

Figure 1.44 Strain distributions along meridional directions of hole-flanged parts in a) AA1050-H111 and b)titanium (grade 2) under press working conditions and multi-stage SPIF. Silva et al.,2013

Despite their inherent advantages in terms of simplicity, flexibility and sustainability, multi-stage hole flanging processes by SPIF have a large deficit in terms of time consumption. In this regard, some attempts have been taken reduce production times by performing hole flanging processes by high-speed SPIF. For instance, in a study by Bambach *et al., 2*014*,* the process was accelerated using a rotating tool set, on which the forming tool was radially and axially displaced, as shown in Figure 1.45.

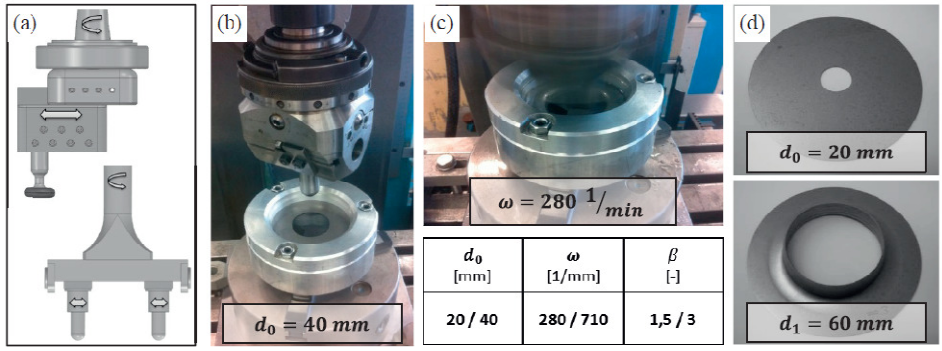

Figure 1.45 High-speed incremental hole flanging: tool designs a), setup b), parameters c) and specimens before and after performing. Bambach et al.2014

Others authors have decided to create new featured tool and tool path strategies to accelerate the process. In Figure 1.46, a basic tool trajectory is compared with the new one tool trajectory and the forming forces and timing.

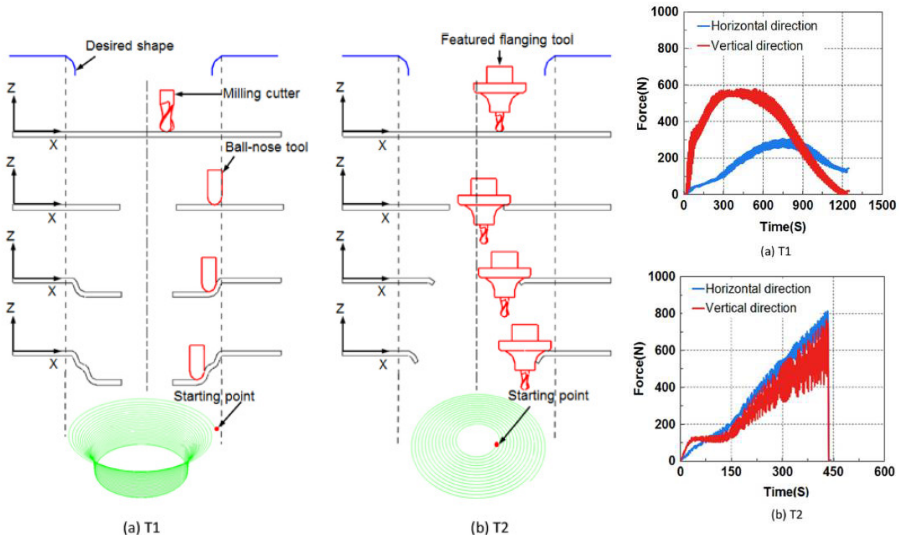

Figure 1.46 Different tool path strategies, forming forces and timing for both tools. Cao et al., 2016

Apart from the studies by Borrego *et al.,*2015, 2016, a systematic study about the capability of performing hole flanging by SPIF in a single stage and an analysis of the mechanics of the process in terms of deformations induced in the part or about the failure modes that define its formability are lacking.

2. MATERIAL CHARACTERIZATION

The aluminium alloy sheet AA7075-O with a thickness of 1.6 mm, which is typically employed in aeronautical applications, is the material selected for this study. The material characterization includes mechanical parameters, such as the flow curve, Young's modulus, ultimate tensile strength, Lankford coefficients and Forming Limit Curve, which is an extensively applied tool in mechanical forming for evaluating formability.

2.1. Mechanical parameters

Generally, the first step after receiving a batch of new material is to perform a tensile test to determine the mechanical properties and compare them with the properties of other batches. A data sheet provides information about the chemical composition and basic mechanical properties but does not provide the flow curve of the desired strain levels.

2.1.1. Tensile test

A tensile test is the most common test for evaluating the elastic-plastic behaviour of a material and is usually performed to calculate Young´s modulus, yield stress, ultimate tensile stress and Lankford coefficients for three different directions (0º rolling, 90º transverse and 45º diagonal direction).

A series of tensile tests was carried out in a universal testing machine at room temperature. The gauge length and width of the tensile specimens were 60 and 12.5 mm respectively according to the standards ASTM E8M-08 (see specimen dimension in Figure *2.1*). The mechanical properties at 0º, 45º and 90º with respect to the rolling direction were also obtained. An extensometer of 25 mm longitudinal reference length and +/-5 mm range was used. Three tests for each direction were performed.

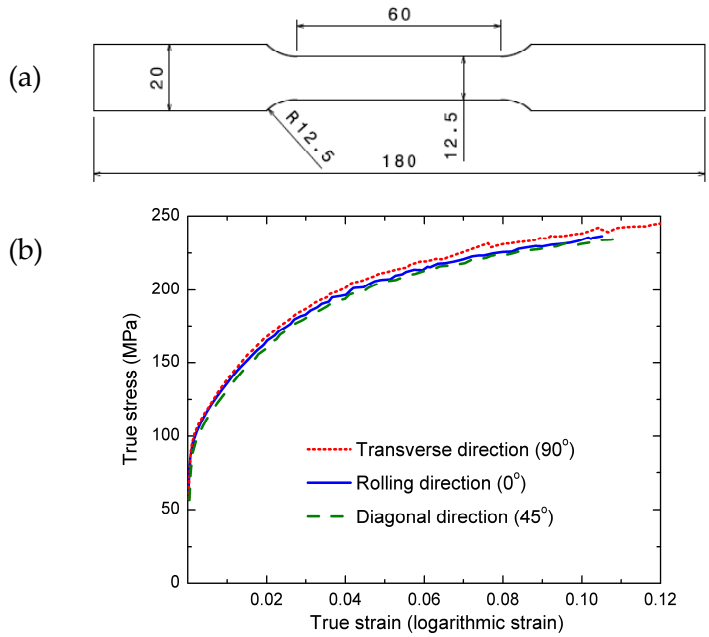

Figure 2.1 a) Geometry of the tensile test specimen and b) strain-stress curves in three different directions

Figure 2.1depicts the true stress-strain curves at 0º, 45º and 90º. The mean values obtained for the yield stress (*Y*), ultimate tensile strength (*UTS*), and Young's modulus (*E*) are displayed in Table 2-1. An average value in the sheet plane is also presented as a reference.

Table 2-1 Material properties of the AA7075-O

Sheet direction	*Y* (MPa)	*UTS* (MPa)	*E* (GPa)
Rolling (0º)	110	214	63.7
Diagonal.,45º)	108	212	61.6
Transverse (90º)	112	218	64
Average: $\frac{x_0+2x_{45}+x_{90}}{4}$	109.5	214	62.5

According to Gilmour et al., 2004, the most accurate correlations between the numerical predictions and the experimental tests for the forming processes that involve high strain levels are achieved by evaluating the Lankford coefficients using plastic strains at levels near the end of uniform strain behaviour. The Lankford coefficients were obtained according to the ASTM 517-00 standard at an engineering strain level of 0.11, following equation (2-1). Once applied, the volume constancy assumes the following form:

$$r = \frac{\varepsilon_2^P}{\varepsilon_3^P} \cong \frac{-\varepsilon_2^P}{\varepsilon_1^P + \varepsilon_2^P} \tag{2-1}$$

where ε_1^p and ε_2^p are the longitudinal principal plastic strain and transverse principal plastic strain, respectively, in the tensile specimen, and ε_3^p is the normalor thickness) strain plastic evaluated by volume constancy from the in plane strains;ε_3^p = - *(*ε_1^p +ε_2^p *).*

Table 2-2 lists the mean values from three tests of the Lankford coefficients at 0º, 45º and 90º and the conventional normal anisotropy coefficient. These values are consistent with the experimental findings of Liu *et al., 2*013 and Durante *et al., 2*009 for the same type of aluminium alloy.

Table 2-2 Lankford coefficients for 0°, 45° and 90°

$r_{0°}$	$r_{45°}$	$r_{90°}$	$\frac{r_{0°} + 2r_{45°} + r_{90°}}{4}$
0.65	0.95	0.81	0.85

2.1.2. Bulge test

According to the tensile test results, only strain levels of approximately 0.12 were achieved. A series of bulge test was performed to extrapolate the flow curve from 0.12 to higher strain levels.

A bulge test consists of an induced equal biaxial strain state by inflating a sheet plate under hydraulic pressure through a circular die (see Figure 2.2). A complete setup that comprises an aluminium sheet plate to be tested between a backing plate and an annular blank holder or die was developed. The backing plate was provided for a container of hydraulic fluid. A blank holder is screwed to the backing plate,

and a draw bed is machined between both the blank holder and the draw bed to provide sufficient clamping force.

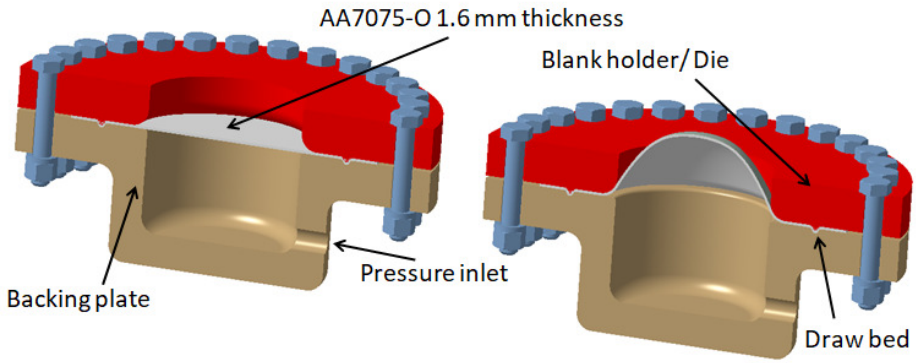

Figure 2.2 Section of the bulge test setup (recreation)

The standard ISO 16808:2014 describes the methodology for calculating the strains and curvature radius at the top of the dome when using video correlations systems (recreation shown in Figure 2.3). Once the test is computed and the top of the dome is localized at the last image before breaking, two circular areas of radius r_1 and r_2 are defined around the top:

$$r_1 = (0.125 \pm 0.025) * d \quad (2\text{-}2)$$

$$r_2 = (0.05 \pm 0.01) * d$$

where d is the die diameter, which is 100 mm in this study. r_1 is used to calculate the area where to perform the best fitting sphere to get the radius of curvature and the strains $\varepsilon_1 = \varepsilon_2$ at the dome of the specimen are estimated using a circular surface of radius r_2

Pressure measurements were directly obtained from a transducer at the inlet of the container. According to Lazarescu *et al.,* 2011, the instantaneous average thickness at the top of the dome can be estimated by assuming material incompressibility, an isotropic behaviour and a spherical shape of the dome using:

$$t = t_o \exp(-2\varepsilon_2) \quad (2\text{-}3)$$

Thus, the equivalent stress and strains can be calculated by

$$\bar{\sigma} = \frac{P\rho}{2t}; \bar{\varepsilon} = \ln\left(\frac{t}{t_o}\right). \text{ (Lazarescu } et\ al.\text{,2011)} \quad (2\text{-}4)$$

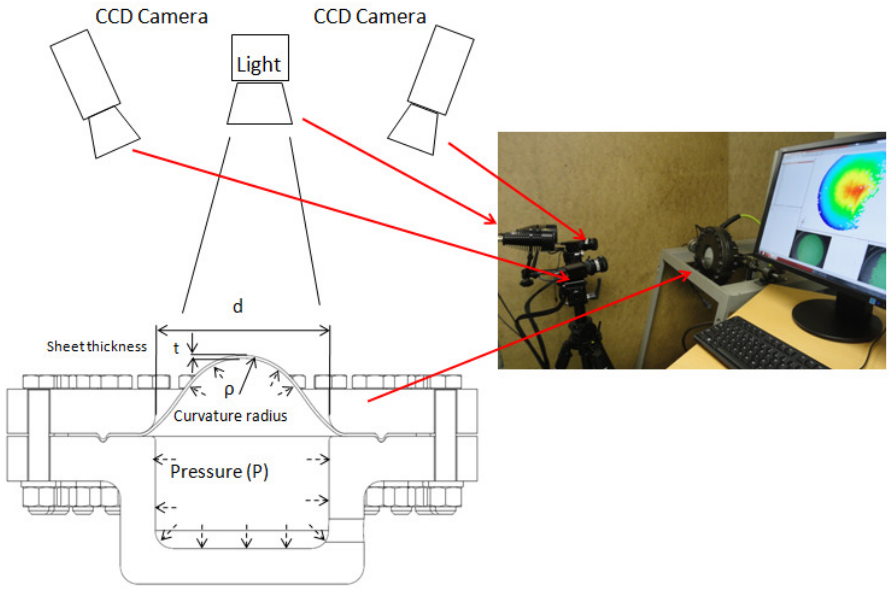

Figure 2.3 Configuration of cameras for the bulge test under the video correlation system

Figure 2.4 shows the true stress-strain curve obtained in the bulge test. The true stress-strain curves at 0º in the tensile test is also depicted for comparison. The bulge curve successfully reproduces the tensile behaviour and is able to extend the stress-strain curve to 0.7 of the equivalent strain.

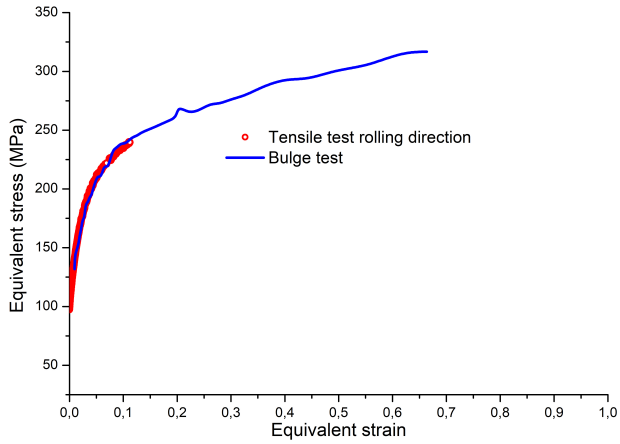

Figure 2.4 Equivalent stress vs equivalent strain for tensile and bulge tests

2.1.3. Stack compression test

Incremental forming is an extraordinary demanding process in terms of strains to perform accurate numerical simulations, which is crucial for obtaining flow curves with high strain levels. The stack compression test is an easy method for obtaining flow curves with higher strain levels due to the absence of necking.

In this test, a pile of discs was axially compressed by two polished and lubricated parallel plates under the action of a hydraulic cylinder (Figure 2.5). Both the compression force and vertical displacement were monitored during the test.

Figure 2.5 Stack compression test setup

The test followed the recommendation of the ASTM E9-09, with the exceptionof the aspect ratio of the stack, which was suggested in $1 \leq h_o/d_o \leq 3$, where h_o and d_o are the height of the stack and the diameter of the stack, respectively. In this study, according to the conclusions of Alves *et al.,*2011, raw materials supplied in form of sheets or plates can be successfully utilized, but due to the difficulties of stacking more than five discs in a stable manner, a pile of five discs with a thickness of 1.6 mm and a diameter of 15 mm ($h_o/d_o \approx 0.5$) was employed. Figure 2.6 shows the agreement between the bulge tests and the stack compression test, which enables the material to be characterized to a 1 strain level.

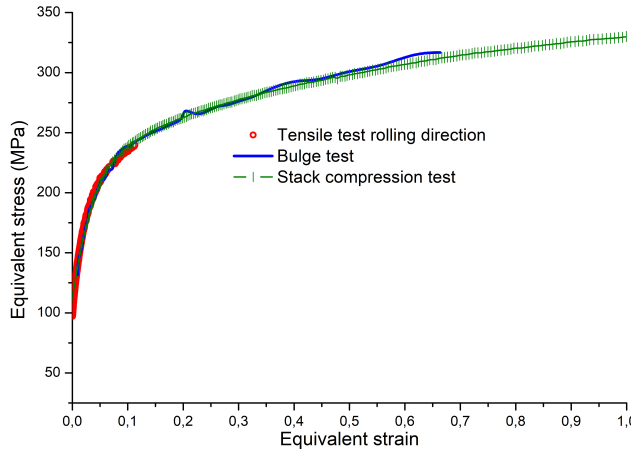

Figure 2.6 Equivalent stress vs. equivalent strain for tensile, bulge and stack compression tests

2.2. Forming Limit Diagrams (FLD)

In general, ductile materials formed by conventional sheet metal forming processes usually start failing due to the onset of localized necking. The material within this neck undergoes an unstable deformation process (plastic instability), following a near plain strain state until fracture occurs. Both necking and fracture are commonly analysed within the principal strain space in the well-known Forming Limit Diagram (FLD). The FLD shows the combinations of two curves:the first curve represents the principal strains in the sheet plane at the onset of local necking (Forming Limit Curve, FLC) and the second curve depicts the principal strains at the beginning of fracture (Fracture Forming Line, FFL).

Figure 2.7 shows the evolution of the FLC and FFL curves for stainless steel AISI 304-H111. Three different regions can be distinguished: one region below the FLC, where the forming is safe; one region between the FLC and the FFL, where the strains evolve instability; and a fracture region for strain levels equal or above the FFL curve.

In the following section, the methodology for determining the FLC and FFL curves for the AA7075-O 1.6 mm thickness sheet is described.

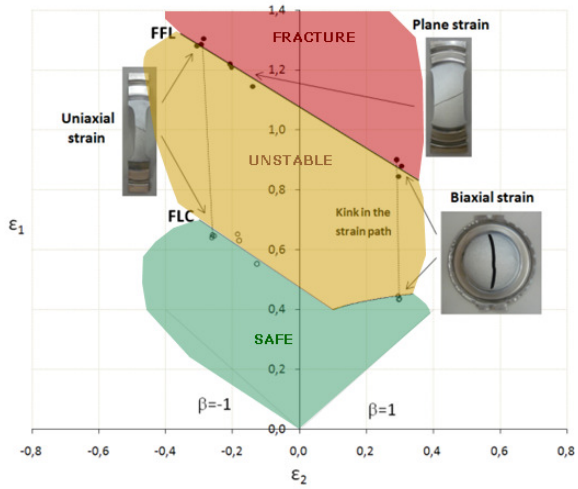

Figure 2.7 Forming Limit Diagram for a ductile material AISI 304-H111. Centeno et al., 2017

2.2.1. Nakazima tests

The characterization of the conventional forming limits by necking and fracture was performed by a series of Nakazima tests with a hemispherical punch that has a diameter of 100 mm, following the testing condition of the standard ISO 12004-2:2008. Figure 2.8 recreates the test.

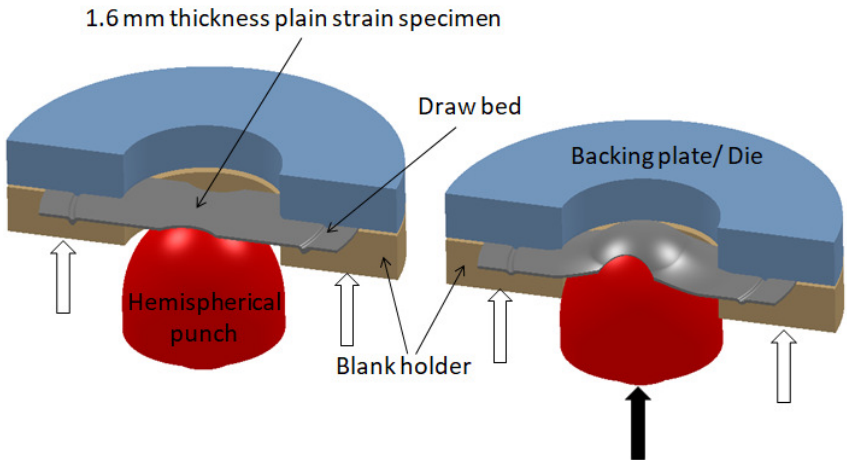

Figure 2.8 Recreation of Nakazima test (section of setup)

The tests were performed on the universal sheet metal testing machine Erichsen 142-20. First, the machine applies force to the specimen through the blank holder against the backing plate. Second, the punch moves to 1 mm/s. The tribological system at the interface punch-sheet was Vaseline + PTFE sheet (0.05 mm in thickness) + Vaseline + PTFE sheet + Vaseline to avoid any friction, and a draw bed was provided to properly support the specimen.

Four different specimen geometries were tested to evaluate the sheet failure at different strain paths (uniaxial strain, near plane strain, biaxial strain and equibiaxial strain). The geometric dimensions of the specimens are shown in Figure 2.9. During the tests, the deformations of the specimens were continuously recorded to failure by digital CCD cameras at a rate of 12 images per second, as shown in the recreation of Figure 2.10. This information is used to evaluate the principal strain in the specimen using the commercial software of Digital Image Correlation (DIC) ARAMIS®.

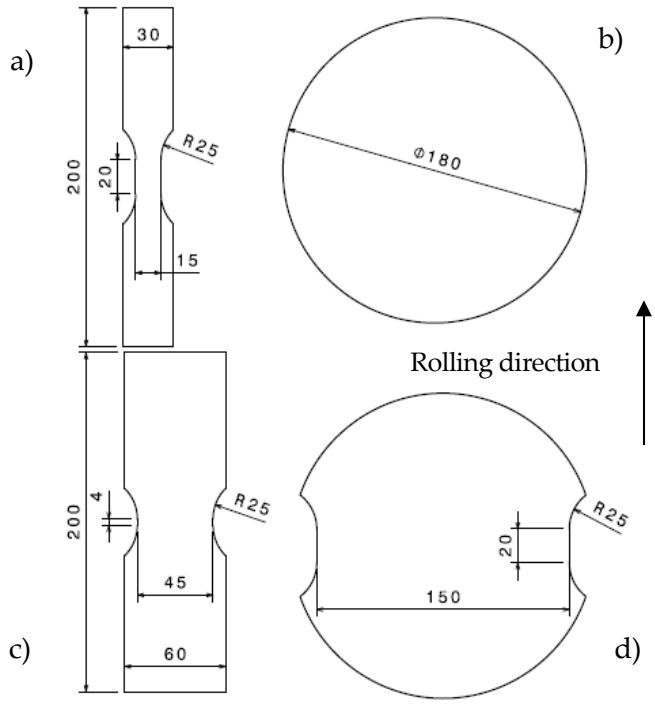

Figure 2.9 Geometry of a) uniaxial, b) equibiaxial, c) near plane strain and d) biaxial strain Nakazima tests

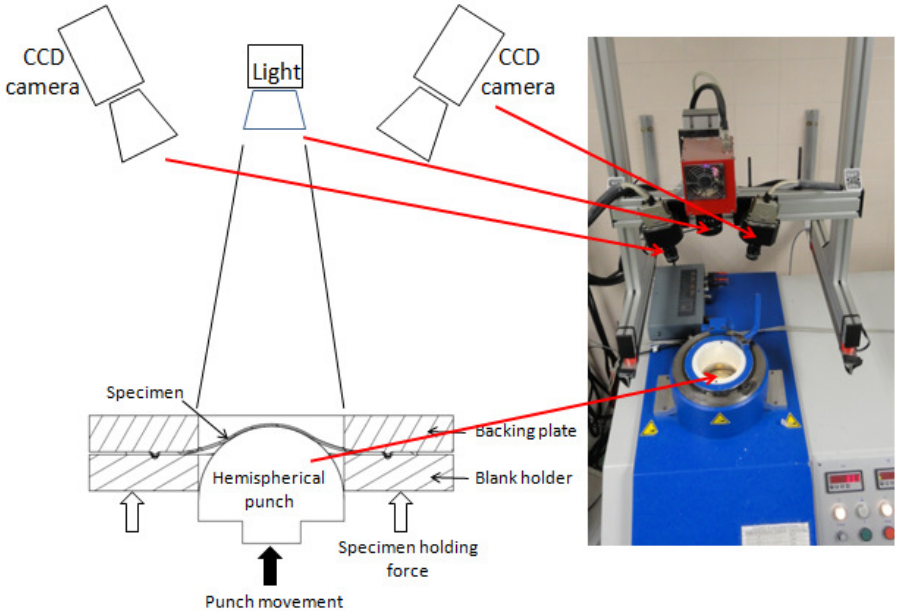

Figure 2.10 Setup of Nakazina tests

2.2.2. Forming limit curve for necking (FLC) and fracture (FFL)

The forming limit curve (FLC) was built following the recommendations given in ISO 12004-2:2008 and using time-dependent methodologies for detecting the onset of localized necking recently proposed by Martinez-Donaire *et al.,*2014. Three specimens of each geometry were evaluated to ensure consistent statistics; the scatter interval and the mean value in each case are also displayed.

The FLC curve is obtained by fitting the experimental results; the curve exhibits a traditional V-shape, which is common in ductile material. The forming fracture limit (FFL) was determined by direct measurement of the sheet thickness, following a methodology similar to that highlighted in Silva *et al.,* 2008. The procedure starts by measuring under a microscope the sheet thickness at the fracture point on both sides of the crack for every tested specimen.

The fracture initiation point is accurately determined by analysing the images recorded by the ARAMIS® system immediately before and after the fracture. In addition, some specimens were cut perpendicularly to the crack at the fracture

initiation site to measure the thickness in the profile view and validate the previous measurements along the crack. The thickness strain at fracture ε_{3f} was subsequently calculated. The minor principal strain in the sheet plane ε_{2f} was estimated as the average value of the minor principal strain along the fracture line measured by ARAMIS® for the last image recorded immediately before the crack appearance. The major principal strain ε_{1f} was then calculated by volume conservation.

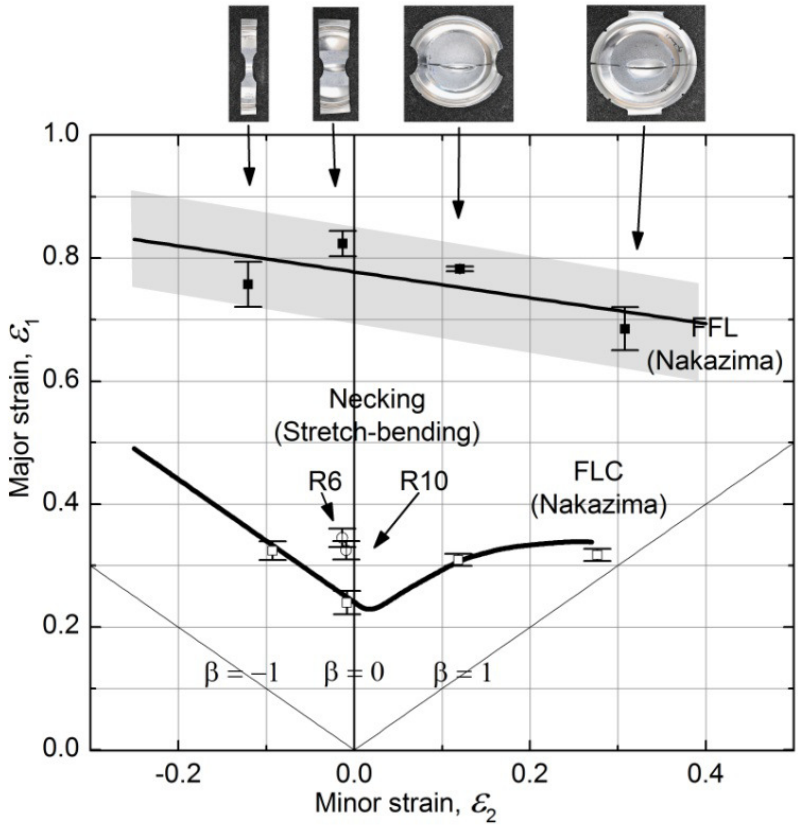

Figure 2.11 Conventional Formability limits at necking (FLC - Forming Limit Curve) and fracture (FFL - Fracture Forming Line) for AA7075-O metal sheets with a thickness of 1.6 mm. Forming limit strains in stretch-bending tests near plane strain for cylindrical punches with radii of 10 and 6 mm. Borrego et al., 2015

The FFL curve, which was linearly fitted from the Nakazima tests, is plotted in Figure 2.11 with a scatter band of 10% of uncertainty in its experimental determination (grey band).The scatter is fairly consistent with the experimental scatter observed by Liu *et al.,* 2013) for the same material.

2.3. Stretch-bending tests

To characterize the sensibility of the material to a severe through-thickness strain gradient, a series of stretch-bending tests using cylindrical punches was performed. These stretch-bending tests on plane strain geometries (Figure 2.9) introduce a controlled through-the-sheet thickness in the failure region due to the punch radius, which will help to explain the influence of the punch profile in hole flanging by conventional press working.

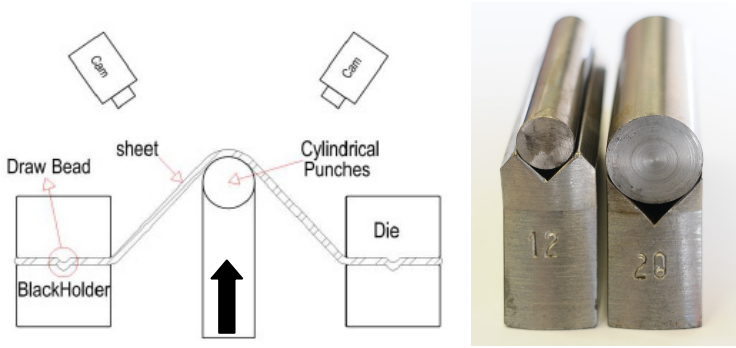

Figure 2.12 Schema of the stretch-bending test, R6 and R10 punches

The stretch-bending test near plane strain conditions was conducted using cylindrical punches with radii of 10 and 6 mm, respectively. The fracture limit strains were obtained using the same methodology employed for the Nakazima specimens (Figure 2.12 shows the schema of testing). The experimental setup and test procedure are detailed in Martinez-Palmeth *et al.,* 2013 and Martinez-Donaire *et al.,* 2014 for a different batch of the same material.

The mean value and scatter band of the necking strain for both punch diameters are shown in Figure 2.11. As expected, the smaller is the punch radius, the higher are the necking strains; both values are above the FLC.

A complete characterization of the true stress-strain curve, anisotropy (Lankford coefficient), strain formability curves, i.e., the conventional FLC and FFL, and the formability in stretch-bending of the AA7075-O 1.6 mm thickness sheet have been presented.

These results will be used in the following chapters to explain the experimental behaviour observed in the process of incremental and conventional hole flanging.

3. HOLE FLANGING BY CONVENTIONAL PRESS WORKING

The aim of this chapter is to contribute to the understanding of the factors that control the formability of the sheet during hole flanging operations using conventional press working. The deformation process of the flange and the influence of the initial hole size and punch profile in the failure and final geometry of the flange are discussed. A series of tests using AA7075-O metal sheets was performed and analysed using three different cylindrical punches with different profile radii (10 mm, 8 mm and 6 mm) and a hemispherical punch (R=47.9 mm). The evolutions of the principal strains along the flange were measured using an optical 3D forming analysis system (ARGUS®). The formability of the flange was analysed via the traditional LFR and conventional FLC. The findings indicated that the FLC was not suitable for analysing the formability of the material along the flange wall, with the exception of the tip of the flange. The real influence of bending induced by the punch and the apparent independence of the punch profile on the flange formability was elucidated.

3.1. Experimental procedure

The tests were performed using an Erichsen 142-20 machine with a blank holder and backing plate with a diameter of 100 mm inner. Figure 3.1 schematically depicts the hole flanging process performed in the laboratory.

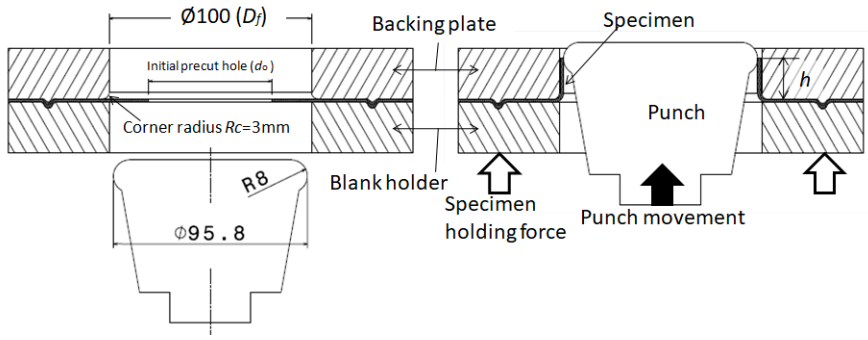

Figure 3.1 Conventional hole flanging process scheme

As shown in the scheme, during the flanging process, the punch expands the material around the pre cut hole in the blank to form a hollow flange. The operation attempts to achieve the final flange with a single pass of the forming tool and is successful when a complete flange that is free of defects is obtained.

Table 3-1 shows the proposed experimental campaign. The blanks were circular, with an external diameter of 180 mm and central pre cut holes with different diameters d_o. The central holes were milled and subsequently grinded with fine grit sandpaper to eliminate any burrs.

Table 3-1 Experimental campaign for hole flanging by conventional press working

Pre cut diameter hole, d_o (mm)	*Die diameter D_f (mm)*	*Punch diameter, D_p (mm)*	*Edge radius R (mm)*
35	100	95.8	6
41			8
58			10
59			47.9
60			
61			
65			
72			
83			

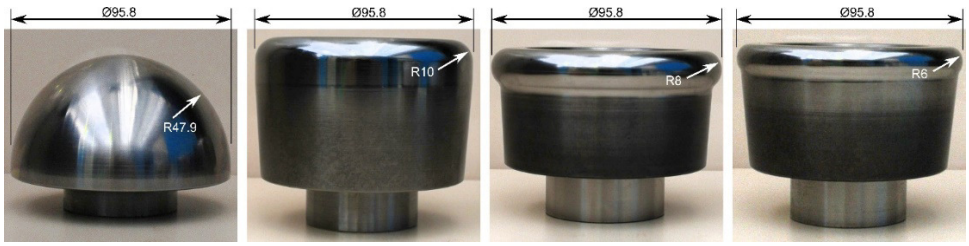

Figure 3.2 Set of punches with different edge radii for hole flanging tests by conventional press working (6 mm, 8 mm, 10 mm and 47.9 mm)

A series of punches with an equal circumferential diameter D_p and different edge radii R was used to analyse the effect of the punch profile on the formability. A circumferential diameter of 95.8 mm and four edge radii of 6 mm, 8 mm, 10 mm and 47.9 mm (hemispherical punch) were selected (see Figure 3.2). The gap between the die and the punch was slightly larger than the sheet thickness to avoid ironing during the forming process. The punches, die and blank holder were fabricated from UNE F1430 steel, tempered and hardened to 60 HRC.

The punch velocity was set to 1 mm/s. The contact between the blank and the punch was lubricated with Vaseline. The blank holding force was set to 85 kN, which was sufficiently high to avoid the blank from drawing in. According to Krichen *et al.,* 2011, the blank holding conditions do not influence the maximum punch load. However, an insufficient holding force may modify the finished flange due to springback effects. Therefore, the use of holding forces that are higher than the maximum reaction force experienced by the punch during the test is always advised.

To study the flange deformation and failure mechanisms, the strains at the outer sheet surface were measured using a circle grid analysis. Blanks were electro etched with a grid of dots with a diameter of 1 mm and centres spaced by 2 mm and the optical 3D forming analysis system ARGUS®, which is used to automatically compute the principal strains at the sheet surface. Measurements were performed at the end of the test or, in the case of failure, after the specimen failed. The final flange height was also measured to evaluate the geometric capabilities of the process.

3.2. Specimen marking for strain measurement

The marking process and limitations in the strain measurement with ARGUS® are discussed in this section.

3.2.1. Electrolytic marking process

The electro etching machine used in this study was an EU-Classic 300 from Ötsling Marking Systems, which provides AC/DC current from 0-24 V. The current flow and voltage selected combined with the electrolyte and felt of the marking head leads to a marking pattern based on black or white dots on the same AA7075-O.

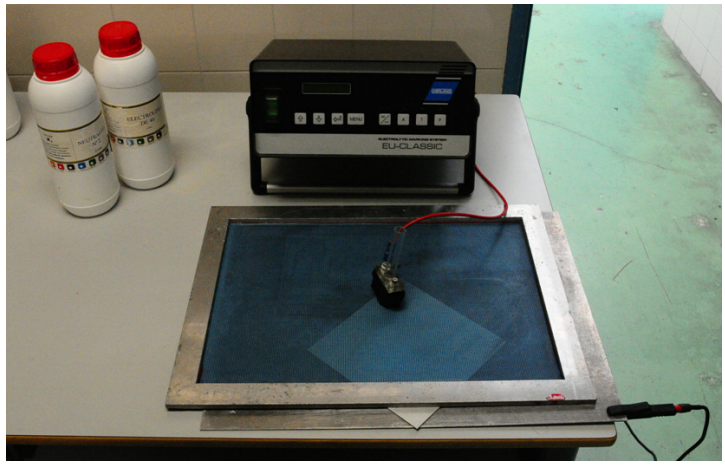

Figure 3.3 Electro etching setup

In our study, a stencil of a dot grid with a diameter of 1 mm and spacing of 2 mm was employed. A dot grid with a diameter of 0.5 mm and spacing of 1 mm was checked for better accuracy. Although this stencil is indicated to strain gradient areas, it easily disappears when a high strain level is reached.

According to the manufacturer, the selected combination of electrolytic, felt, current flow and different voltages for black markings did not meet our expectations for high-demanding strain states in hole flanging by the SPIF process. They did not provide sufficient contrast between the black colour of the points and the shiny aluminium sheet background. The solution passed by finding a method to increase the contrast by increasing the black colour of the points or whitening the background of the aluminium sheet.

To increase the black colour of the points, a sand blasting process of the surface prior to electro etching increased the contrast; however, a compression strain state was induced in the sand-blasted surface. This solution was discarded.

Figure 3.4 Examples of black on white and white on black markings

For whitening the background prior to electro etching, a Keller solution was applied (93.5% H_2O, 1.5% HCl, 2.5% HNO_3 and 2.5% HFl). After plunging the sheet blank in the solution and electro etching, perfect black dots were visible in the white background (see Figure 3.4 left). This technique yields positive results in terms of sufficient contrast between the black and white colours for high strain levels and will be employed in the hole flanging by SPIF discussed in section 4.

In the case of a conventional press forming test, where lower strain levels were achieved at the outer surface of the specimen, both black on white or white on black marking can be applied. In our case, a white on black marking was performed using deep marking settings. Note that ARGUS® reads the shiny aluminium patina as a black background when no direct light is falling on it.

The optical 3D forming analysis system ARGUS® computes the strains after the hole flanging process by comparing the centre distance of the previously electro etched dotted pattern in the outer surface of the specimen with the centre distance of the initial dotted pattern, which is an internal parameter of the software that can be adjusted according to the dot grid stencil used during the marking process. (ARGUS User Manual v6.2 rev-a, 17/09/2009.)

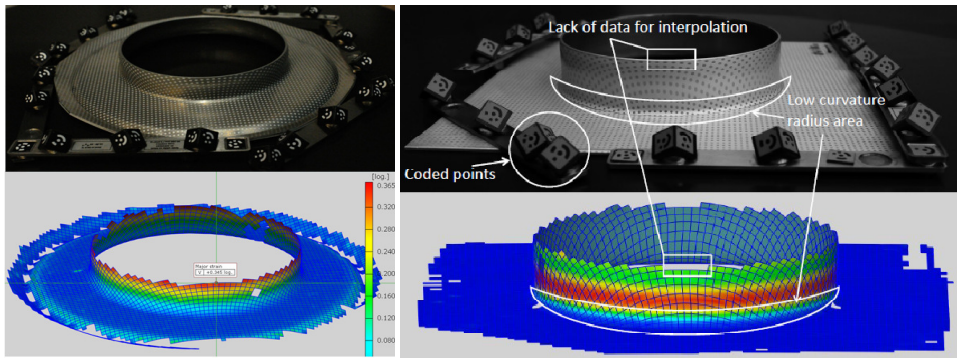

Figure 3.5 Specimen before and after ARGUS computation; an example in conventional and SPIF processes

Figure 3.5 shows a typical setup for measuring the strains using the ARGUS® system and the major principal strain contour map. Specimens for conventional and incremental hole flanging are shown. The main drawback of the software is that it cannot compute strains near the edges of the sheet due to the lack of data for interpolation. Thus, in this study, only the strains at the hole edge have been calculated from direct measurement of the initial and final perimeters of the hole and the initial and final sheet thickness and assuming material volume constancy.

3.3. Experimental results

In this section, the tests results are described. The influence of the punch profile on the deformation of the flange is discussed.

Table 3-2 Series of conducted conventional press working hole flanging tests

Edge radius, R (mm)	Initial pre cut hole diameter, d_o(mm)								
	35	41	58	59	60	61	65	72	83
6	F		F	F/N	N	O	O	O	O
8		F	F	F/N	N	O	O	O	O
10			F	F/N	N	O	O	O	O
47.9			F	F/N	N	O	O	O	O

Table 3-2 summarizes the results of the hole flanging process using AA7075-O produced by conventional press working in blanks with different pre cut hole diameters d_o.The experimental plan is shown in Table 3-1. The different punches are identified by their edge radius R. The label "O" indicates a successful test in terms of obtaining a complete hole-flanged part that was free of defects; "N" indicates tests that exhibited necking without fracturing the flanges; and "F" indicates specimens with fractured flanges.

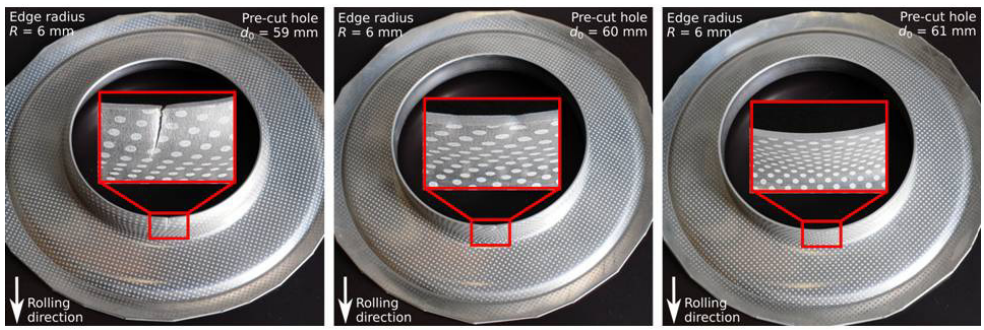

Figure 3.6 Flanges from pre cut hole diameters of 59 (fractured), 60 (necked) and 61 mm (successful) with a 6 mm edge radius

A series of increasing values of d_o was tested to determine the successful flanges. Intermediate pre cut holes were tested until a difference equal or less than 1 mm in diameter was reached between the successful tests and the failed tests. The necking situations were verified using at least two different tests.

Figure 3.6 shows tests for the pre cut holes with a 59 mm, 60 mm and 61 mm diameter using a punch with a 6 mm edge radius. A successful flange was obtained for d_o equal to 61 mm (labeled as "O" in Table 3-2), whereas incipient necking at the hole tip was observed for d_o equal to 60 mm (labeled as "N" in Table 3-2), and a meridional crack was clearly developed for d_o equal to 59 mm (labeled as "F" in Table 3-2).

Table 3-3 Experimental results and process parameters of the successful tests

Edge radius, R (mm)	d_o (mm)	$d_f \approx D_p$ (mm)	h (mm)	Bending ratio t_o/R	HER (d_f/d_o)	LFR ($d_f / d_{o,min}$)
6	61	95.8	18.2	0.27	1.57	1.57
6	65		16.4		1.47	
6	72		13.2		1.33	
6	83		7.6		1.15	
8	61	95.8	18.2	0.20	1.57	1.57
8	65		16.4		1.47	
8	72		13.0		1.33	
8	83		7.7		1.15	
10	61	95.8	18.2	0.16	1.57	1.57
10	65		16.5		1.47	
10	72		13.0		1.33	
10	83		7.7		1.15	
47.9	61	95.8	17.6	0.03	1.57	1.57
47.9	65		15.9		1.47	
47.9	72		12.9		1.33	
47.9	83		7.5		1.15	

The mode of failure observed in all situations was the initiation of a neck at the edge of the flange, which developed until the material fractured. The onset of necking appeared preferentially oriented along the rolling direction, as shown in Figure 3.6.

Table 3-3 presents the geometric parameters that were measured in the successful parts of the different pre cut holes. The final hole diameter d_f was assumed to be the punch diameter D_p, neglecting the slight springback experienced by the flange after removing the punch, as D_p was always the largest diameter that ran through the hole.

The flange height h was measured at four different positions around the flange (approximately every 90°). The bending ratio, which is defined as the ratio of the initial sheet thickness to the punch edge radius (t_o/R), is also presented. This ratio quantifies the severity of local bending induced on the sheet thickness during the forming operation. With the exceptionof the hemispherical punch, the values were nearly identical for a given pre cut hole d_o when the bending ratios ranged from 0.16 to 0.27.

3.4. Formability analysis based on the LFR

As mentioned in the introduction, the forming severity during conventional circular hole flanging is measured by the hole expansion ratio (*HER*), and the formability is quantified by the limiting forming ratio (*LFR*). These parameters are defined as follows:

$$HER = \frac{D_p}{d_0} \qquad \therefore \qquad LFR := \frac{D_p}{d_{0,min}} \tag{3-1}$$

Figure 3.7 graphically depicts the information in Table 3-3, where flange height is dimensionalized by the final hole diameter d_f or the punch diameter D_p on the vertical axis versus the *HER* one the horizontal axis. The higher is the *HER* value, the higher is the non dimensional flange height.

Note that all punch radii evolutions overlap, and the *LFR* or maximum *HER*, which is indicated by a dotted line, remained constant with *R* and was equal to 1.57, which indicates that the punch profile did not significantly influence successful flange formation, i.e., the flange formability. Similar conclusions have been noted by other authors, e.g., Leu *et al.,* 1999 and Huang *et al.,* 2001a. In their studies, they noted that the formability during hole flanging processes appeared to be unaffected by the punch profile. The reason for this insensibility will be

subsequently discussed. The dotted line joining the origin with the test indicates a suggested evolution as no data were available. For completeness, the dashed line in this process represents the physical limit for which the flange never becomes thicker on average, that is, the undeformed flange height $(d_f - d_o)/2$ should always be smaller than its average deformed height h.

For a given *HER*, the flange height decreases with the bending ratio (t_o/R). As subsequently explained, in practice, due to the special geometry of the test, the tensile stress state of the edge of the pre cut hole produces a contraction of the flange, which is enhanced by the bending ratio and friction conditions of the punch. Smaller punch edge radii can reduce the contraction of the flange.

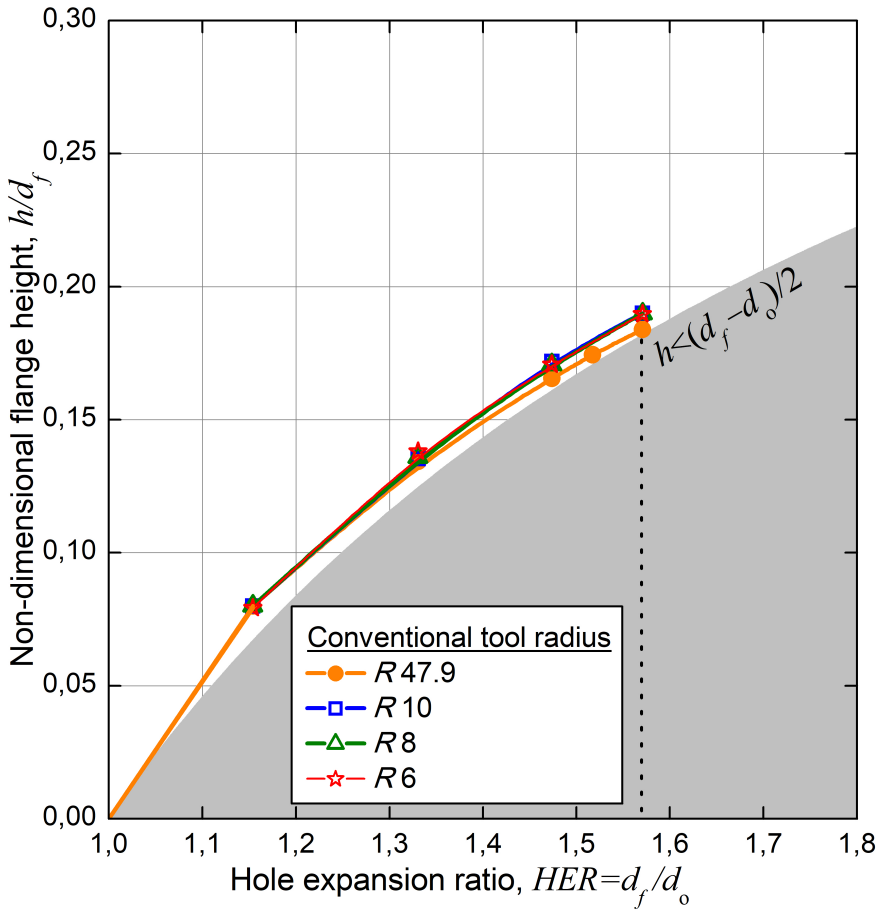

Figure 3.7 Non-dimensional flange height (h/d_f) of successful conventional hole-flanged sheets for different pre cut diameters

3.5. Formability analysis based on the FLC

Conventional FLC is currently the most useful tool during the designing stage of press working operations for evaluating the formability of a metal sheet. In general terms, safe operation is warranted when the strains in the sheet are well below the FLC.

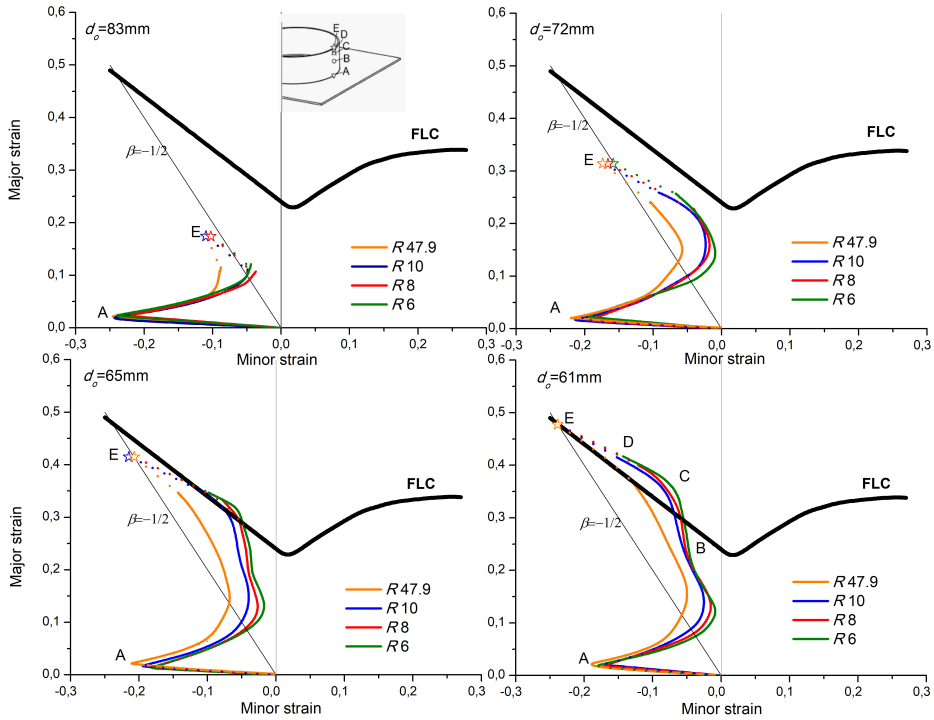

Figure 3.8 In-plane strains along the meridional direction for all successful hole flanged parts fabricated using different punches

Figure 3.8 shows the in-plane strains along the meridional direction of finished flanges from all successful tests, i.e., the 61 mm, 65 mm, 72 mm and 83 mm pre cut holes using the cylindrical punches (6 mm, 8 mm, and 10 mm edge radius) and the hemispherical punch, respectively. The inspection directions were oriented along the rolling direction according to the preferential failure orientation.

The principal strains, which were computed using ARGUS®, are represented by a solid line and cover points from the base to nearly the edge of the flange. The strain at the exact flange edge, which was obtained using direct measurement as indicated in section 0, is depicted with a star. The gap between the last point

measured using ARGUS® and the hole tip is depicted by a dotted line and was estimated to be approximately 1 mm. The major strain direction and minor strain direction correspond to the circumferential direction and meridional direction, respectively, of the part, i.e., the directions along and across the flange.

As shown in the figure, the evolution of the in-plane principal strains on the outer surface of the flange exhibits a two-shaped curve. The strain shows significant contraction in the meridional direction, especially at the base of the flange, due to the bending of the flange around the die radius, followed by stretching of the flange wall in the circumferential direction and ending in pure uniaxial tension at the exact flange edge. This contraction in the meridional direction increases with the punch edge radius, where minor strain values are more negative for the larger punch edge radius (R=47.9 mm). For other punches that were tested, no significant differences were observed.

The most remarkable fact noted in Figure 3.8 is that, with the exception of the hemispherical punch, the strain curves for the pre cut hole with a 61 mm diameter are clearly above the FLC. According to the traditional analysis using FLC, these parts should have failed at some point along the flange, which did not occur. This phenomenon of exceeding the FLC without failure when analysing conventional hole flanging can also be observed in the experimental studies of several researchers, such as Silva *et al.,* 2013 for Ti6Al4V and Montanari *et al.,* 2013 and Cristino *et al.,* 2015 for AISI304L; however, this phenomenon has not been analysed.

Two events are a priori candidates for explaining the inability of conventional FLC to describe the failure during hole flanging by press working. The first event is the bending induced by the punch edge radius, and the second event is the non proportionality of the strain path.

3.5.1. Bending effect

Bending induced by forming tools has a beneficial effect on the formability as it enables higher strains at the sheet surface before failure occurs. The bending effect and its contribution in the enhancement of formability in press working (see, e.g.,Vallellano *et al.,*2008, 2010, Luo and Wierzbicki, 2010 and Morales-Palma *et al.,*2013) and incremental sheet-forming processes (see e.g.,Silva *et al.,*2011), Seong *et al.,* 2014), and Centeno *et al.,* 2014)) have been extensively discussed in this research field.

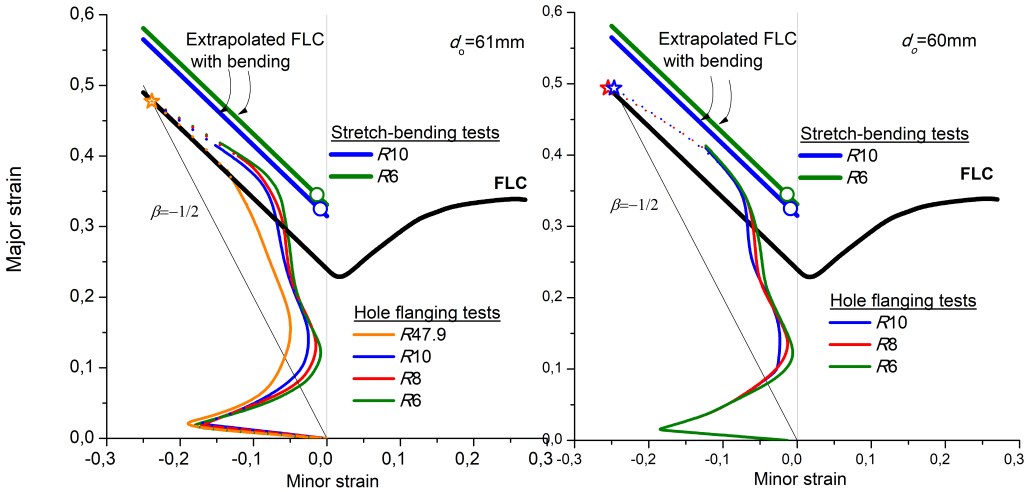

Figure 3.9 In-plane strains along the meridional direction for hole-flanged parts using pre cut holes with a 61mm (successful) and 60mm (necked) diameter and different punch edge radii. Comparison with the results for the stretch-bending tests using cylindrical punches with a 6 and 10mm radius and the extrapolated FLC with the bending contribution

Figure 3.9 shows the in-plane strains along the meridional direction for the hole flanging tests with 61 mm and 60 mm pre cut hole diameters and different punch edge radii. The first graph (on the left) corresponds to the minimum pre cut hole that is necessary to fabricate a successful flange, and the second graph (on the right) corresponds to the maximum pre cut hole that is necessary to obtain a flange that is necked at the hole tip.

To quantify the effect of bending, a series of stretch-bending tests was developed using cylindrical punches with a 10 and 6 mm radius, which corresponded to the maximum and minimum edge radii in the cylindrical hole flanging punches. Both forming limit strains from the stretch-bending tests are depicted in Figure 3.9 near the plane strain (open symbols). See section 0 for a detailed description of these tests. Assuming a constant strain thickness during the appearance of necking, two parallel lines on the left-hand side of the FLC were extrapolated through the uniaxial region in the principal strain diagram from the experimental limit strains. These lines may be considered as an estimation of the FLCs with the bending contribution. As expected, the smaller is the bending radius, the higher is the estimated FLC value. As shown, the differences between the 6 mm radius results and 10 mm radius results were not very significant.

The strain evolutions for all cylindrical punches of hole flanging in Figure 3.9 are below their estimated FLCs with bending, which indicates that failure by necking was not expected to occur in the flange wall when the effect of bending is considered. When the influence of bending disappears near the hole edge, the conventional FLC again dominates the failure of the sheet. The flanges finally fail in this zone (see the results for the 60 mm pre cut hole diameter in Figure 3.9).

3.5.2. Strain path effect

The strain path has a strong influence on the onset of necking. Experimental studies by Graf *et al.,*1994 and Stoughton *et al.,*2012 and theoretical/numerical studies by Barata da Rocha *et al.,*1985, Yoshida *et al.,*2007 and He *et al.,*2014 have shown that changes in the strain path significantly affect the shape and location of the FLC.

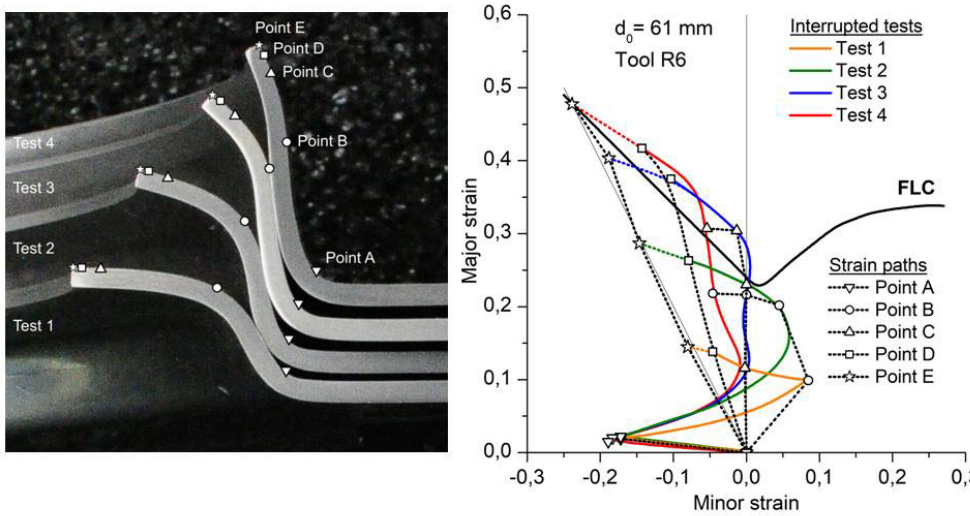

Figure3.10 In-plane strain paths during the hole flanging process obtained from the interrupted tests using the pre cut 61 mm hole and a 6 mm punch edge radius

To analyse the strain path evolution during flange formation, a given blank with the same pre cut hole was tested, and the punch stroke was interrupted at different heights. Figure3.10 (left) shows the flange for four interrupted tests using a pre cut 61 mm hole and a cylindrical punch with a 6 mm edge radius.

The principal strains were measured at the end of each test, and the strain history at five points (A-E) along the meridional direction of the flange is represented in

Figure3.10 (right). Point E, which is located at the hole tip, underwent pure uniaxial tension and increased linearly and proportionally from the origin to the final stage. Point D and Point C, which are located at the transition region between the hole tip and the flange wall, evolved from uniaxial stretching to near plane strain, respectively. These points followed a linear strain path during most of the deformation process, with the exception of the last step, where they exhibited a certain lack of proportionality. Point B, which is located at the flange wall, experienced a significant non proportional strain path, starting in biaxial stretching and ending in uniaxial stretching. Point A, which is located at the die radius, underwent severe compression and followed a linear path.

According to these results, a clear non proportionality in the strain paths was observed for the points in the flange wall. However, the strain paths tended to become proportional at the flange edge zone, and reached a complete proportionality at the exact hole edge. Since the strains in the area near the edge of the flange exceeded those of the conventional FLC, the effect of the non proportionality in the strain paths was not expected to have a relevant influence. In the author's opinion, the bending effect should be the factor that controls the apparent enhancement in the formability around the edge zone of the flange, which was clearly influenced by the punch profile.

In hole flanging by the conventional process, the punch edge radius primarily affected the meridional strain, i.e., the minor principal strains along the flange. Therefore, the smaller is the punch edge radius, the higher is the minor strain, which produced a shift in the strain curves to the right in the principal strain diagram. This shift is clearly observed in Figure 3.8, which compares the strain curve for the hemispherical punch and those for the cylindrical punches. The differences between the cylindrical punches are less apparent due to the experimental scatter. This shift was also responsible for the lower value of the flange height exhibited by the semi-spherical punch (see the h values in Table 3-3).

The condition for the onset of necking at the hole tip must be fulfilled at the intersection of the FLC with the line of pure uniaxial tension, as noted by Yu *et al.,* 2015. Figure 3.9 right shows the uniaxial tension line according to the Mises behaviour, i.e., $\beta = -0.5$. This condition is well satisfied by the experimental results, in which the small deviations are attributed to the experimental scatter and the inherent anisotropy of the sheet. The *LFR* value must also be intrinsically associated with this intersection point and can be expressed as a function of the limiting major strain at the onset of necking in uniaxial tension ($\varepsilon^*_{1,UT}$) as follows:

$$\varepsilon_1|_{holetip} = \ln\left[\frac{\pi D_p}{\pi d_{0,min}}\right] = \ln[\mathrm{LFR}] \coloneqq \varepsilon^*_{1,UT} \qquad \therefore \qquad \mathrm{LFR} \coloneqq e^{\varepsilon^*_{1,UT}} \tag{3-2}$$

As previously discussed, the material at the hole tip is free of the influence of punch bending, which agrees with the fact that the *LFR* is a material that is constant and independent of the punch edge radius. This result shows complete agreement with the results of Huang and co-workers (Leu *et al.,* 1999 and Huang *et al.,*2001a), with the exception that they suggested that the fracture strain of the simple tension test can be adopted as a necking criterion at the flange tip, instead of the necking strain proposed here. As shown in Figure3.10 left and according to Eq. (3-2), a value of major strain at necking in the uniaxial tension$\varepsilon^*_{1,UT}$ of 0.47 yields a LFR value of 1.6, which shows agreement with the experimental value of 1.57.

3.6. Forming forces and final shape

This section presents an analysis of the vertical forces involved in the process and the final shape of the hole flange.

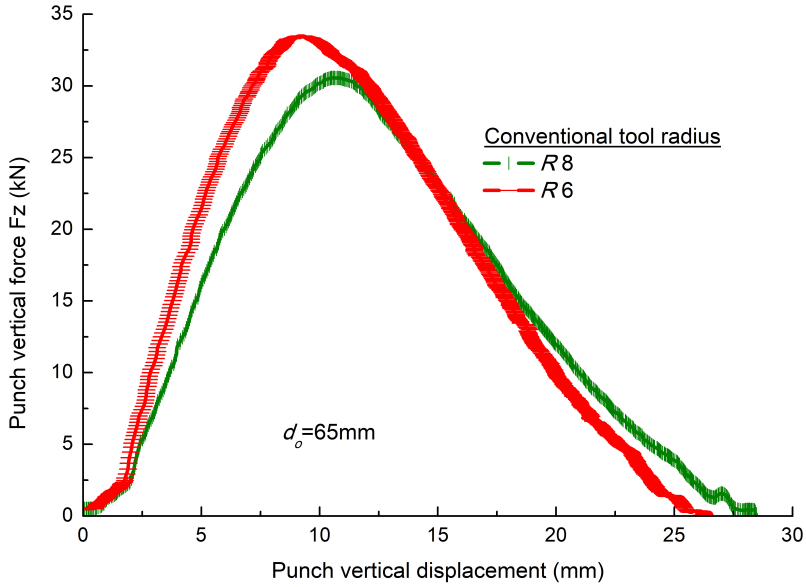

Figure 3.11 Vertical forming forces for a 65 mm diameter pre cut hole and punch corner radii of 8 mm and 6 mm

As explained in section 0, the natural tendency of the flange in conventional hole flanging is a shortening of the length of the flange. The use of low punch corner radii hinders this natural tendency, and higher punch forces are required to successfully perform the hole flanging, as noted by Huang *et al.,* 2001. Using numerical simulations, they also demonstrated that the increase in the friction coefficient produces the same effects as reducing the punch corner radii, which also increases the forming forces.

Figure 3.11 shows the vertical forming forces experienced by the specimen with an initial pre cut hole that has a diameter of 65 mm and is exposed to two different punch corner radii: 8 mm and 6 mm. In both cases, the forces rapidly increase to reach a maximum value and decrease to zero at the end of the test. This maximum value increases as the punch edge radius decreases. The peak of the forces appears earlier for smaller corner radii, which reflects that larger edge radii perform a more progressive flanging operation.

To visualize the shape and thickness of the flange, Figure 3.12 presents the diametrical section of the flange for the test of the 61 mm pre cut hole formed with the punch with an 8 mm edge radius. This section has been extracted by scanning the formed specimen with the 3D Geomagic Capture scanner. The red lines represent the theoretical flange with a diameter of 95.8 mm.

Two relevant facts common to all tested specimens: the relative uniformity in thickness distribution, and the relative amount of springback exhibited by the specimen. As discussed in subsequent chapters, the former will be an advantageous feature with respect to the process of incremental hole flanging in a single stage, where asthe latter will be a clear disadvantage.

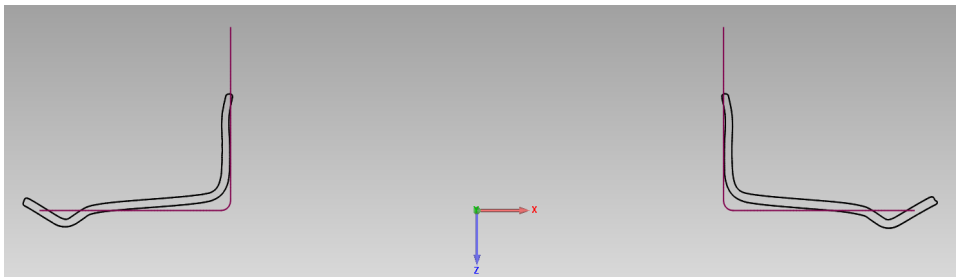

Figure 3.12 Section of specimen successfully conformed with a R=8 mm corner radius punch and 61 mm pre cut hole, which was scanned and compared with the theoretical profile

3.7. Conclusions

The formability of the hole-flanged parts fabricated using press working was analysed via the *LFR* and the conventional FLC. The influence of the punch profile on the deformation process and flange failure was discussed. A series of conventional hole flanging tests using a 1.6 mm 7075-O aluminium alloy sheet were performed using three cylindrical punches with different edge radii and a hemispherical punch. The main conclusions of this study can be summarized as follows:

- The failure mode prevailing at the formability limit was the initiation of necking at the edge of the flange.

- For the successful parts fabricated with cylindrical punches with bending ratios that range from 0.16 to 0.27, the heights of the flanges were nearly identical for a given pre cut hole d_o. The hemispherical punch produced slightly lower flanges.

- The *LFR* is a suitable measure of the formability in conventional hole flanging operations as this parameter directly quantifies the maximum stretching of the material at the hole tip, where failure occurs in practice. The LFR remained constant with *R* and was equal to 1.57.

- In general, conventional FLC was not a suitable tool for analysing the formability of the material along the flange, with the exception of the flange tip.

- The evolution of the in-plane principal strains on the outer surface of the flange exhibited a two-shaped curve. With the exception of the hemispherical punch, the strain curves for the pre cut holes near but below the formability limit were clearly above the FLC; however, failure did not occur. This event was observed in the area of the wall near the edge of the flange.

- The bending effect seemed to be the main factor that controlled the apparent enhancement in the formability in this area, which was clearly influenced by the punch profile.

- The punch edge radius primarily affected the final value of the meridional strain, i.e., the minor principal strains along the flange. A smaller punch edge radius induced a shift in the strain curves to the right in the principal

strain diagram. This shift was responsible for the lower value in the flange height exhibited by the semi-spherical punch.

- The condition for the onset of necking at the flange tip was fulfilled at the intersection of the FLC with the line of pure uniaxial tension. The *LFR* value was associated with this intersection point, which explains why the *LFR* is a material constant that is independent of the punch profile and can be obtained as $LFR = exp\ (\varepsilon_{1,UT}^{*})$, where $\varepsilon_{1,UT}^{*}$ is the major strain at the onset of necking in uniaxial tension.

In the next chapter, the formability and geometric capabilities of the hole flanging process by single point incremental forming (SPIF) in a single stage is discussed to critically evaluate the technological differences with respect to the conventional method by press working.

4. HOLE FLANGING BY SINGLE STAGE SPIF

The aim of the present chapter is to contribute to the understanding of the formability of metal sheets in the demanding operation of single-stage hole flanging by SPIF. Three important points need to be discussed: (1) the physical mechanisms that control the sheet failure during this process, (2) the maximum flange that can be successfully formed by SPIF in a single stage and (3), the geometrical capabilities of the process in terms of thickness distribution and flange shape.

A series of experimental tests of AA7075-O metal sheets has been performed and analysed using three different tool radii (10, 8 and 6 mm) and two spindle speed values (0 and 1000 rpm). The surface roughness and thickness profile along the flanges on the final parts are also analysed. The forming forces are analysed to anticipate the failure of the metal sheet.

4.1. Experimental procedure

The single-stage hole flanging tests were performed on a three-axis milling CNC machine EMCO VMC-200. The experimental setup is shown in Figure 4.1. The SPIF setup comprised a blank holder and a backing plate with a 100 mm diameter hole; both were fixed to the machine table via a rigid rig.

The sheet metal blanks, which were initially without pre cut holes but electrochemically etched, were fixed upside down by the holder over the backing plate. The pre cut holes were milled and the edges were sanded to remove any burr. This sequence guaranties that the pre cut holes and tool are perfectly centre.

Once the pre cut hole was finished and the tool was changed by the forming tool, the specimen was ready to be incrementally deformed, as shown in Figure 4.1 (a).

To analyse the effect of the sheet thickness-to-tool radius ratio (t_o/R) on formability, three different radii were employed (R = 6, 8 and 10 mm). The forming tools are shown in Figure 4.2.

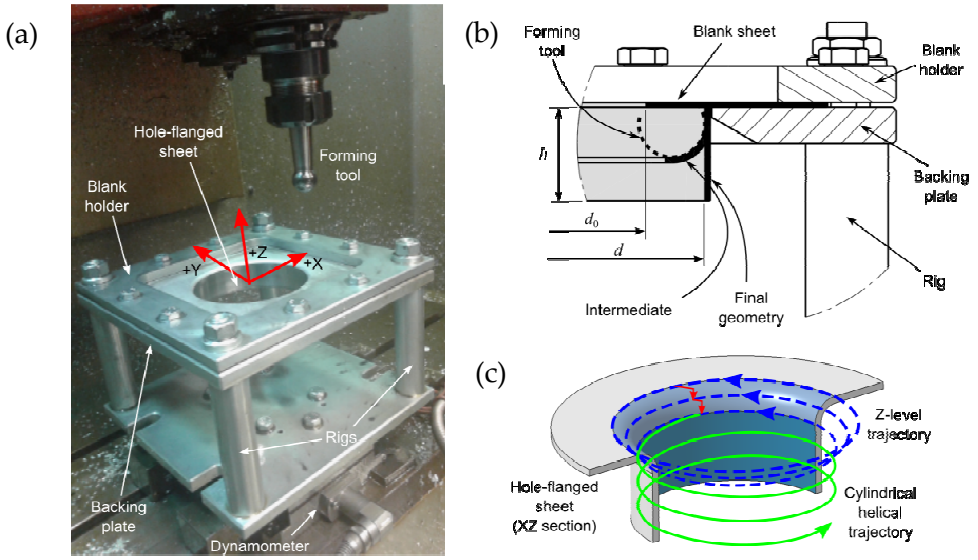

Figure 4.1 (a) Experimental setup for SPIF. (b) Scheme of the single-stage hole flanging process by SPIF. (c) Scheme of the z-level trajectory for the conical frustum and cylindrical helical path

Figure 4.2 Forming tools used for SPIF

Figure 4.1 (b) shows the scheme of the process. The test attempts to achieve the final theoretical geometry of the hole flanged sheet in a single pass of the forming tool. In this case, a final cylindrical hole with an inner diameter d_f= 95.8 mm is programmed.

A series of pre cut holes d_o was machined on the sheet blanks to obtain the formability limit of the single-stage hole flanging process by SPIF. This limit is defined as the maximum $HER = d_f / d_o$ that ensures a complete flange that is free of defects, i.e., the *LFR*. The final flange height *h* and thickness are also measured to evaluate the geometric capabilities of the process.

The forming trajectories to perform the hole flanging tests were modelled and simulated in CATIA V5® using a machining workbench. A virtual model of the experimental setup was employed to optimize the trajectories according to the desired final geometry of the flange.

The tool trajectory was divided into two steps, as represented in Figure 4.1 (c). The tool follows a z-level anticlockwise path of concentric circles with a decreasing diameter to smoothly adjust the sheet to the backing plate. The second step is a cylindrical helical anti-clockwise path. A step down of 0.2 mm/turn is utilized in both steps. Note that a simpler alternative to the second step is to use a trajectory of successive circular paths of constant diameters at different depths. However, a drawback of this alternative is that the vertical force showed a significant peak when the tool went down between two circular paths, which increased the probability of premature failure in the sheet at this location.

Two tool rotation conditions were tested:0 rpm and 1000 rpm clockwise. The condition of 0 rpm represents a tool that cannot rotate at all, i.e., a locked tool. The feed rate was set to 1000 mm/min.

To minimize the friction effects, a special lubricant for metal forming applications, Castrol Iloform TDN81, was continuously applied between the forming tool and the sheet during deformation.

A Kistler® dynamometer was placed between the machine-table and the SPIF frame (see Figure 4.1(a)) to measure the forming forces in the X-, Y- and Z-axes during the tests. The forces were acquired using the commercial software LabVIEW®. As a reference, the typical duration of a SPIF test was approximately 40-45 minutes for the successful specimens and approximately 15-20 minutes for the fractured specimens. Approximately 15 minutes were initially taken for milling and deburring the hole.

To study the deformation and failure mechanisms, the strains at the outer sheet surface were obtained by measuring with the optical 3D forming analysis system ARGUS®. To analyse the geometric capability of the process, finished flanges of successful specimens were cut to measure the final height, the sheet thickness distribution along the produced flange and the surface roughness.

4.2. Results

According to the experimental procedure, six series of tests were performed for three different tool radii (R = 6, 8 and 10 mm) and two spindle speeds (0 and 1000 rpm clockwise). Table 4-1 lists the values of the pre cut hole diameters d_o and their results. The label "O" represents a successful test in terms of obtaining a complete hole-flanged part with no defects, "X" indicates fractured specimens, and "D" denotes specimens that have a complete flange but exhibit surface defects. To determine the forming capability for each test condition, a series of increasing values of d_o was tested to achieve a successful flange. Intermediate pre cut holes were tested until a difference of less than or equal to 1 mm in diameter between successful tests and failed tests was reached.

Note that the failed test (X and/or D) closest to the first successful test was repeated at least twice in all cases to confirm the failure. In the case of the successful tests, only a few tests in the frontier of formability were repeated. In both cases, the results showed a high repeatability.

Table 4-1 Series of SPIF tests

Tool R (mm)	Spindle (rpm)	Initial pre cut diameter of the hole, d_o (mm)													
		55	56	57	57.5	58	59	60	61	62.5	63.5	64.5	65	70	82
6	0			X				X		X	X	O	O	O	O
6	1000										X	O	O		
8	0			X				X	O	O			O		
8	1000						X	O	O						
10	0	X	X	D	O	O			O				O		O
10	1000	X	X	O	O										

Figure 4.3 shows pictures of the closest successful-failed test pair for every tool radius at 0 rpm. The failed tests were interrupted as soon as the initiation of a crack was observed. Three deformation zones can be distinguished on the in-process workpiece: the cylindrical flange that is already formed, the curved sheet in contact with the tool in the process of forming, and the still-flat sheet that is

being radially stretched. The latter is essential to the success of the operation as the larger is this zone, the greater is the deformation resistance. Similar findings are also observed at 1000 rpm.

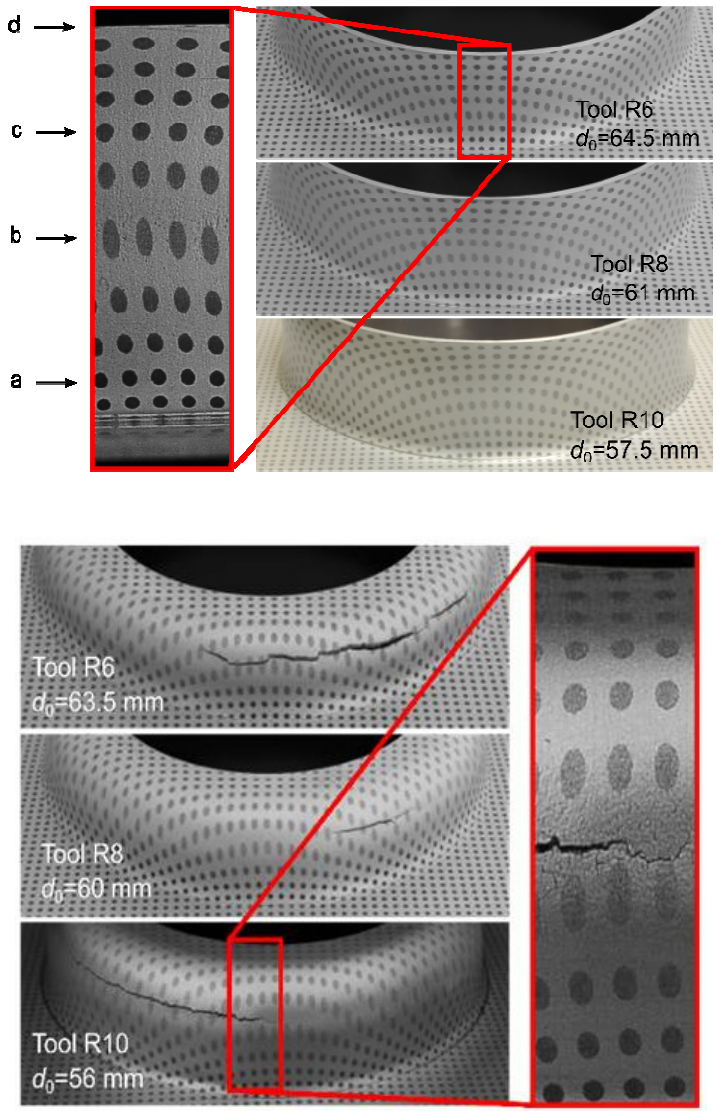

Figure 4.3 Pictures of the closest success-failed test pair with a spindle speed of 0 rpm. Details of the deformed sheets

Table 4-2 Experimental results and process parameters in successful tests with a tool rotation of 1000 rpm

Tool R (mm)	d_o (mm)	d_f (mm)	h (mm)	HER (d_f /	LFR (HER_{max})	t_o/R	TR ($\bar{t}/t_o$)
6	64.5	94.3	22.3	1.46	1.46	0.27	0.56
6	65	94.3	21.4	1.45		0.27	0.58
8	60	94.8	26.4	1.58	1.58	0.20	0.54
8	61	94.7	24.6	1.55		0.20	0.56
10	57	94.8	26.6	1.66	1.66	0.16	0.57
10	57.5	94.8	25.5	1.65		0.16	0.59

Table 4-3 Experimental results and process parameters in successful tests with a tool rotation of 0 rpm

Tool R (mm)	d_o (mm)	d_f (mm)	h (mm)	HER (d_f / d_o)	LFR (HER_{max})	t_o/R	TR ($\bar{t}/t_o$)
6	64.5	94.4	23.6	1.46	1.46	0.27	0.53
6	65	94.4	22	1.45		0.27	0.56
6	70	94.4	16	1.35		0.27	0.66
6	82	95.2	8.8	1.16		0.27	0.70
8	61	94.8	24.8	1.55	1.55	0.20	0.56
8	62.5	94.7	22	1.52		0.20	0.61
8	65	94.7	19	1.46		0.20	0.66
10	57.5	94.8	26.8	1.65	1.65	0.16	0.56
10	58	94.6	25.5	1.63		0.16	0.58
10	61	94.8	21	1.55		0.16	0.66
10	65	94.8	17.8	1.46		0.16	0.71
10	82	95.3	8.3	1.16		0.16	0.75

Table 4-2 and Table 4-3 present different geometric and process parameters measured in the successful parts for different pre cut holes for spindle speeds of 1000 rpm and 0 rpm, respectively. The flange height h and the final hole diameter d_f were measured at four different positions around the flange (approximately every 90º). A Mitutoyo digital calliper with a resolution of 0.01 mm was employed. The tables list the mean value of h and d_f; their standard deviation was slower than 0.15 mm in both cases. Note that d_f slightly differs from its theoretical value of 95.8 mm. Apart from the intrinsic experimental scatter, these differences seem to be primarily attributed to the elastic deflection of the tool and the elastic springback of the sheet observed in the tests. As a result, a slight trend to obtain smaller final holes with a smaller tool radius, i.e., with more flexible tools, is observed.

The tables also present four different process parameters that are used to analyse the process. The *HER* and the *LFR* were defined in the introduction. The bending ratio is defined as the ratio of the initial sheet thickness-to-tool radius (t_o/R), which quantifies the severity of local bending induced by the forming tool. The average thickness ratio is defined as the ratio of the average thickness $\bar{t}$ of the final flange to the initial sheet thickness ($\bar{t}/t_o$). The interest in these parameters to explain the deformation process is discussed in the following sections.

A comparison of the results at 1000 and 0 rpm reveal that the higher spindle speed slightly decreases the minimum pre cut hole allowed and seems to yield marginally shorter flanges for the same pre cut hole. This fact should be considered with caution since these differences are small in both cases and may be influenced by the intrinsic dispersion in the experimental tests and measures. As will be subsequently discussed, increasing the tool rotation provides clear beneficial effects, such as a more uniform thickness distribution in the final flange, a reduction in the roughness at the surface in contact with the tool and a slight decrease in the forming force.

4.3. Strain analysis and failure mechanism

The strain analysis of the outer sheet surface enables an understanding of the physical mechanism that controls the sheet failure. By comparing the strain distribution evolution from successful tests to failed tests, this mechanism can be clearly observed.

Figure 4.4 shows the strain evolution in the flange for specimens with different pre cut holes (58, 57.5, 57 and 56 mm diameters), formed with a 10 mm tool radius at

0 rpm. The principal strains were measured along the flange in line *a-b-c-d* (see the left legend in Figure 4.3). The strain evolutions in the FLD describe a loop, beginning from the bottom of the flange (point *a*), reaching a maximum value near the midway (point *b*) and ending at the flange edge (point *d*). Strains measured with ARGUS® are identified with closed symbols, whereas strains calculated at the flange edge (point *d*) are represented by open stars. In the failed specimens, the fracture strains measured on the crack lips are represented by open symbols. In all cases, the strains are above the FLC for necking obtained by the Nakazima tests, which indicates that necking is clearly postponed or suppressed. This inhibition of necking has also been reported by Silva *et al.,*2011 and Centeno *et al.,*2014 in SPIF processes. The smaller is the pre cut hole diameter, the higher is the major strain in the central region of the flange (point *b*).

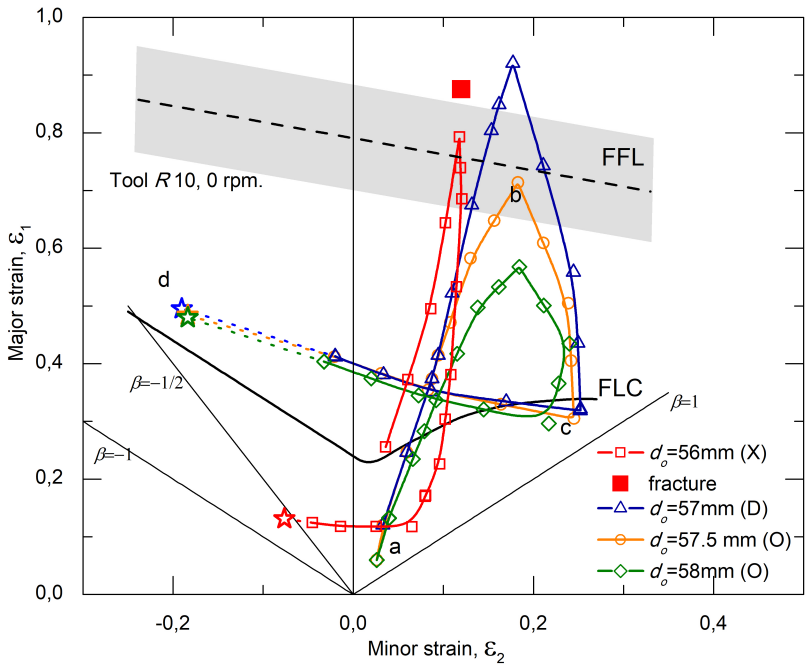

Figure 4.4 FLD with the evolution of strain paths along the final flange for different pre cut hole diameters for a R10 tool radius at 0 rpm

In this series, the holed specimens with diameters of 58 and 57.5 mm were successfully formed (labelled with "O" in Table 4-1), whereas the holed specimen with a diameter of 56 mm fractured before completing the flange (labelled with "X"). As expected, the former exhibited strain loops below the FFL, whereas the latter clearly crossed the FFL. Special attention should be paid to the specimen

with a hole diameter of 57 mm (labelled with "D") for which surface microcracks were detected in the flange, although a complete flange was obtained. This attention ensures that a major principal strain above the FFL is attained without showing a clear coalescence into a macrocrack. This test is illustrated and discussed at the end of this section.

Figure 4.5 presents the strain loops obtained for successful specimens with different tool radii at 0 rpm. The selected tests are the specimens with the minimum pre cut hole according to

Table 4-3.

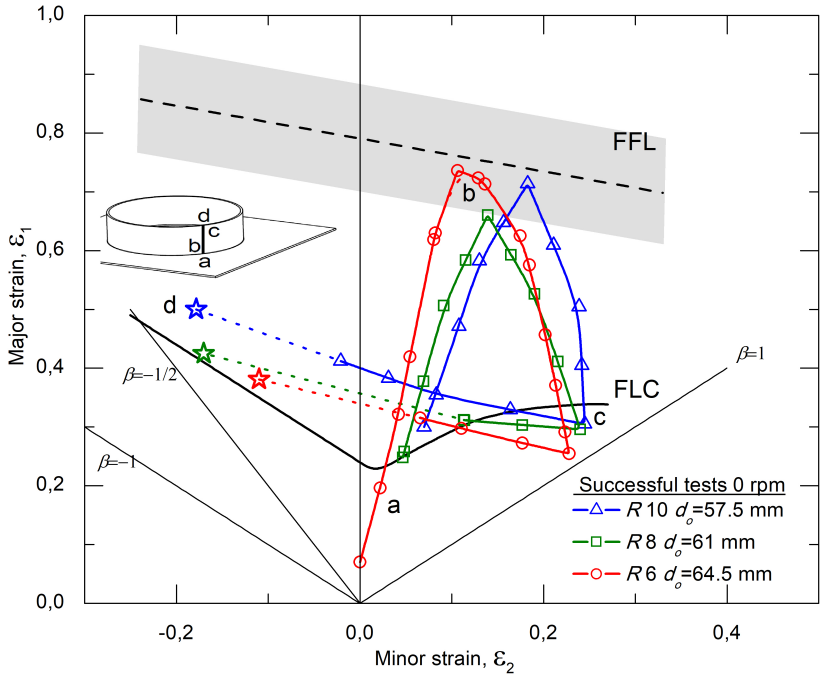

Figure 4.5 FLD with the evolution of strain paths along the final flange for successful tests with the minimum pre cut hole diameters at 0 rpm

Deformation along the flange can be divided into two parts. The first part is zone *a-b-c*, where the material is primarily deformed by in-plane stretching under biaxial strain conditions. Here, the major principal strain, in the axial direction, reaches a maximum value at point *b* near the central region of the flange and starts to decrease. This strain is driven by the concurrence with an increasing circumferential stretching in the flange. At point *c*, note that the major principal

strain direction changes from the axial direction (in zone *a-b-c*) to the circumferential direction (in zone *c-d*). The second part is zone *c-d*, near the hole edge, where the material is primarily subjected to circumferential stretching and bending. In this region, the strain state evolves from equibiaxial stretching (point *c*) to uniaxial tension at the hole edge (point *d*). Similar results have been obtained at 1000 rpm, which are not represented here for clarity. These evolutions are consistent with the previous work of Alkas-Yonan *et al.,*2014 for hole flanging by SPIF using multiple-stage strategies.

The strain evolutions for the failed tests near the first successful flange for each tool radius are depicted in Figure 4.6. Only the results at 0 rpm are presented for clarity.

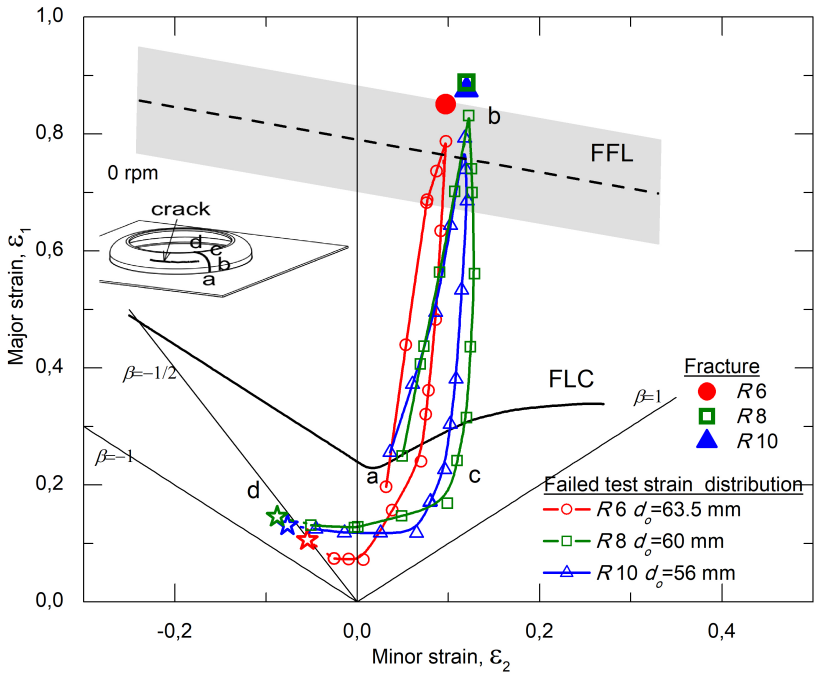

Figure 4.6 FLD with the evolution of strain paths along the final flange for failed tests closest to success at 0 rpm

As shown, the strain loop becomes steeper and sharper than that in the successful tests, which denotes a more severe deformation of the material. The low deformation levels exhibited in the zone *c-d* are consequences of the test interruption once the crack appeared (see the illustration in Figure 4.6). The

fracture strains at point *b* measured on the crack lips are shown by open marks. As expected, the fracture strain is reasonably located above the FFL scatter band obtained with the Nakazima tests.

As previously mentioned, the failed tests were interrupted as soon as a crack was observed. To analyse the failure mechanism, these specimens were cut across the crack at the fracture initiation site. The sections were mechanically polished and observed under a microscope. Figure 4.7 shows the fractographies of the failed specimens formed with the tool radii R = 6, 8 and 10 mm and pre cut holes of 63.5 mm, 60 mm and 56 mm, respectively.

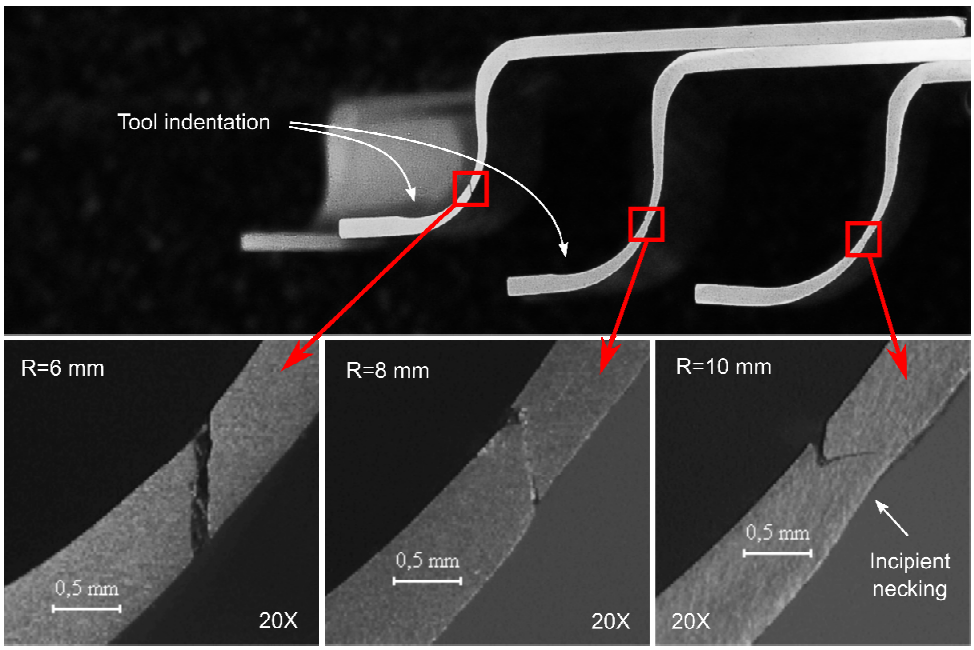

Figure 4.7 Fractographies of the failure zone for failed tests

The fractographies of the smaller tools, i.e., radii of 6 and 8 mm, show a clear through-thickness shear crack without any evidence of local necking in the crack initiation zone. This finding indicates that local necking was completely suppressed, and ductile fracture was the only active mechanism of failure. However, in the fractography of the tool with a radius of 10 mm, an incipient necking zone is clearly evidenced. According to a previous deformation analysis, the necking mechanism was inhibited at a very early stage, which changed the failure mode from necking to ductile fracture. This inhibition and even suppression of necking are causes of the enhancement of formability exhibited in

the SPIF processes, which is primarily attributed to the beneficial effect of the local and incremental deformation and the bending induced in the material, as discussed in Silva *et al.,*2011 and Centeno *et al.,*2014.

Another interesting effect appreciated in Figure 4.7 is the level of indentation performed by the tool into the sheet. As the tool radius decreases, a deeper indentation mark between the curved zone and the still-flat flange is observed. This indentation hinders the material flow from the flat flange to the formed wall (formed flange). Thus, the higher is the restriction, the higher is the stretching of the formed flange. Any event to facilitate this flow, such as improving lubrication and reducing the step-down, should yield a slight enhancement in formability.

The results conclude that the failure mechanism in the single-stage hole flanging by SPIF, either by necking or directly by fracture, is highly influenced by the strain/stress gradient through the sheet thickness, which is typically characterized by the bending ratio. Generally, a high bending ratio should improve the formability of the flange. This finding is consistent with previous research by Morales-Palma *et al.,*2013 on stretch-bending and Silva *et al.,*2011 and previous research by Centeno *et al.,*2014 on SPIF. However, an excessive bending ratio may reduce the expected enhancement of formability by blocking the material flow around the forming tool. Recent work by Al-Ghamdi *et al.,*2015 suggests the existence of a threshold tool radius that maximizes the formability in SPIF.

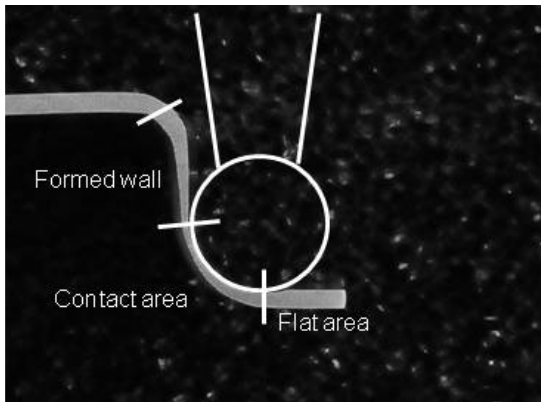

Figure 4.8 Deformation zones on the in-process workpiece

Three deformation zones can be distinguished on the in-process workpiece (see Figure 4.8), the cylindrical flange that is already formed, the curved sheet in contact with the tool during the process of forming and the still-flat sheet that is being radially stretched. The latter is essential to the success of the operation as the larger is this zone, the greater is the deformation resistance. The location of the

fractures exposed in Figure 4.7show agreement with the studies of Fang *et al.,* 2014,who propose an analytical model of the deformation and fracture of the sheet in AA1100 and consider the bending and strain hardening effect. Fang theoretically proved that the fracture occurs first on the outer side of the wall at the transition area between the contact and non-contact zone due to the bending effect.

To conclude this subchapter, a specimen with a 57 mm diameter pre cut hole and a 10 mm forming tool radius at 0 rpm that is labelled with "D" in Table 4-1 are discussed.

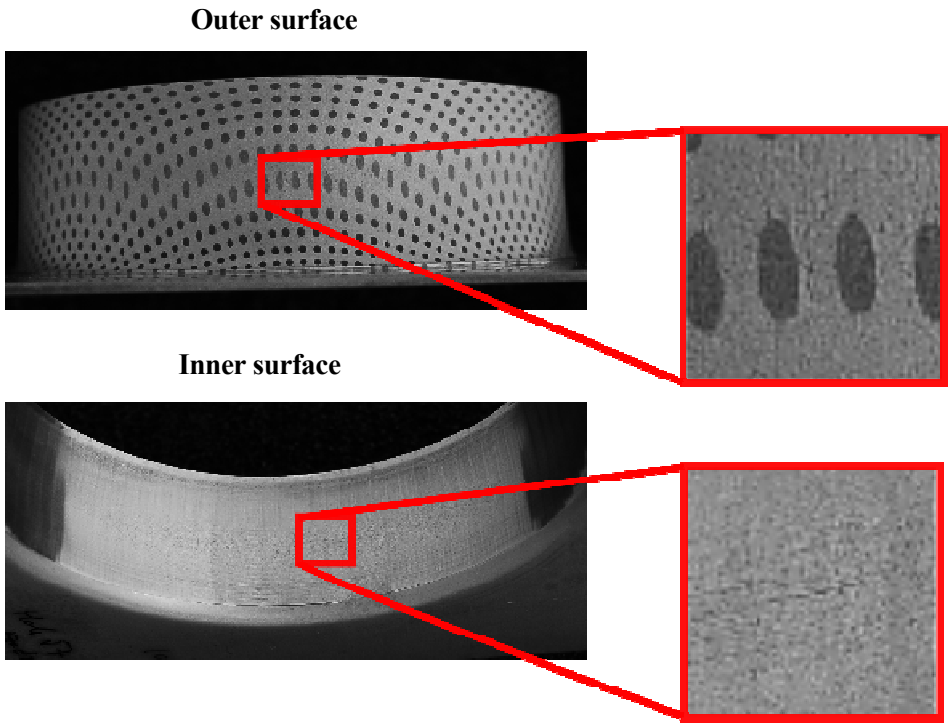

Figure 4.9 Worst surface quality of the flange obtained in the test with a 10 mm tool radius, 57 mm initial hole diameter and 0 rpm spindle speed: tiny microvoids at the outer surface and grooves in the inner surface follow the forming tool path

Figure 4.9 shows the surface quality of this specimen. The central area of the finished flange exhibits visible grooves that follow the forming tool path at the inner surface and microvoids and microcracks at the outer surface. This figure shows the sheet has already reached its formability limit, being the prelude to ductile fracture by coalescence of these microcracks. As a consequence of these surface defects, the

measured strains at the flange centre may be very inaccurate, overestimating the real values. This seems to be the explanation for the strain evolution of the meridional cut well above the FFL shown in Figure 4.4 for this test.

A similar effect may explain the behaviour observed for the test with an 8 mm radius tool at 1000 rpm and a 60 mm diameter pre cut hole, which exhibits a flange height and *TR* value that is substantially higher than those obtained with the smallest tool. In this case, only sporadic microvoids and microcracks were observed at the flange surface, which contradicts the previously observed generalized pattern. As a result, this test was labelled "O" in Table 4-1 instead of "D". Although a functional flange seems to be produced, the material is beginning to exhibit signs of exhaustion, such as a flange that is more lengthened than expected, which should not be confused with an effective gain in formability.

4.4. Formability analysis based on the LFR

*As mentioned in the previous section, the forming severity in conventional circular hole flanging is measured by the hole expansion ratio (*HER*), and the formability is quantified by the limiting forming ratio (*LFR*).*

Table 4-3 shows the values of the *HER* and *LFR* for the successful tests at 0 rpm. The *LFR* increases as the tool radius increases, that is, the higher is the tool radius *R*, the smaller is the minimum pre cut hole diameter that is required to obtain a successful flange. For the tools analysed here, the higher *LFR* value was 1.65 for the tool with a 10 mm radius. This result appears to conflict with accepted SPIF trends, which show that formability in SPIF increases as the tool radius decreases, as previously discussed.

The explanation for this apparent inconsistency in the *LFR* in measuring the formability in incremental hole flanging is that this parameter only considers the maximum strain at the hole edge (circumferential strain), assuming that failure will appear at this location. As previously discussed, failure in incremental hole flanging is controlled by the severe stretching and thinning in the material of the flange. Failure is governed by the deformation in the entire flange, particularly by the axial strain around the middle of the flange instead of only the circumferential strain at the hole edge.

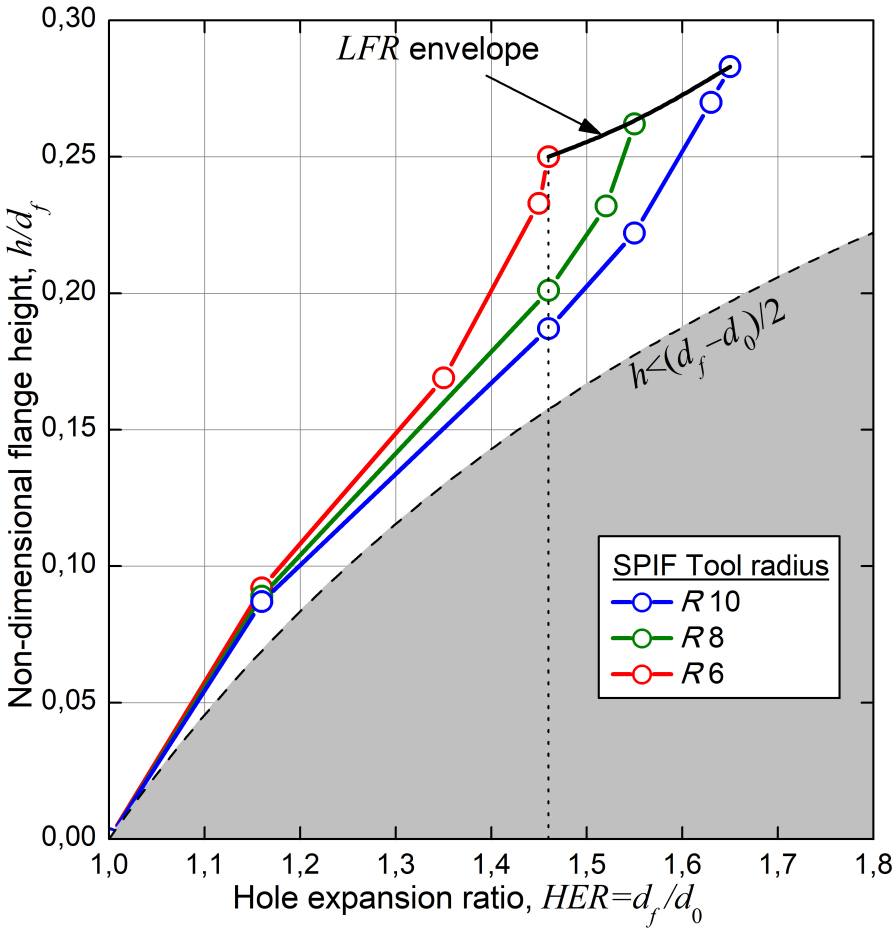

Figure 4.10 Non-dimensional flange height (h/d_f) of successful hole-flanged sheets for different pre cut diameters at 0 rpm

A direct parameter that quantifies the stretching that the flange underwent is the flange heighth presented in

Table 4-3. Figure 4.10 depicts the evolution of the non-dimensional flange height h/d_f versus the *HER*. For a given *HER* (for instance, the vertical dotted line), the non-dimensional flange height h/d_f increases as the tool radius decreases, which shows agreement with the expected trend and indicates that the formability of the flange increases as the bending ratio (t_o/R) increases.

Note that the non-dimensional flange height h/d_f in Figure 4.10 has been extrapolated to zero for a pre cut hole d_0 that is equal to the final hole d_f (HER = 1). For large pre cut holes (typically, HER<1.2), the flange height is practically independent of the tool radius and no gain in formability is obtained from reducing the tool radius. As indicated in the previous chapter, the physical limit for the flange height is depicted (dashed line).

According to these results, a more appropriate parameter for measuring the formability of the flange is the thickness ratio, which is obtained by assuming volume constancy during the flange deformation. This approach yields the formula

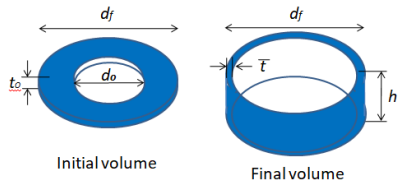

$$\pi d_f h \bar{t} = \frac{\pi}{4}(d_f^2 - d_0^2)t_0 \qquad (4\text{-}1)$$

where $\bar{t}$ is the average thickness in the finished flange. Note that this equation realistically combines the axial, the circumferential and the thickness deformation undergone by the flange. Thus, the average thickness ratio (TR) may be written as follows:

$$TR = \frac{\bar{t}}{t_0} = \frac{d_f^2 - d_0^2}{4 d_f h} \quad \rightarrow \quad TR = \frac{1 - 1/HER^2}{4(h/d_f)} \qquad (4\text{-}2)$$

As shown in Eq. (4-2), for a given HER, the higher is the flange, the lower is the average thickness ratio. The experimental values of TR are shown in Table 4-3. For a given HER, TR decreases as the bending ratio (t_o/R) increases. As expected, in practice, smaller tools are able to further stretch the material of the flange provided that the initial pre cut hole is above the critical hole established by the minimum radius tool.

A similar trend is also observed in tests at 1000 rpm, as shown in Table 4-2. An exception is obtained for the tool with an 8 mm radius, which yield a TR value that is notably smaller than that obtained with the 6 mm radius tool.

4.5. Thickness, surface roughness and flange shape

The thickness profiles were measured with a Nikon SMZ800 microscope (magnification, x20) and commercial image processing software. Figure 4.11 presents the thickness profile along the flange in the rolling direction obtained in two hole flanging tests at 0 and 1000 rpm. No significant differences were observed in the shape of the profiles measured in other directions. The results correspond to tests performed with a 6 mm radius tool in blanks with a 64.5 mm diameter hole.

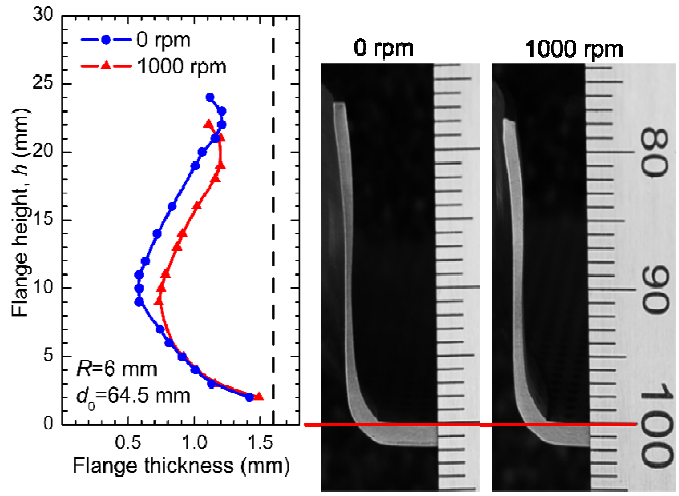

Figure 4.11 Sheet thickness along the flange formed with spindle speeds of 0 and 1000 rpm

The thickness reduction presents a wavy profile along the flange height, with a maximum reduction of 62% (0 rpm) and 53% (1000 rpm) around the middle of the flange (point *b* in Figure 4.3 (upper)). The experimental results of multi-stage hole flanging noted by Cui *et al.,*2010 present a similar evolution in the thickness distribution by forming a successive conical frustum of an increasing angle to 90º. Although the thickness distribution provided by SPIF can be improved using an appropriate multi-stage strategy, as reported by Skjoedt *et al.,*2010 and Mirnia *et al.,*2014, assuming its geometrical restrictions, a single-stage strategy may provide functional flanges in considerably less time.

As deduced from Figure 4.11, a higher spindle speed yields a final flange with a

slightly more uniform thickness profile, which reduces the risk of sheet failure. Durante *et al.,*2009 attributed this effect to friction reduction and increased temperature. The lower friction reduces the forming force and stretching stresses, which promotes a lower thickness reduction in the area that is being deformed.

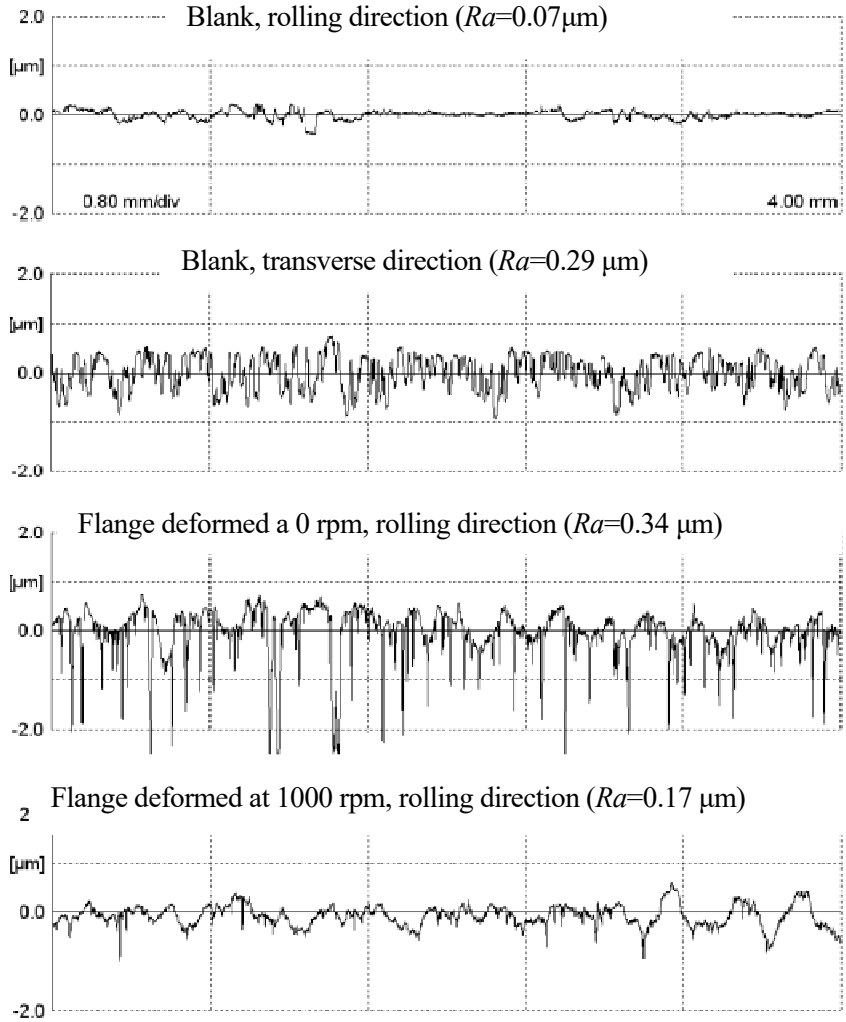

Figure 4.12 Roughness profile Ra of a blank sheet (0° and 90° RD) and deformed flange (0 and 1000 rpm),which correspond to a specimen tested with a 6mm tool radius and 65 mm initial hole diameter

Another beneficial effect of increasing the tool rotation is the lower roughness

observed in the inner sheet surface in contact with the tool. Figure 4.12 shows the roughness profile *Ra* that is measured in the blank prior to forming, in the rolling and transverse directions and in the final flange at 0 and 1000 rpm. A Mahr® M1 perthometer was employed. *Ra* is reduced by almost 50% when the speed rotation is increased from 0 rpm (0.34 μm) to 1000 rpm (0.17 μm). Note that the absolute values of *Ra* are highly dependent on the step down, which is fixed to 0.2 mm in all tests in this study.

This improvement of superficial quality has also been attributed to friction reduction by Durante *et al.,*2009. Numerous authors have recently investigated new tools and techniques to reduce friction in SPIF to enhance the formability and surface quality, e.g., using laser surface texturing tools, as proposed by Xu *et al.,* 2013, or oblique roller ball tools, as suggested by Lu *et al.,*2014.

The final shape must be considered. In Figure 4.13, two sections are superposed, red and black. The section in red is the section of the theoretical shell that is used to program the theoretical flange profile by CATIA® V5 to a final hole flange with a diameter of 95.8 mm. The black section is the result of a hole flanging by SPIF using a tool diameter of 16 mm and a pre cut hole with a diameter of 61 mm. The scanned image and section were performed with the 3D Geomagic Capture® scanner with a precision between 0.060 and 0.118 mm depending on the capture distance.

Due to the non symmetry of the forming process (the tool is shaping on one side while nothing occurs on the opposite side) and the stiffness of the tool, which acts as a small cantilever beam (stiffness is especially low for small tool diameters), achieving a theoretical final diameter is challenging.

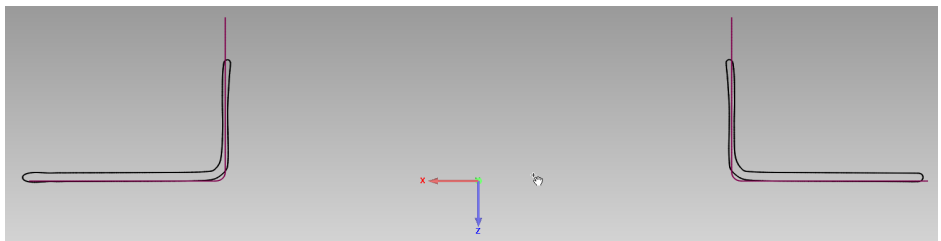

Figure 4.13 Section of specimen R8 with a pre cut hole with a61mm diameter, scanned and compared with the theoretical profile.

Although low springback effects were also observed, the tendency seemed to be regular and only a wider tool trajectory design would be sufficient for achieving a 95.8 mm diameter hole flange.

4.6. Forming Forces

According to part geometry and tool trajectories, the two main force components involved in the process are the vertical force F_z and the horizontal force F_h. The former, which is directly measured by the dynamometer, is primarily related to the stiffness in the axial direction of the flange and the friction force in the tool due to the material flow from the flat part towards the flange in the wall. The latter is related to the circumferential deformation of the flat part and the friction force in the direction of the tool feed, which can be calculated from the measured forces F_x and F_y as

$$F_h = \sqrt{F_x^2 + F_y^2} \tag{4-3}$$

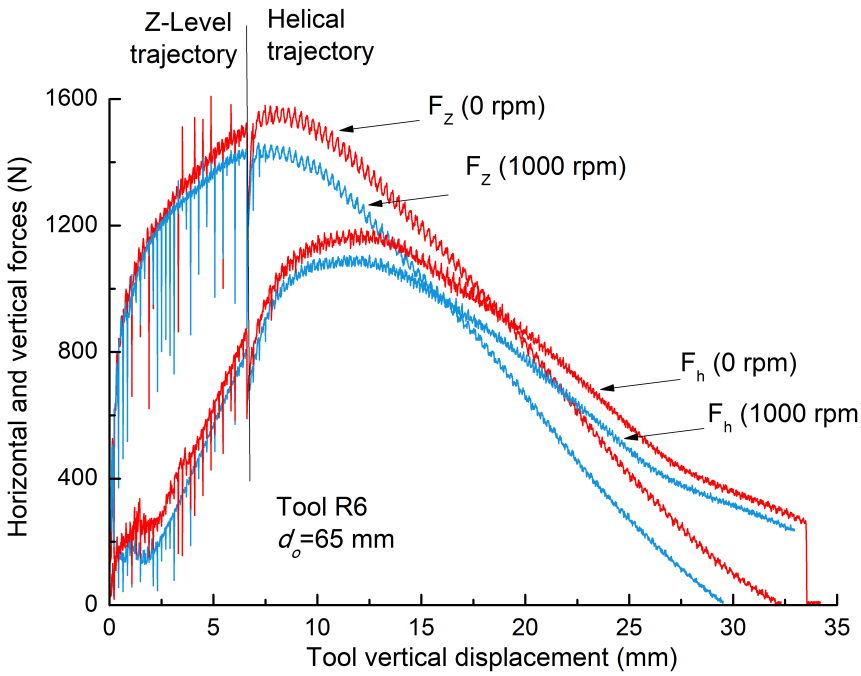

Figure 4.14 Horizontal and vertical force components vs. tool vertical displacement for successful tests at different spindle speeds.

Figure 4.14 compares the typical evolution of F_h and F_z in two successful tests with a tool radius of 6 mm at 0 and 1000 rpm. As expected, smaller forming forces are required at 1000 rpm. In both cases, the vertical force F_z predominates over F_h at early stages of the forming process. This force rapidly increases to a maximum value and decreases to zero at the end of the test. The horizontal force shows a similar evolution but subsequently reaches the maximum value. A nonzero value is obtained at the end of the test due to the springback force exerted by the formed flange over the tool. In both cases, the transition between the z-level and the helical path of the tool is identified.

A comparison of the evolution of the horizontal force-to-vertical force ratio (F_h/F_z) during the test for a successful specimen and a failed specimen is interesting. Figure 4.15 shows this ratio for the successful tests discussed in Figure 4.14 (65 mm diameter pre cut hole) and their nearest failed tests (63.5 mm diameter pre cut hole). Excluding the initial z-level phase, in successful tests, the F_h/F_z ratio monotonically increases during the helical phase until the flange is finished. However, in failed tests, the F_h/F_z ratio shows a maximum value and then decreases until failure occurs. This evolution was observed in all tests analysed in this study.

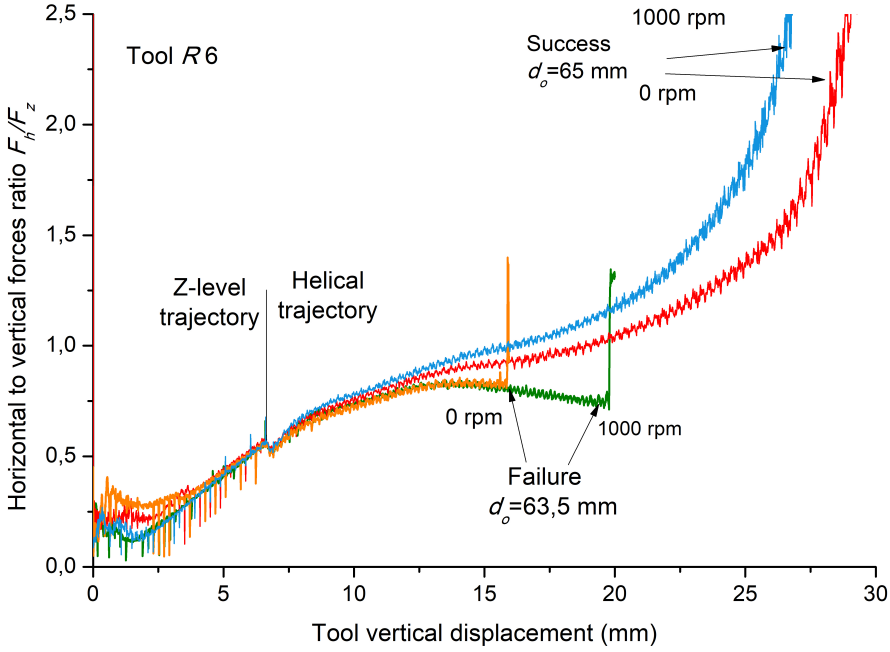

Figure 4.15 Horizontal-to-vertical forces ratio (F_h / F_z) for successful and failed tests at different spindle speeds

The explanation for this increasing F_h/F_z ratio in successful tests is based on the fact that the material in the wall is more resistant than the still non deformed material in the flat part (below the forming tool), yielding an appropriate material flow to form the flange. However, the appearance of a maximum and the subsequent decrease in the F_h/F_z ratio indicates that the deformation in the wall is more intense than in the flat part, giving rise to a failure by excessive stretching of the wall.

Apart from the physical explanation, note that the appearance of this maximum in the forces occurs in advance of the final failure. Therefore, monitoring this force ratio during the process may help to anticipate the sheet failure and control the process in practice.

To study the tool punch radius effect in forming forces, Figure 4.16 compares the three axial forming forces of the tool radii 6 mm, 8 mm and 10 mm for the same initial 65 mm diameter pre cut hole and 0 rpm spindle speed.

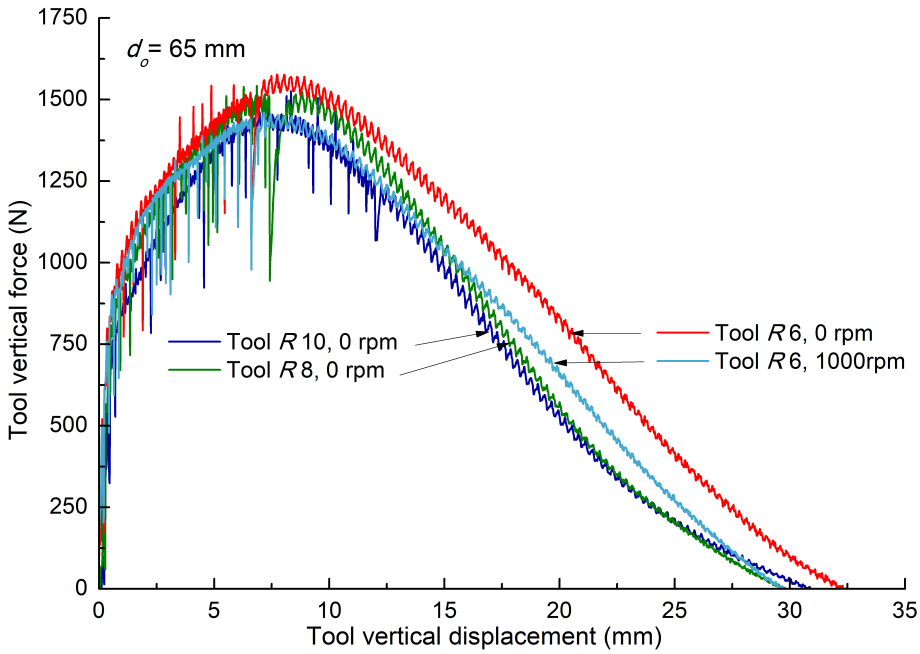

Figure 4.16 Vertical Forces for an initial pre cut hole with a 65 mm diameter and punch tool radii of 6, 8 and 10 mm

Although the total amount of material to be conformed was the same for all three tests, the larger radius of the punch allowed the material to flow more easily from

the flat part to the wall than the smaller radius; thus, the axial forces were lower. Reducing the friction coefficient by increasing the spindle speed can balance the punch radius effect. Figure 4.17 shows the radial force evolution for a punch tool radius of 10 mm and 8 mm at 0 rpm and 6 mm with and without a spindle speed for the same initial pre cut hole of 65 mm diameter. Contrary to the axial force evolution, a larger tool radius produces higher radial forces due to the amount of material involved in the forming process.

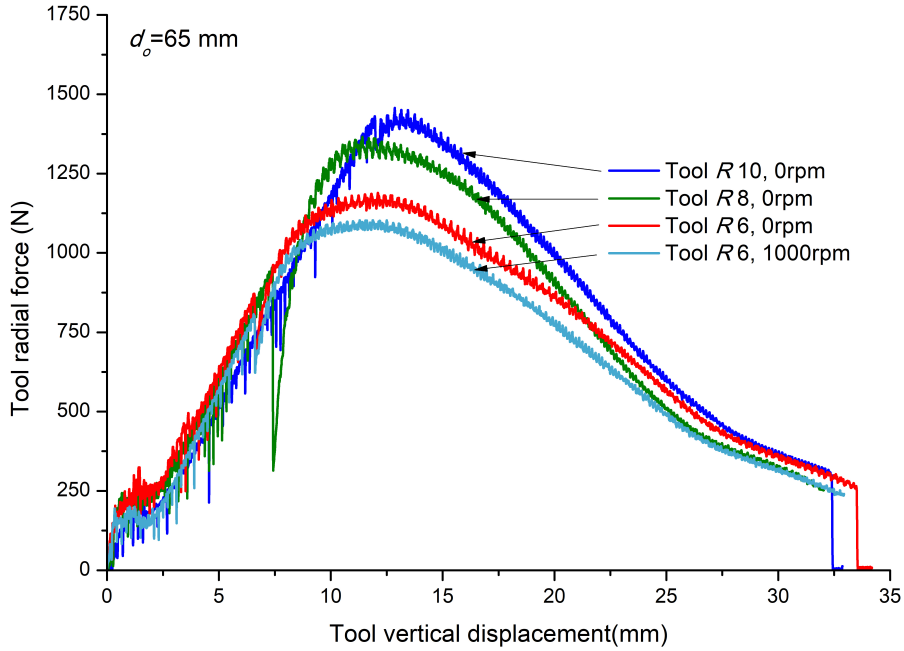

Figure 4.17 Radial forces for an initial pre cut hole with a 65 mm diameter and punch tool radii of 6, 8 and 10 mm

4.7. Conclusions

The capability of SPIF to successfully perform hole flanging operations using a single-stage strategy has been analysed. The material is a 7075-O aluminium alloy sheet with a thickness of 1.6 mm. A series of sheet metal blanks with different pre cut holes has been incrementally deformed using three different hemispherical forming tools with radii of 10 mm, 8 mm and 6 mm and two spindle speeds, 0 and 1000 rpm clockwise. The main conclusions can be summarized as follows:

- The dominant failure mechanism in this process has been determined. As discussed, the sheet failure is produced by biaxial stretching near the midway of the deformed flange instead of uniaxial tension at the hole edge, as usually observed in conventional hole flanging operations.

- Typical for SPIF, the bending ratio t_o/R has an important role in the failure mode. For the smaller tools (6 mm and 8 mm radii), the mechanism of failure is ductile fracture with a complete suppression of local necking. For the larger tool (10 mm radius), the observed mechanism is ductile fracture with postponed necking at the very early stage.

- A higher limiting forming ratio *LFR* obtained is 1.66 for the larger tool radius. For the tools in this study, the *LFR* increases as the tool radius increases.

- As failure in incremental hole flanging occurs via severe stretching and thinning of the flange, the non-dimensional flange height (h/d_f) and the average thickness ratio ($\bar{t}/t_o$) seem to be more appropriate parameters for evaluating the geometric capability of the process. Thus, as the tool radius decreases, h/d_f increases and $\bar{t}/t_o$ decreases for a given initial pre cut hole. This finding shows agreement with the expected trend in SPIF, which indicates that the capability of forming a flange increases as the bending ratio (t_o/R) increases.

- The use of spindle speed does not significantly increase the formability in terms of the minimum pre cut hole to be successfully machined. However, spindle speed provides other interesting advantages, such as better surface quality, a more regular thickness profile along the flange and a reduction in forming forces. Therefore, the use of spindle speed is highly recommended in this demanding single-stage process.

- To increase the dimensional accuracy and due to low springback effects, initial theoretical tool trajectories need to be modified.

- The evolution of forming forces during the process, particularly the ratio of the horizontal component to the vertical component, can be useful in predicting sheet failure in practice.

In the next chapter, a comparison between the conventional hole flanging process and the incremental hole flanging process will be presented.

5. CONVENTIONAL *VS.* INCREMENTAL HOLE FLANGING

In this chapter, the two forming processes to produce the hole flanged parts analysed in previous chapters (single point incremental forming in a single stage and conventional press working) are compared from both a formability point of view and a technological point of view. The formability is analysed in terms of the strain distribution, failure modes, failure location, formability limits and tool radius effect. The technical features that are considered include the geometrical properties, such as flange height and thickness distribution, dimensional accuracy, machine requirements and processing time.

5.1. Selection of experimental results for comparison

The comparison between the two manufacturing technologies in this thesis to produce hole flanged parts is performed via the experimental results. As discussed in chapters 3 and 4, an extensive experimental campaign was planned to capture the limit between the successful flanges and failed flanges obtained with different forming conditions.

Table 5-1 lists the results of all experimental tests. The failed and successful flanges by single-stage SPIF and conventional press working are distinguished with “X” and “O”, respectively. “Tool” represents either the tool radius in SPIF or the punch edge radius in conventional hole flanging.

There are a priori different criteria to select a set of tests to compare both manufacturing processes. In terms of geometric features, analysing the tests performed with identical blanks, that is, specimens with the same pre-cut-hole (d_0), seems to be appropriate. In this regard, successful flanges from 61 and 65 mm pre cut hole diameters have been chosen. These flanges are highlighted in bold symbols in Table 5-1.

Table 5-1 Compilation of experimental hole flanging tests by single-stage SPIF and conventional press working ("X" - failed flange; "O" - successful flange). Specimen candidates for comparison are denoted by boldface symbols

Tool	Hole flanging process		Initial pre cut hole diameter, d_o (mm)																		
			35	41	55	56	57	58	58	59	60	61	63	64	65	65	70	72	82	83
R6	SPIF in a Single stage	0 rpm					X				X		X	X	O	**O**	O		O	
		1000 rpm												X	O	**O**				
	Press-working		X						X		X	**O**				**O**		O		**O**
R8	SPIF in a Single stage	0 rpm					X				X	**O**	O			**O**				
		1000 rpm								X	O	**O**								
	Press-working			X					X		X	**O**				**O**		O		**O**
R10	SPIF in a Single stage	0 rpm			X	X	X	O	O			**O**				**O**			O	
		1000 rpm			X	X	O	O												
	Press-working								X		X	**O**				**O**		O		**O**
R47.9	Press-working								X		X	**O**				**O**		O		**O**

To evaluate the differences in the sheet strain distribution, a comparison of the tests from equal blanks (equal pre cut hole) and similar bending conditions induced by the forming tool is desirable. As shown in Table 5-1, two pairs of candidates are tested from 60 and 61 mm pre cut hole diameters with a 8 mm tool radius or punch edge radius. These tests correspond to a successful flange and failed flange in SPIF at 0 rpm and in a conventional press.

Note that the comparison of both technologies is restricted to 7075-O aluminium sheets with a thickness of 1.6 mm with hole flanges with an inner diameter of 95.8 mm. Therefore, although qualitative results should maintain, different results might be obtained for others materials and/or geometries.

5.2. Strains distribution in the flange

The analysis of the strain distribution in the outer sheet surface is the key to understanding the geometrical differences among the flanges manufactured by both forming processes. As previously mentioned, the tests from the 61 mm pre cut hole diameter with 8 mm tool radius in SPIF and the 8 mm edge radius in conventional press working are selected for this analysis.

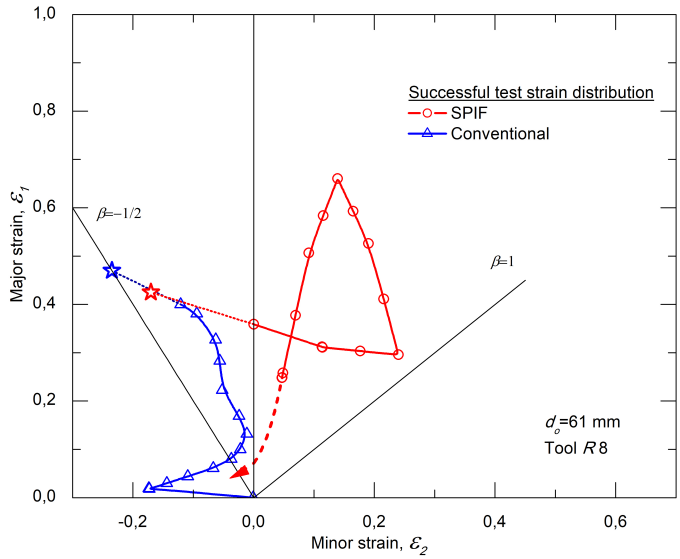

Figure 5.1 Evolution of the principal strains along the flange in SPIF and conventional press for a pre cut hole with a diameter of 61 mm and 8 mm tool radius

Figure 5.1 presents the principal strain distribution along the flange in the rolling direction at the outer sheet surface for both successful tests. As in previous chapters, the solid lines represent the strains that are directly measured with ARGUS®. The starting points are the estimation of the strain values at the edge of the flange by direct measurement of the edge thickness and the circumferential length of the flange to obtain their corresponding strains and apply volume constancy to estimate the meridional strain.

Note the loop presented by the in-plane principal strain in SPIF in contrast with the evolution in conventional press working. This strain inversion is a consequence of the attempt to cross the SPIF strains with the first-quadrant bisector. This finding can be better appreciated in Figure 5.2, where the strains in the circumferential and meridional directions are displayed instead of the principal major-minor strain. The SPIF strain intersects the bisector in two locations along the flange.

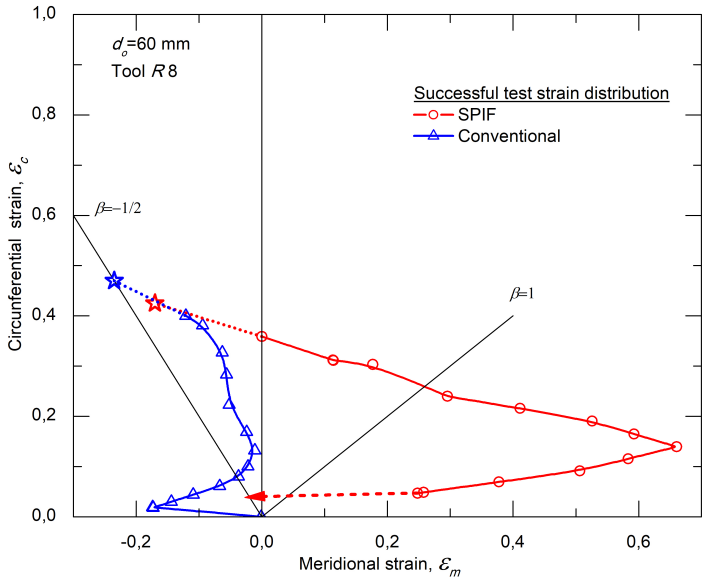

Figure 5.2 Evolution of meridional and circumferential strain along the flange in SPIF and conventional press for a pre cut hole with a diameter of 61 mm and 8 mm tool radius

A comparison of the strain evolution in both processes indicates that the level of circumferential strains is almost the same in both cases because this strain is primarily geometrical; the level of the circumferential strains is also related to the change in length between an undeformed circumference and its corresponding

deformed circumference. However, meridional strains are completely different. While an SPIF strain displays a high positive value around the middle of the flange, the strain in press working shows a moderate negative evolution. According to this observation, the SPIF process produces higher flanges than the conventional process. Conversely, flanges with a more uniform thickness distribution are expected to be obtained by the conventional process instead of the incremental process. The negative meridional strain exhibited at the bottom of the flange in the conventional process is attributed to the severe bending in the sheet induced around the die edge. The same tendency is expected in SPIF.

5.3. Comparison of formability

5.3.1. Analysis based on the FLD

As discussed in previous chapters, different mechanisms of failure occur in press working and the SPIF process. The former is controlled by the local plastic instability, which yields the appearance of necking, and the latter is governed by the ductile fracture of the material with a notable delay or total suppression of the development of this neck.

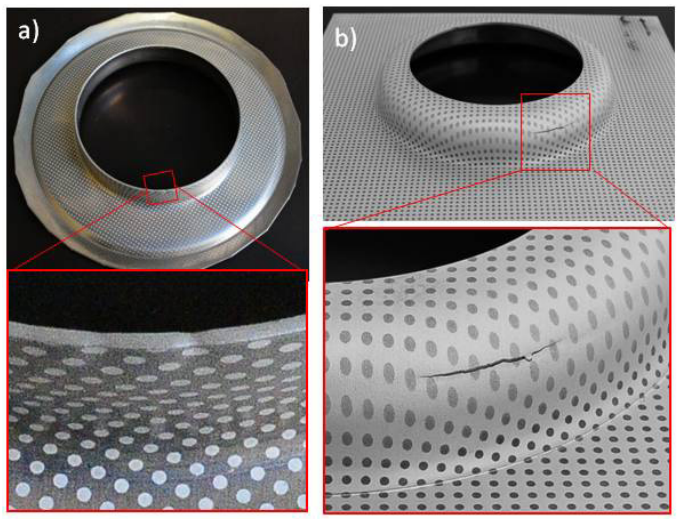

Figure 5.3 Comparison of the mechanisms of failure between both flanging processes. Failed tests with a 60 mm pre cut hole diameter andan 8 mm tool radius by conventional press forming (a) and single-stage SPIF at 0

rpm (b)

Figure 5.3 shows the mechanisms of failure and initiation sites in both processes. These tests correspond to non-successful specimens with a 60 mm pre cut hole diameter formed with an 8 mm tool radius in SPIF and an 8 mm punch edge radius in a conventional press. In the case of press working (Figure 5.3 a), the formation of a neck is visible at the edge of the flange, while a mode-I type of crack is observable around the middle of the flange wall in incremental sheet forming (Figure 5.3 b).

These two events are graphically compared in Figure 5.4. The evolution of principal strains along the flange is represented in the FLD for the same tests shown in Figure 5.3. The major-minor strain evolution for press working intersects the FLC at the edge of the flange (see the start point). As discussed in chapter 3, the FLC is the appropriate failure locus to analyse the formability in this process. The reader is invited to reread this chapter for a detailed explanation about the possibility of strains in the wall flange above the FLC without activating the plastic instability. Conversely, in the single-stage SPIF process, this intersection occurs with the FFL in the wall, far from the flange edge. As established in chapter 4, the FFL is a suitable limiting curve to predict the flange fracture and evaluate the flangeability in sheet incremental forming processes.

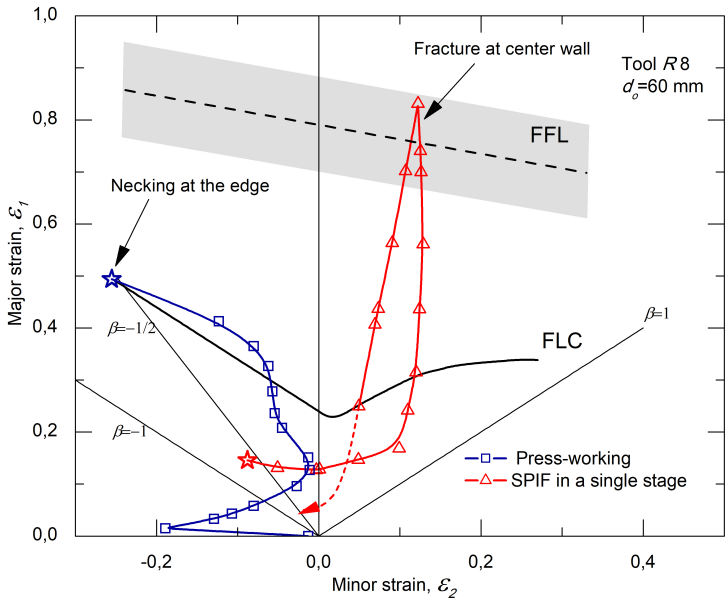

Figure 5.4 Major-minor strain diagram for successful and unsuccessful test strain paths under single stage SPIF and conventional forming processes

5.3.2. Analysis in terms of the LFR

As discussed in chapter 3, the Limiting Forming Ratio (*LFR*) (see Eq. (1-1)) is the parameter that is traditionally employed to quantify the formability in hole flanging operations. Table 5-2 summarizes the *LFR* values obtained in both single-stage SPIF and press working process using different tool radii (*R*6, *R*8, *R*10 and *R*47.9 (only press working)).

Table 5-2 Summary of LFR values in hole flanging by press working and single-stage SPIF and their corresponding non-dimensional height and average thickness of the flange for these specimens

Hole-flanging		Tool *R*6				Tool *R*8			
Single-stage SPIF	Spindle (rpm)	d_0 mm	*LFR*	h/d_f	$\bar{t}/t_0$	d_0 mm	*LFR*	h/d_f	$\bar{t}/t_0$
	0	64.5	1.46	0.25	0.53	61	1.55	0.26	0.56
	1000	64.5	1.46	0.24	0.56	60	1.58	0.28	0.54
Press-working		61	1.57	0.19	0.78	61	1.57	0.19	0.78
Hole-flanging		Tool *R*10				Tool *R*47.9			
Single-stage SPIF	Spindle (rpm)	d_0 mm	*LFR*	h/d_f	$\bar{t}/t_0$	d_0 mm	*LFR*	h/d_f	$\bar{t}/t_0$
	0	57.5	1.65	0.28	0.56	-	-	-	-
	1000	57	1.66	0.28	0.57	-	-	-	-
Press-working		61	1.57	0.19	0.78	61	1,57	0,18	0,81

Three facts can be clearly highlighted. The first fact is the insensitivity of the *LFR* to the punch edge radius in conventional press working, as discussed in detail in chapter 3, where the *LFR* is 1.57. The second fact, which was analysed in chapter 4, is the relative increase in the *LFR* value as the tool radius increases in single-stage SPIF. The maximum *LFR* obtained in this case is 1.66. The third fact is that the gain in formability measured via the *LFR* is not significant in practical terms. Both processes present an approximate *LFR* value of 1.6.

This fact highlights the ability of the *LFR* to compare the formability between both processes. As previously discussed in chapter 4, this parameter considers the maximum circumferential strain at the hole edge, which is consistent with the failure site in a conventional hole flanging operation but far from the failure location observed in SPIF. Two parameters were proposed to measure the

formability of the flange: the non-dimensional height of the flange (h/d_f), as a measure of the stretching undergone by the material in the flange in the meridional direction, and the average thickness ratio ($\bar{t}/t_o$), as a measure of the reduction in thickness undergone by the material in the flange (see Eq. (4-2)). Thus, the higher is the value of h/d_f and the lower is the $\bar{t}/t_o$, the higher is the formability.

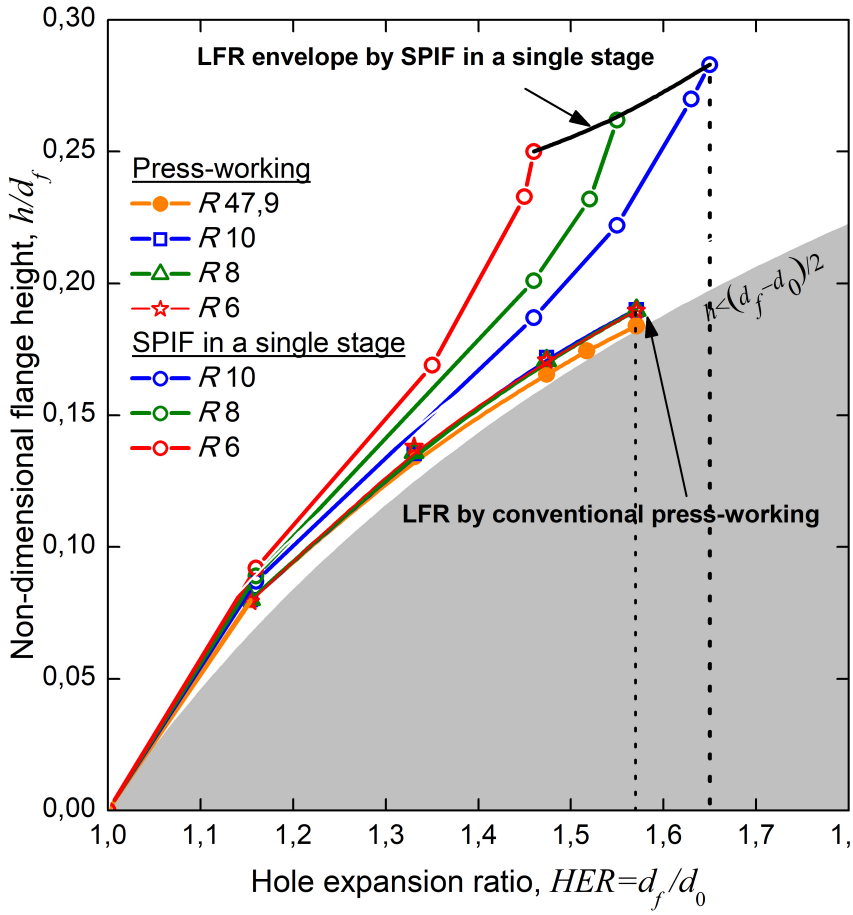

Figure 5.5 Evolution of the non-dimensional flange height (h/d_f) vs. HER of successful hole flanging tests manufactured by press working and single-stage SPIF at 0 rpm

These two parameters are displayed in Table 5-2. As expected, both show insensitivity to the punch edge radius in conventional press working, with values

of approximately 0.19 and 0.78 for non-dimensional height and average thickness ratio, respectively. However, these values significantly different in SPIF, where values of h/d_f, which range from 0.25-0.28, and values of$\bar{t}/t_o$, whichrange from 0.53-0.56, are typically observed at 0 rpm. Similar values are obtained at 1000 rpm, that is, h/d_fvalues from 0.24-0.28 and $\bar{t}/t_o$values from 0.54-0.57.

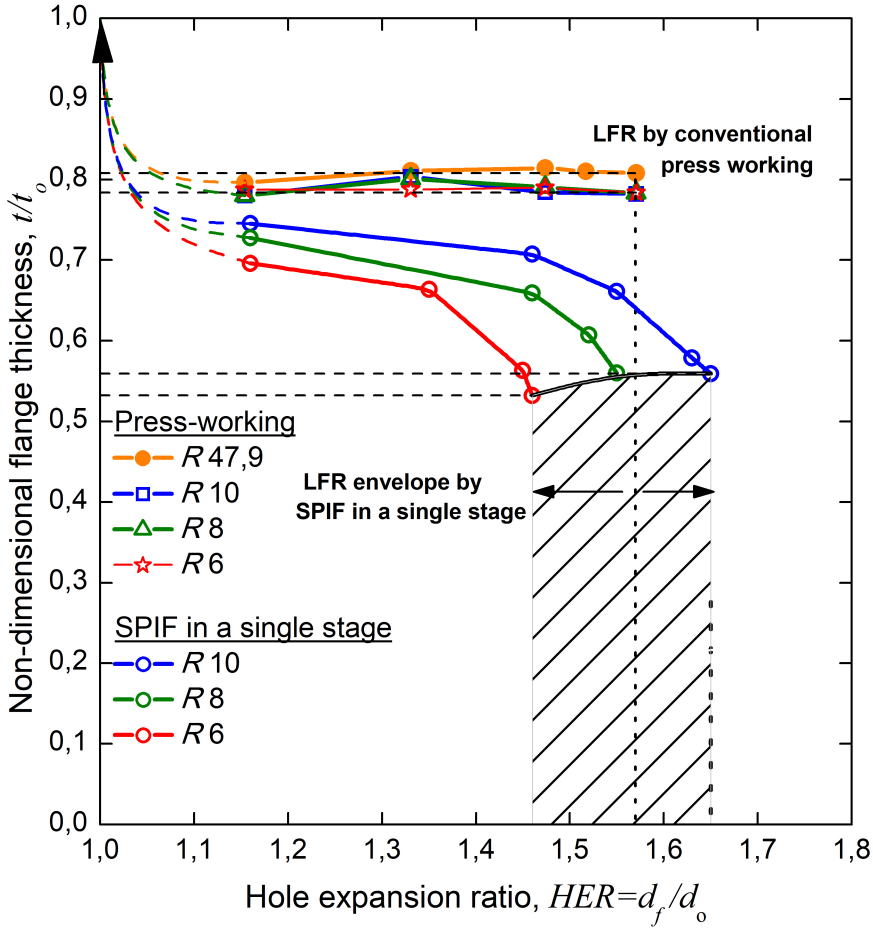

Figure 5.6 Evolution of the average thickness ratio ($\bar{t}/t_o$) vs. HER of successful hole flanging tests manufactured by press working and single-stage SPIF at 0 rpm

Figure 5.5 and Figure 5.6 graphically depict the differences between press working and single-stage SPIF at 0 rpm. All successful hole flanging tests manufactured by both processes are compiled. The experimentally achieved

ranges of h/d_f, $\bar{t}/t_o$ and *LFR* versus *HER* are visualized. Comparing their evolution, the results concluded that single-stage SPIF exhibits a significant enhancement in formability regarding the press working, which is approximately quantified at approximately 40% in terms of relative flange height (h/d_f) and approximately 30% in terms of relative thickness reduction ($\bar{t}/t_o$). This improvement does not manifest when using traditional *LFR* as a measure of flangeability, which reflects the fact that this parameter does not reproduce the mechanism of failure in hole flanging by SPIF.

5.4. Geometrical features

The final shape of the flange is another important factor to compare the feasibility of both processes. The geometrical feature of flanges obtained in tests with a 61 mm pre cut hole diameter and a 8 mm tool radius for press working and SPIF at 0 rpm are analysed.

Figure 5.7 details both specimens before they were processed. They were cut along the meridional direction of the flange and polished. The flange profiles were scanned using the scanner model 3D Geomagic Capture to measure their local shape and thickness evolution.

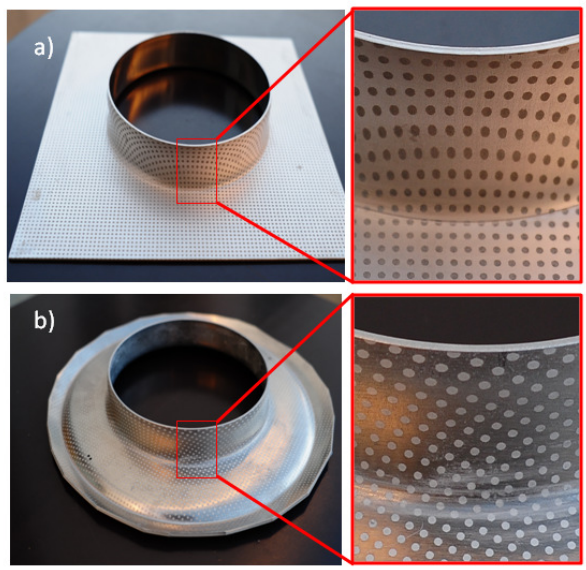

Figure 5.7 Flanged specimens with a pre cut hole with a diameter of 61 mm and 8 mm tool radius by SPIF at 0 rpm (a) and press working (b)

Figure 5.8 displays the flange profile of both specimens. The continuous red line represents the theoretical internal profile of the flange. The distortion is visible in both cases. In the SPIF case, the flange accurately reproduce the theoretical shape at the base and shows a slight inward distortion at the wall. This wall distortion is primarily attributed to the springback of the flange but can also be influenced by the tool deflexion that is exhibited to a certain extent in this process. In the case of press working, although distortion of the wall is similar or even seems to improve regarding the incremental case, the flange shows an important springback at the base. This springback is directly related to the blank-holder force and clamping condition during the tests. This distortion may be improved by increasing the blank-holder force and modifying the clamping system. However, this analysis is beyond the scope of this study, which was originally focused on the comparative evaluation of the formability between both hole flanging processes.

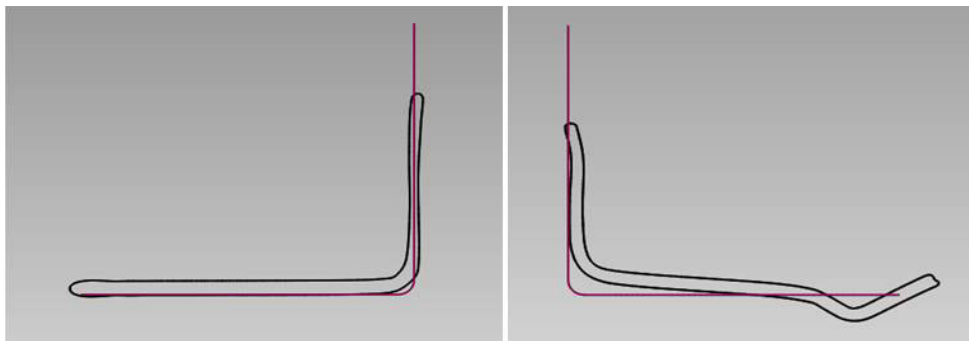

Figure 5.8 Comparison of flange profile from specimens with a 61mm pre cut hole diameter and 8 mm tool radius by SPIF at 0 rpm (left) and press working (right)

The thickness distribution versus the flange height in both tests are shown in Figure 5.9. As discussed in section 0, the thickness distribution in the incremental flange is considerably more irregular than that in press working, as a result of the high strain gradient exhibited in the meridional direction in this process (see Figure 5.2). The large thickness reduction obtained around the middle of the flange is also observed.

According to the Figure 5.9, the local and incremental deformation induced in the single-stage SPIF can intensively stretch the material, which enables higher and thinner flanges for a given *HER* parameter. Conversely, the conventional hole flanging process provides shorter but thicker (more robust) flanges for an identical specimen. Thus, the practical application and service requirements of the flange will determine the more suitable process in each case.

Note that multi-stage SPIF is the most common alternative to the single-stage

process to improve the material distribution during a flanging operation. As highlighted by several researchers (Morales-Palma *et al.,*2017, Skjoedt *et al.,* 2008, 2010, Verbert *et al.,*2008, Duflou *et al.,*2010, Liu *et al.,*2014), multi-stage strategies are able to control the excessive thinning and can improve the dimensional accuracy of the flange. However, apart from an increase in the process complexity, the main drawback is the notable increase in process time as the number of stages (steps) increases.

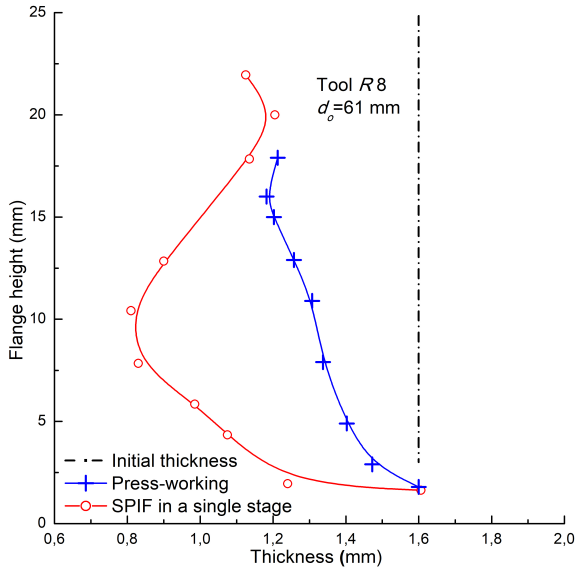

Figure 5.9 Comparison of flange height and thickness for specimens with a 61mm pre cut hole diameter and 8 mm tool radius by SPIF at 0 rpm and press working

5.5. Forming forces and process time

Force requirements and production time are determining factors in the selection of a suitable technology.

Hole flanging by conventional press working requires heavy machinery and dedicated dies and punches for each flanging size. Assuming that the press is available, the high cost of these accessories renders the process acceptable only large production batches.

An incremental hole flanging operation requires considerably less force than a conventional operation, which enables the operation in a standard CNC machine.

In this case, the auxiliary structure and forming tools are substantially less expensive and more versatile than conventional hole flanging dies, which renders incremental sheet forming processes profitable for small production batches. However, their main weakness is the high processing time required for a conventional operation.

This comparison could be completed by quantifying the level of force and process time that is required for performing the hole flanging tests by single-stage SPIF and conventional press presented in this study. The optimization of these process variables was not the aim of this study; thus, the differences listed in Table 5-3 are estimates of the results expected in industrial operations.

Table 5-3 Summary of maximum forming force in z-direction and processing time in both hole flanging operation for tests with a 65 mm pre cut hole diameter and 8 mm tool radius

Hole flanging Operation	Max. forming force (kN)	Processing time (min)		
		Hole milling and deburring	*Set-up time*	*Hole flanging*
Single-stage SPIF: *feed rate: 1000 mm/min, 0 rpm* *stepdown: 0.2 mm/rev, 8 mm tool*	1.5	15	3	30
Conventional press working: *cylindrical punch - 8 mm edge radius* *punch speed: 0.1 mm/s*	30.5		1	1

Table 5-3 summarizes the maximum forming force in the z-direction (vertical) and the processing time required to perform a hole flanging test with a 65 mm pre cut hole diameter and 8 mm tool radius by both technologies. As described in previous chapters, the feed rate and stepdown per revolution used for single-stage SPIF was 1000 mm/min and 0.2 mm/rev, respectively, and the punch speed for press working was 0.1 mm/s.

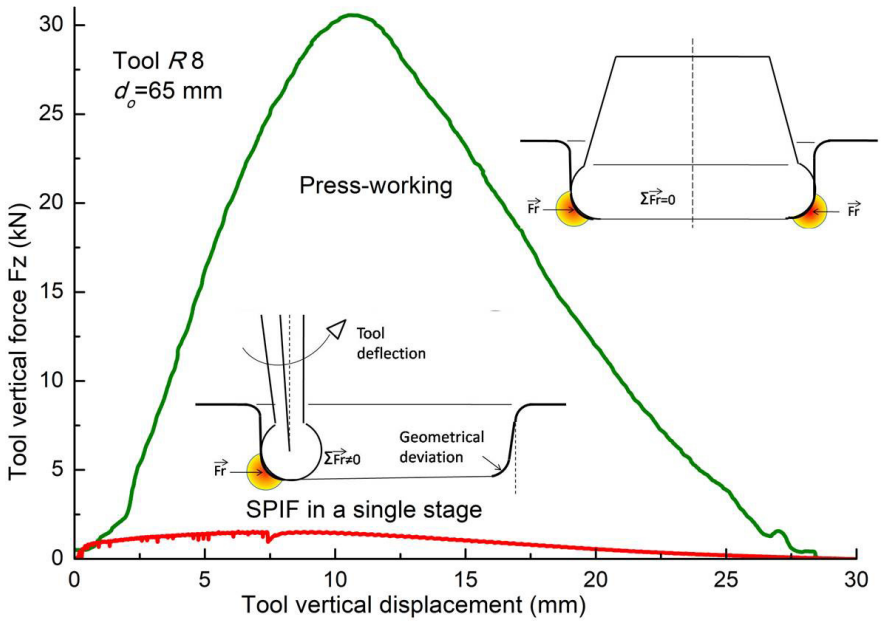

Figure 5.10 Evolution of forming force vs. tool travel in z- direction in single-stage incremental and conventional hole flanging for tests of 65 mm pre cut hole diameter and 8 mm tool radius

Figure 5.10 depicts the evolution of the tool registered in the z-direction as a function of the tool travel in both forming operations. As expected, the maximum force in conventional forming is one order of magnitude higher than the incremental one. As shown in Table 5-3, the maximum forces are approximately 30.5kN and 1.5kN, that is, a difference of approximately 20 times between operations.

Regarding the processing time, the trend reverses. The processing time can be split into three parts: (1) the time for milling and deburring of the initial hole, which is a common operation in both forming processes, (2) the set-up time of the test, that is, the time required to place the specimen, apply the tribological system, and select the process parameters or CNC program, and (3) the hole flanging time, i.e., the time required by the tool to form the flange. Table 5-3 shows the time spent in each of these phases. The flanging time is critical; it is one order of magnitude higher in incremental forming than conventional forming for these tests. This difference can be considerably modified in an industrial context.

5.6. Conclusions

Two hole flanging processes conventional press working and the single-stage incremental forming have been critically compared in terms of flangeability, geometrical features of the finished part and required forming force and time. The main conclusions drawn are summarized as follows:

- Regarding the strain in the flange, the main difference between both processes is derived from the evolution of the meridional strain. In single-stage SPIF, this strain displays a high positive value around the middle of the flange, which is responsible for a longer and thinner flange thanthe flange in the conventional process.

- The analysis based on the FLD satisfactorily reflects the mechanisms that control the flangeability in both processes. In press working, the failure is triggered by necking at the flange edge and controlled by the FLC. In incremental forming, the failure initiates by ductile fracture near the middle of the flange wall and is then controlled by the FFL.

- The traditional *LFR* is not an appropriate parameter for measuring the flangeability in hole flanging by SPIF as it does not capture the physics of failure of this process. A *LFR* value of approximately 1.6 is obtained for both processes.

- Alternatively, the non-dimensional flange height (h/d_f) and the average thickness ratio ($\bar{t}/t_o$) are more suitable for evaluating the flangeability in both processes. In terms of these parameters, the single-stage SPIF exhibits a significant enhancement in formability regarding the press working. A gain in flangeability of approximately 40% and 30% is quantified using h/d_f and $\bar{t}/t_o$, respectively.

- Regarding the flange geometry, the single-stage SPIF is able to perform higher and thinner flanges for a given *HER* parameter. The thinner area locates near the middle of the flange.

- For the tests analysed in this study, the maximum force in conventional forming is one order of magnitude higher than that in single-stage SPIF. This this trend reverses when the processing time is considered.

Without considering the restrictions induced by the volume of production, the

results conclude that conventional press working is preferred to produce shorter, thicker and more homogeneous flanges, whereas single-stage SPIF is better for manufacturing longer and thinner flanges with more flexibility in shape.

6. CONCLUSIONS AND FUTURE WORKS

The capability to successfully perform circular flanges in a 7075-O aluminium alloy sheet with a thickness of 1.6 mm using single-stage SPIF and conventional press working methods has been discussed.

A series of sheet metal blanks with different pre cut holes was conventionally press worked using three cylindrical punches with a diameter of 94.8 mm, different edge radii (10, 8 and 6 mm) and a hemispherical punch (47.9 mm). In hole flanging by a single stage SPIF process, a series of sheet metal blanks with different pre cut holes has been incrementally deformed to a final hole with an inner diameter of 94.8 mm using three different hemispherical forming tools with the same radii (10 mm, 8 mm and 6 mm) and two spindle speeds 0 and 1000 rpm clockwise.

Both forming processes have been analysed and compared in terms of strain evolution, mode of failure, geometric features of the fabricated flanges, such as flange height and shape, thickness distribution, surface roughness, and process features, such as forming forces and time. The formability study was performed based on the classical *LFR* parameter and the conventional FLD obtained from Nakazima tests. Two alternative parameters were proposed to better quantify the flangeability.

This chapter presents a brief compilation of the main conclusions of this study as highlighted Chapters 3, 4 and 5. The reader is referred to these previous chapters for an exhaustive and detailed description of the conclusions.

6.1. Conclusions

The main conclusions of this study can be separated into three categories: formability issues, geometric features and process features.

- ***Formabilty***

The sheet failure in hole flanging by single stage SPIF is produced by biaxial

stretching around the midway of the deformed flange instead of by uniaxial tension at the hole edge, as observed in hole flanging by conventional press working.

According to the deformation analysis of failed specimens by single stage SPIF, the necking mechanism is inhibited at a very early stage, which changes the failure mode from necking to ductile fracture. The bending ratio t_o/R has an important role in the failure mode. For the smaller tools (6 mm and 8 mm radius), the mechanism of failure is ductile fracture with a complete suppression of local necking. For the larger tool (10 mm radius), the observed mechanism is ductile fracture with postponed necking in the very early stage. This inhibition and suppression of necking is the cause of the enhancement of formability that is exhibited in SPIF processes, which is primarily attributed to the beneficial effect of the local and incremental deformation and bending induced in the material.

In the case of failed specimens by conventional press working, the failure mode prevailing at the formability limit was the initiation of necking at the edge of the flange. The condition for the onset of necking at the flange tip of conventional press working hole flanging was fulfilled at the intersection of the FLC with the line of pure uniaxial tension. The *LFR* value was associated with this intersection point, which explains why the *LFR* is a material constant and independent of the punch profile. The following expression is proposed: $LFR = exp\ (\varepsilon^*_{1,UT})$, where $\varepsilon^*_{1,\mathrm{UT}}$ is the major strain at the onset of necking in uniaxial tension.

The traditional *LFR* is a suitable measure of the formability in conventional hole flanging operations as this parameter directly quantifies the maximum stretching of the material at the hole tip, where failure occurs in practice. However, this parameter is not appropriate for measuring the flangeability in hole flanging by SPIF as it cannot capture the physics of failure. The *LFR* values achieved by the incremental process and conventional process are very similar, that is, 1.6 and 1.57, respectively, do not show any enhancement on formability by either process. As failure in incremental hole flanging occurs via severe stretching and thinning of the flange, two alternative parameters that quantify these events were proposed: the non-dimensional flange height (h/d_f) and average thickness ratio ($\bar{t}/t_o$). In terms of these parameters, the single-stage SPIF exhibits a gain in flangeability of approximately 40% and 30%, with respect to the press working process. These parameters also captures the expected increase in formability exhibited by SPIF processes, with an increase in the bending ratio (t_o/R) induced by the forming tool.

The conventional FLC and FFL obtained from Nakazima tests have not been

demonstrated to be suitable to evaluate the formability in all points of a flange in both processes. In the case of hole flanging by single stage SPIF, points around the middle of the flange with principal strains that easily overcome the FFL are observed. In conventional press forming, some points near the flange edge exhibit strains above the FLC. The reason for the former seems to be based on the effect of triaxiality in the ductile fracture of the material (Martins *et al.,*2008). The level of triaxiality is clearly lower in the incremental process than in the Nakazima tests, which postpones the onset of fracture. The latter is primarily attributed to the effect of bending induced in the sheet by the punch edge radius, which has a beneficial effect by delaying the initiation of necking in the sheet (Centeno et al., 2012).

In this work, note that the use of spindle rotation in the SPIF process does not significantly increase the formability in terms of the minimum pre cut hole to be successfully manufactured. However, spindle rotation provides a better surface quality, a more regular thickness distribution in the flange and a reduction in forming forces.

- ***Geometric features***

From an industrial point of view, other important aspects in hole flanging operations are the geometric features of the fabricated flange. The main conclusions regarding the dimensional accuracy, flange height and thickness distribution are summarized here.

For a given pre cut hole (i.e., a given *HER*), the conventional hole flanging operation can fabricate shorter, thicker and more homogeneous flanges than the single-stage SPIF operation, which would be more appropriate for manufacturing longer and thinner flanges with greater flexibility in shape. The thinner area is located around the middle of the flange.

When the flange provides support for another element, such as a threaded or welded joint, the thickness distribution is the weak point in single stage SPIF, and thus, the use of spindle speed is recommended to obtain a more regular thickness profile along the flange. Due to the presence of positive meridional strains in the outer surface of the specimen compared with the small negative meridional strains in conventional press working, the average thickness in single stage SPIF is smaller than that in conventional press working and has a less uniform thickness distribution for a given *HER* and tool radius or punch edge radius. The higher the meridional strain level, the higher the flange height.

The lack of dimensional accuracy causes rejection in production lines and

additional cost. In the conventional press working process, where the geometry of the flange is imposed by the punch shape, the dimensional precision is tuned by controlling the springback of the flange. In the case of the single-stage SPIF process, the dimensional precision can be increased by the design of new trajectories to counterbalance the springback of the flange and the tool deflexion. A greater homogeneous thickness distribution can be achieved using multi-stage SPIF strategies, which is significantly less aggressive than single-stage SPIF strategies (see, e.g., Morales et al.2017).

- ***Process features***

Machine requirements are important factors when choosing a technology. Conventional hole flanging operations require heavy machinery and dedicated punches and dies for each hole size. An incremental hole flanging operation, not only in single-stage, requires one order magnitude less force than a conventional hole flanging operation, can be performed in a standard CNC machine, and requires much less costly accessories to perform a large variety of hole flanging operations, which renders the investment profitable for small production batches.

The forming force and process time are important requirements from a production point of view. Regarding the former, the tests analysed in this study indicate that the maximum force in conventional forming is one order of magnitude higher than that in single-stage SPIF. However, this trend reverses when the process time is considered. In this study, the forming forces required in conventional forming reached a maximum of three orders of magnitude greater than that observed in incremental forming. Although the production time in a single-stage SPIF process can be reduced by increasing the feed-rate and the stepdown, differences are technologically unavoidable. The suitability of the press forming process when considering high productivity is confirmed.

6.2. Future works

This section describes the next steps that can be performed to complete the study developed in this thesis. Some of this research is currently in progress, as outlined in three points:

- The first step involves the characterization of the FFL via incremental forming tests.

  One of the main conclusions of this study is that FFL calculated by Nakazima

tests seems not to be an accurate curve for comparing the strains obtained in SPIF. A series of SPIF tests with different strain conditions should be executed to determine the appropriated FFL locus for incremental forming conditions or to explore other alternatives to anlyse the formability limits of the material instead of the traditional FLD analysis.

- The second step suggests the numerical simulation of both incremental processes and conventional processes.

  Some peculiarities experimentally observed in incremental hole flanging that are related to the process of fracture are founded on the evolution of the stresses, e.g., stress triaxiality, which are induced in the sheet during the flanging process. These events can be only analysed by virtually simulating the experimental tests using an FE model. The development of an accurate and computationally effective model is mandatory for a comprehensive analysis of the process.

- The third step focuses on the improvement of the flange thickness distribution.

The lack of uniformity in thickness is a major drawback of the single-state SPIF process. The study of new forming strategies, for instance, by optimizing the tool trajectories or the number of forming stages or the use of innovative tools, are tasks to be accomplished in the future as well as explore its application on new materials and other types of flanges.

7. REFERENCES

Alves, L.M., Nielsen, C.V., Martins, P.A.F. 2011. Revisiting the Fundamentals and Capabilities of the Stack Compression Test. Experimental Mechanics 51:1565–1572.

Ambrogio, G.; De Napoli, L.; Filice, L.; Gagliardi, F.; Muzzupappa, M. 2005. Application of incremental forming process for high customized medical product manufacturing. J. Mater. Process. Tech. 162, 156–162.

Ambrogio, G., Filice, L., Gagliardi1, F., Micari, F., 2005. Sheet incremental forming: A new process configuration allowing a sheet metal material controlled flow under the blank.holder. Proc. of Advanced Technology of Plasticity–Proceeding of the 8th ICTP, October 913, Verona (Italy), pp. 351-352.

Amino, H.; Lu, Y.; Ozawa, S.; Fukuda, K.; Maki, T. 2002. Dieless NC forming of automotive service panels. In Proceedings of the Conference on Advanced Techniques of Plasticity, Yokohama, Japan, October 27–November 1.

Amino, M., Mizoguchi, M., Terauchi, Y., Makic, T., 2014. Current Status of "Dieless" Amino's Incremental Forming. Procedia Engineering Volume 81, Pages 54-62.

Al-Ghamdi, K.A., Hussain, G. 2015. Threshold tool-radius condition maximizing the formability in SPIF considering a variety of materials: Experimental and FE investigations. International Journal of Machine Tools and Manufacture 88, pp. 82-94

Alkas-Yonan, Y., Silva, MB., Martins, PAF., Tekkaya, AE., 2014. Plastic flow and failure in single point incremental forming of PVC sheets. Express Polymer Letters 8(5):301–311.

ARGUS v6.2 User Manual v6.2 rev-a, 17/09/2009.

ARAMIS User Manual v6.3 rev-b, 09/07/2013.

ASTM E8M-08, Standard Test Methods for Tension Testing of Metallic Materials.

ASTM E9-09, Standard Test Methods of Compression Testing of Metallic Materials at Room Temperature.

ASTM E517-00, Standard Test Method for Plastic Strain Ratio r for Sheet Metal.

Azevedo, N.G., Farias, J.S., Bastos, Teixeira, P.b, Davim, J.P., Alves de Sousa, R.J.. 2015. Lubrication aspects during Single Point Incremental Forming for steel and aluminum materials. International Journal of Precision Engineering and ManufacturingVolume 16, Issue 3, Pages 589-595

Bagudanch, I., Lozano-Sánchez, L.M., Puigpinós, L., Sabatera, M., Elizalded, L.E., Elías-Zúñigab, A., Garcia-Romeu, M.L., 2015. Manufacturing of polymeric biocompatible cranial geometry by single point incremental forming. Procedia Engineering 132, 267 – 273.

Bambach, M., Voswinckel, H., Hirt, G., 2014, A new process design for performing hole-flanging operations by incremental sheet forming. Procedia Engineering 81(C):2305-2310.

Barata da Rocha, Barlat F., Jalinier, J.M. 1985. Prediction of the forming limit diagrams of anisotropic sheets in linear and non-linear loading. Materials Science and Engineering 68: 151–164.

Bastos, R N.P., Alves de Sousa, R. J.,. Fernandes Ferreira, J. A.,2016 Enhancing time efficiency on single point incremental forming processes. Int J Mater Form 9:653–662.

Borrego, M., Morales-Palma, D., Martínez-Donaire, A. J., Centeno, G., Vallellano, C., 2015. On the study of the single-stage hole-flanging process by SPIF. Procedia Engineering 132, 290–297.

Borrego, M., Morales-Palma, D., Martínez-Donaire, A.J., Centeno, G., Vallellano, C. 2016. Experimental study of hole-flanging by single-stage incremental sheet forming. Journal of Materials Processing Technology 237, pp. 320-330.

Cawley, B., Adams, D., and Jeswiet, J. 2013. Examining Tool Shapes in Single Point Incremental Forming. Proceedings of NAMRI/SME, Vol. 41.

Centeno, G., Doblas, F.J., Martínez-Palmeth, L.H., Martínez-Donaire, A.J., Vallellano, C. 2012. FEA of the bending effect in the formability of metal sheets via incremental forming. Steel Research International Volume SPL. ISSUE, Pages 447-450.

Centeno, G., Silva, MB., Cristino, VAM., Vallellano, C., Martins, PAF., 2012, Hole-flanging by incremental sheet forming. International Journal of Machine

Tools and Manufacture 59: 46-54.

Centeno, G., Silva, B., Vallellano, C., Martins, P., 2012, Manufacturing of sheet metal flanged parts using multi-stage SPIF, Steel Research International, Sp. Ed. Metal Forming, pp.271-274.

Centeno, G., Bagudanch, I., Garcia-Romeu, M.L., Martinez-Donaire, A.J., Vallellano, C., 2013. Experimental study on the overall spifability of AISI 304 sheets under different bending conditions. Key Engineering Materials 554-557, pp. 2293-2298.

Centeno, G., Bagudanch, I., Martínez-Donaire, AJ., García-Romeu, ML., Vallellano, C., 2014. Critical analysis of necking and fracture limit strains and forming forces in single-point incremental forming. Materials and Design 63,20-29.

Centeno, G., Martínez-Donaire, A.J., Bagudanch, I., Morales-Palma. D., Garcia-Romeu, M.L., Vallellano, C., 2017. Revisiting formability and failure of AISI304 sheets in SPIF: Experimental approach and numerical validation. *Metals*, *7*(12), 531

Cristino, VAM., Silva, MB., Wong, PK., Tam, LM., Martins, PAF., 2015, Hole-flanging of metals and polymers produced by single point incremental forming, Int. J. of Mat. Prod. Technology 50(1):37-48.

Cui, Z., Gao, L., 2010, Studies on hole-flanging process using multistage incremental forming. CIRP Journal of Manufacturing Science and Technology 2:124–128.

Duflou, J.r., Callebaut, B., Verbert, J., De Baerdemaeker, H., 2008. Improved SPIF performance through dynamic local heating. International Journal of Machine Tools & Manufacture 48, 543–549.

Duflou, JR., Verbert, J., Belkassem, B., Gu, J., Sol, H., Henrard, C., Habraken, AM. 2008. Process window enhancement for singlepoint incremental forming through multi-step tool paths. CIRP Ann Manuf Technol 57(1):253–256.

Durante, M., Formisano, A., Langella, A. ,Capece Minutolo, F.M.,2009. The influence of tool rotation on an incremental forming process. Journal of Material Processing Technology 209, 4621-4626.

Durante, M., Formisano, A., Langella, A.,2011. Observations on the Influence of

Tool-Sheet Contact Conditions on an Incremental Forming Process. JMEPEG 20:941–946.

Emmens, WC, van den Boogaard, AH., 2009a. An overview of stabilizing deformation mechanisms in incremental sheet forming. Journal of Materials Processing Technology 209,3688–3695.

Emmens, WC, van den Boogaard, AH., 2009b. Incremental forming by continuous bending under tension: An experimental investigation. Journal of Materials Processing Technology 209, issue 14 5456–5463.

Emmens, WC, Sebastiani, G., van den Boogaard, AH., 2010. The technology of Incremental Sheet Forming—A brief review of the history. Journal of Materials Processing Technology 210, 981–997.

EP 1560668, Tuominen, T., 2002, Method and apparatus for forming three-dimensional shapes in a sheet metal.

EP 1899089, Callebaut, B., Duflou, J., Verbert, J., 2005. Asymmetric incremental sheet forming system.

Fan, G., Gao, L., Hussain, G., Wu, Z., 2008. Electric hot incremental forming: A novel technique. International Journal of Machine Tools & Manufacture 48, 1688–1692.

Fang, Y., Lu, B. ,Chen, J., Xu, D.K., Ou, H., 2014. Analytical and experimental investigations on deformation mechanism and fracture behavior in single point incremental forming. Journal of Materials Processing Technology 214 (8), 1503-1515.

Fiorentino, A., Feriti, G.C., Ceretti, E., Giardini, C. 2018. Capability of iterative learning control and influence of the material properties on the improvement of the geometrical accuracy in incremental sheet forming process. International Journal of Material Forming 11(1), pp. 125-134

Fratini, L., Ambrogio,G., Di Lorenzo, R., Filice, L.,Micari, F., 2004. Influence of mechanical properties of the sheet material on formability in single point incremental forming. CIRP Annals Volume 53, Issue 1,Pages 207-210.

Geiger, M.,Merklein, M.,2003, Determination of forming limit diagrams – A new analysis method for characterization of materials' formability, Annals of the CIRP, Vol. 52/1:213-216.

Gilmour, K.R., Leacock, A.G., Ashbridge, M.T.J.,2004. The influence of plastic strain ratios on the numerical modelling of stretch forming. Journal of Materials Processing Technology. 152, Issue 1, 116-12.

Giraud-Moreau, L., Belchior, J., Lafon, P., Lotoing. L., Cherouat, A., Courtielle, E., Guines, D., Maurine, P. 2018. Springback effects during single point incremental forming: Optimization of the tool path. AIP Conference Proceedings 1960,160009

Graf , A., Hosford, W., 1994. The influence of strain-path changes on forming limit diagrams of Al 6111T4. International Journal of Mechanical Sciences 36, 897-910.

Golabi, S., Khazaali, H.,2014. Determining frustum depth of 304 stainless steel plates with various diameters and thicknesses by incremental forming. Journal of Mechanical Science and Technology 28 (8), 3273-3278.

Gupta, P., Jeswiet, J., 2018. Effect of temperatures during forming in single point incremental forming. J. Int J Adv Manuf Technol 95: 3693.

He, J., Zeng, D. ,Zhu, X., Xia, C. ,Li, S., 2014. Effect of nonlinear strain paths on forming limits under isotropic and anisotropic hardening. International Journal of Solids and Structures 51, 402–415.

Huang, Y.M.,Chien, K.H.,2001b. The formability limitation of the hole-flanging process. Journal of Materials Processing Technology 117, 43-51.

Huang, Y.M.,Chien, K.H.,2001a. Influence of the punch profile on the limitation of formability in the hole-flanging process. Journal of Materials Processing Technology 113, 720-724.

Huang, Y.M.,Chien, K.H.,2002. Influence of Cone Semi-Angle on the Formability Limitation of the Hole-Flanging Process. Int J Adv Manuf Technol 19, 597–606.

Hussain, G., Gao, L., 2007. A novel method to test the thinning limits of sheet metals in negative incremental forming. International Journal of Machine Tools & Manufacture 47, 419–435.

Hussain, G., Gao, L., Hayat, N., Cui, Z., Pang, Y.C., Dar, N.U.,2008. Tool and lubrication for negative incremental forming of a commercially pure titanium sheet. journal of materials processing technology 203, 193–201.

Hussain, G., Khan, H.R., Gao, L., Hayat, N. 2013. Guidelines for Tool-Size Selection for Single-Point Incremental Forming of an Aerospace Alloy. Materials and Manufacturing Processes, 28:3, 324-329.

Iseki, H., Kato, K., Sakamoto, S., 1989. Flexible and incremental sheet metal forming using a spherical roller. Proc. 40th JJCTP, pp. 41-44.

Iseki, H., Kato, K., Sakamoto, S., 1991. Flexible and incremental sheet bulging using a path-controlled spherical roller (a trial manufacture of the bulging machine). Proc.1991. JSCTP, pp. 515-518.

Iseki, H., Kato, K., Sakamoto, S., 1992a. Flexible and incremental sheet bulging using a path-controlled spherical roller. Trans. JSME 58 (554), 3147-3155.

Iseki, H., Kato, K., Kumon, H., Ozaki, K., 1992b. Flexible and incremental sheet bulging using a few spherical rollers. Trans. JSME 59 (565), 2849-2854.

Iseki, H., Shioura, T., Kato, Satou , K., 1994. Practical development of flexible and incremental sheet metal bulging machine. Proc. 1994. JSCTP, pp. 573-576.

Iseki, H., Shioura, T., Satou , K., 1996. Practical development of press-molding machine with small punching tool. Proc. 5th ICTP, Columbus OH, USA, October 7-10, 1996, pp. 935-938.

Isik, K., Silva, MB., Tekkaya, AE., Martins, PAF., 2014. Formability limits by fracture in sheet metal forming. Journal of Materials Processing Technology 214:1557-1565.

ISO 12004-2:2008, Metallic materials — Sheet and strip — Determination of forming-limit curves — Part 2: Determination of forming-limit curves in the laboratory.

ISO 16808:2014, Determination of biaxial stress-strain curve by means of bulge test with optical measuring systems.

Jackson, K.P.; Allwood, J.M.; Landert, M. 2008. Incremental forming of sandwich panels. Journal of Materials Processing Technology 204, 290–303.

Jeswiet, J.; Hagan, E. Rapid prototyping of a headlight with sheet metal. In Proceedings of SheMet International Conference, Leuven, Belgium, April 2–3, 2001.

Jeswiet, J., Micari, F., Hirt, G., Bramley, ,A., Duflou, J, Allwood, J.M., 2005. Asymmetric single point incremental forming of sheet metal. CIRP Annals-Manufacturing Technology 54:88–114.

Jeswiet, J.; Duflou, J.; Szekeres, A.; Levebre, P. Custom manufacture of a solar cooker: A case study. Journal Advanced Materials Research 2005, 6–8, 487–492.

Ji, Y.H., Park , J.J., 2008. Formability of magnesium AZ31 sheet in the incremental forming at warm temperature. journal of materials processing echnology 2 0 1, 354–358.

Johnson W.,Chitkara N.R.,Minh H.V., 1977. Deformation modes and lip fracture during hole-flanging of circular plates of anisotropic material, American Society of Mechanical Engineers (76 -WA/Prod-15).

Kacem, A.,Krichen, A.,Manach, P.Y.,2011. Occurrence and effect of ironing in the hole-flanging process. Journal of Materials Processing Technology 211, 1606–1613.

Kacem, A.,Krichen, A.,Manach, P.Y, Thuillier, S.,Yoon, J.W.,2013. Failure prediction in the hole-flanging process of aluminium Alloys. Engineering Fracture Mechanics 99, 251–265.

Kacem, A.,Krichen, A.,Manach, P.Y., 2015. Finite element analysis of hole-flanging process with various anisotropy assumptions. International Journal of Advanced Manufacturing Technology 80, 11–19.

Krichen, A.,Kacem, A.,Hbaieb, M.,2011. Blank-holding effect on the hole-flanging process of sheet aluminum alloy. Journal of Materials Processing Technology 211, 619–626.

Lăzărescu, L., Comşa, D.S., Banabic, D.,2011. Determination of stress-strain curves of sheet metals by hydraulic bulge test. AIP Conference Proceedings Volume 1353, 2011, Pages 1429-1434.

Leu D.K.,Chen T.C.,Huang Y.M.,1999. Influence of punch shape on the collar-drawing process of sheet steel. Journal of Materials Processing Technology 88, 134-146.

Li, Y.,Daniel, W.J.T.,Liu, Z.,Lu, H.,Meehan, P.A.,2015. Deformation mechanics and efficient force prediction in single point incremental forming. Journal of Materials Processing Technology 221, 100-111.

Li, Y., Liu, Z., Daniel, W.J.T., Meehan, P. A. 2014. Simulation and Experimental Observations of Effect of Different Contact Interfaces on the Incremental Sheet Forming Process, Materials and Manufacturing Processes, 29:2, 121-128.

Li, Z., Lu, S., Zhang, T., Mao, Z., Zhang, C., 2018. A Simple and Low-Cost lubrication Method for Improvement in the Surface Quality of Incremental Sheet Metal Forming. Trans Indian Inst Met 71(7):1715–1719.

Liu, Z.,Li, Y.,Meehan, P. A.,2013. Experimental investigation of mechanical properties, formability and force measurement for AA7075-O aluminium alloy sheets formed by incremental forming. International Journal of Precision Engineering and Manufacturing 14, 1891–1899.

Lu, B.,Fang, Y.,Xu, D.K.,Chen, J.,Ou, H.,Moser, N.H.,Cao, J.,2014. Mechanism investigation of friction-related effects in single point incremental forming using a developed oblique roller-ball tool. International Journal of Machine Tools and Manufacture 85, 14–29.

Liu, Z., Daniel, WJT., Li, Y., Liu, S., Meehan, PA. 2014. Multi-pass deformation design for incremental sheet forming: analytical modeling, finite element analysis and experimental validation. J Mater Process Technol 214(3):620–634.

Luo, M., Wierzbicki, T., 2010. Numerical failure analysis of a stretch-bending test on dual-phase steel sheets using a phenomenological fracture model. International Journal of Solids and Structures 47: 3084–3102.

Malhotra, R., Xue, L., Belytschko, T., Cao, J., 2012. Mechanics of fracture in single point incremental forming. Journal of Materials Processing Technology 212,1573– 1590.

Maqbool F, Bambach M, 2017. Revealing the Dominant Forming Mechanism of Single Point Incremental Forming (SPIF) by Splitting Plastic Energy Dissipation. 17th International Conference on Sheet Metal, SHEMET 2017. 183: 188-193.

Martínez-Donaire, A.J., García-Lomas, F.J., Vallellano, C., 2014. New approaches to detect the onset of localised necking in sheets under through-thickness strain gradients. Materials and Design 57, 135–145.

Martínez-Palmeth, L.H. ,Martínez-Donaire, A.J., Centeno, G., García-Lomas, F.J., Vallellano, C. 2013. Formability of automotive H240LA steel sheets in stretch - Bending processes. Procedia Engineering 63, pp. 669-677.

Martins, P.A.F., Bay, N. Skjoedt, M., Silva, M.B., 2008. Theory of single point incremental forming. CIRP Annals-Manufacturing Technology 57 (2008) 247–252.

Mason, B., 1978. Sheet metal forming for small batches. Bachelor Thesis, Univ of Nothingham.

Mason, B., Appleton. E., 1984. Sheet metal forming for small batches using sacrificial tooling. Proc. 3rd Int.Conf. on Rotary Metalworking. Kyoto, Japan, pp.495-511.

Matsubara, S. 1994. Incremental backward bulge forming of a sheet metal with a hemispherical tool - A study of a numerical control forming system. Journal of the Japan Society for Technology of Plasticity 35, 1311–1316.

Mirnia, M.J., Mollaei Dariani, B., Vanhove, H., Duflou, J.R., 2014. Thickness improvement in single point incremental forming deduced by sequential limit analysis. International Journal of Advanced Manufacturing Technology 70, 2029–2041.

Montanari, L.,Cristino, V.A.,Silva, M.B.,Martins, P.A.F.,2013. A new approach for deformation history of material elements in hole-flanging produced by single point incremental forming. International Journal of Advanced Manufacturing Technology 69 (5), 1175–1183.

Montanari, L., Cristino ,VA., Silva, MB., Martins, PAF., 2013, A new approach for deformation history of material elements in hole-flanging produced by single point incremental forming. International Journal of Advanced Manufacturing Technology, 69(5-8):1175-1183.

Morales-Palma, D.,Vallellano, C.,García-Lomas, F.J.,2013. Assessment of the effect of the through-thickness strain/stress gradient on the formability of stretch-bend metal sheets. Materials and Design 50, 798–809.

Morales-Palma, D., Borrego, M., Martínez-Donaire, A.J., Centeno, G., Vallellano, C. Preliminary investigation on homogenization of the thickness distribution in hole-flanging by SPIF. Procedia Manufacturing 13, pp. 124-131.

Rodriguez, P.P. Incremental sheet forming: Industrial applications. In International Seminar on Novel Sheet Metal Forming Technologies, Jyvaskyla, Finland, February 16, 2006.

Seong, D.Y., Haque ,M.Z., Kim, J.B., Stoughton, T.B., Yoon, J.W. 2014. Suppression of necking in incremental sheet forming. International Journal of Solids and Structures 51, 2840–2849.

Shamsari, M., Mirnia, M.J., Elyasi, M., Baseri, H., 2018. Formability improvement in single point incremental forming of truncated cone using a two-stage hybrid deformation strategy. Int J Adv Manuf Technol 94, 2357–2368.

Silva, M.B., Skjoedt, M.,Martins, P.A.F., Bay, N.,2008. Revisiting the fundamentals of single point incremental forming by means of membrane analysis. International Journal of Machine Tools & Manufacture 48, 73–83.

Silva, MB., Nielsen, PS., Bay, N., Martins, PAF., 2011, Failure mechanisms in single point incremental forming of metals. International Journal of Advanced Manufacturing Technology 56,893-903.

Silva, MB., Teixeira, P., Reis, A., Martins, PAF., 2013, On the formability of hole-flanging by incremental sheet forming. Proceedings of the Institution of Mechanical Engineers, Part L: Journal of Materials: Design and Applications 227(2):91-99.

Skjoedt, M., . Hancock, M.H., Bay, N., 2007. Creating Helical Tool Paths for Single Point Incremental Forming. Key Engineering Materials Vol 344. pp 583-590.

Skjoedt, M., Bay, N., Endelt, B., Ingarao, G., 2008. Multi stage strategies for single point incremental forming of a cup. J Mater Form 1(1):1199–1202.

Skjoedt, M., Silva, M.B., Martins, P.A.F., Bay, N., 2010. Strategies and limits in multi-stage single-point incremental forming. Journal of Strain Analysis for Engineering Design 46, 33–44.

Soussi H.,Masmoudi N.,Krichen A.,2016. Analysis of geometrical parameters and occurrence of defects in the hole-flanging process on thin sheet metal, Journal of Materials Processing Technology 234: 228–242.

Stoughton, T.B., Yoon, J.W. 2012. Path independent forming limits in strain and stress spaces. International Journal of Solids and Structures 49(25), pp. 3616-3625.

Tang, S.C.,1981. Large elasto-plastic strain analysis of flanged hole forming. Computers and Structures 13, 363-370.

Takano, H.; Kitazawa, K.; Goto, T., 2008. Incremental forming of nonuniform sheet metal: possibility of cold recycling process of sheet metal waste. Int. J. Mach. Tool Manufact.48, 477–482.

US 3316745, Berghahn, W.G., Murray, G.F. 1967. Method of dielessly forming surfaces of revolution.

US 3342051, Leszak, E. 1967, Apparatus and process for incremental dieless forming.

US 6748780, Luttgeharm, C.A., 2001, Numerically controlled forming method.

Vallellano, C., Morales, D., García-Lomas, F. J., 2008. A Study to Predict Failure in Biaxially Stretched Sheets of Aluminum Alloy 2024-T3. Materials and Manufacturing Processes 23, 303–310.

Vallellano, C., Morales, D., Martinez, A.J. ,Garcia-Lomas, F.J. 2010. On the use of concave-side rule and critical-distance methods to predict the influence of bending on sheet-metal, International Journal of Material Forming, 3 (suppl. 1): 1167-1170.

Verbert, J., Belkassem, B., Henrard, C., Habraken, AM., Gu, J., Sol, H., Lauwers, B., Duflou, JR. 2008. Multi-step Toolpath approach to overcome forming limitations in single point incremental forming. Int J Mater Form 1(1):1203–1206.

Xu, D.,Wu, W.,Malhotra, R.,Chen, J.,Lu, B.,Cao, J.,2013. Mechanism investigation for the influence of tool rotation and laser surface texturing (LST) on formability in single point incremental forming. International Journal of Machine Tools and Manufacture 73, 37–46.

Yamada, Y.,Koide,M.,1967. Analysis of the bore-expanding test by the incremental theory of plasticity. International Journal of Mechanical Sciences 10,1-14.

Yoshida, K., Kuwabara, T., Kuroda, M. ,2007. Path-dependence of the forming limit stresses in a sheet metal. Int. J. Plast. 23: 361–384.

Yu, X., Chen, J., Chen, J. 2016. Influence of curvature variation on edge stretchability in hole expansion and stretch flanging of advanced high-strength steel. International Journal of Advanced Manufacturing Technology 86(1-4), pp. 1083-1094 .

Young, D., Jeswiet, J., 2005. Wall thickness variations in single-point incremental forming. Proc. Instn Mech. Engrs Vol. 218 Part B: J. Engineering Manufacture.

Zhang, J., 2007, Roboterbasiertes inkrementelles Blechumformen.Ph.D. thesis, Ruhr-Universitaet Bochum.

Marcos Borrego Puche

Analysis of single stage SPIF process applied to the hole flanging operation

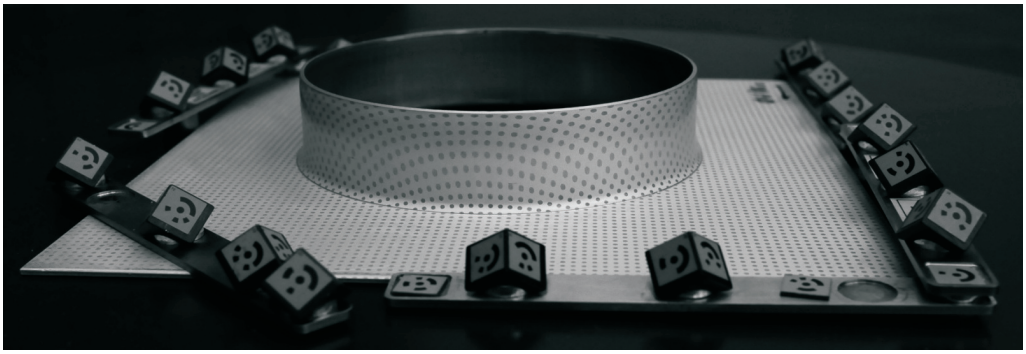

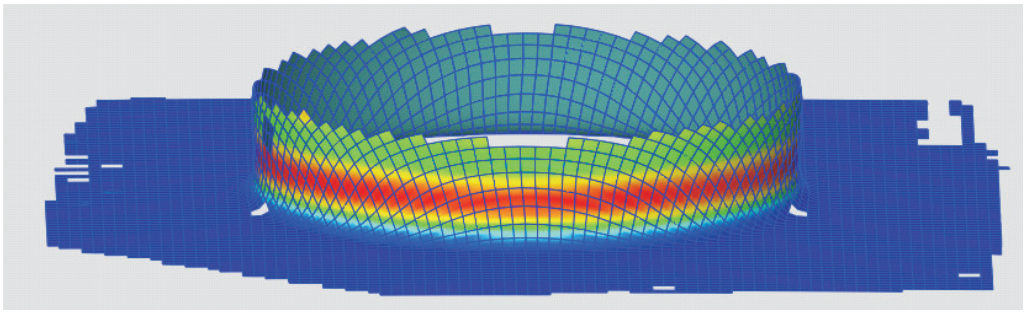

GOBIERNO DE ESPAÑA
MINISTERIO DE ECONOMÍA Y COMPETITIVIDAD

DPI-2012-32913

2018